RHEINISCH-WESTFÄLISCHE TECHNISCHE HOCHSCHULE AACHEN

GRADUATE SCHOOL LECTURES 2014

PART II

OPTICAL PROPERTIES OF NANOSTRUCTURED MATTER

THE MODEL OF METAL NANOPARTICLES

UWE KREIBIG

ALMUTH HILGER,

HEINZ HÖVEL,

MICHAEL QUINTEN

I. Physikalisches Institut IA

der R W T H Aachen / BRD

kreibig@physik.rwth-aachen.de

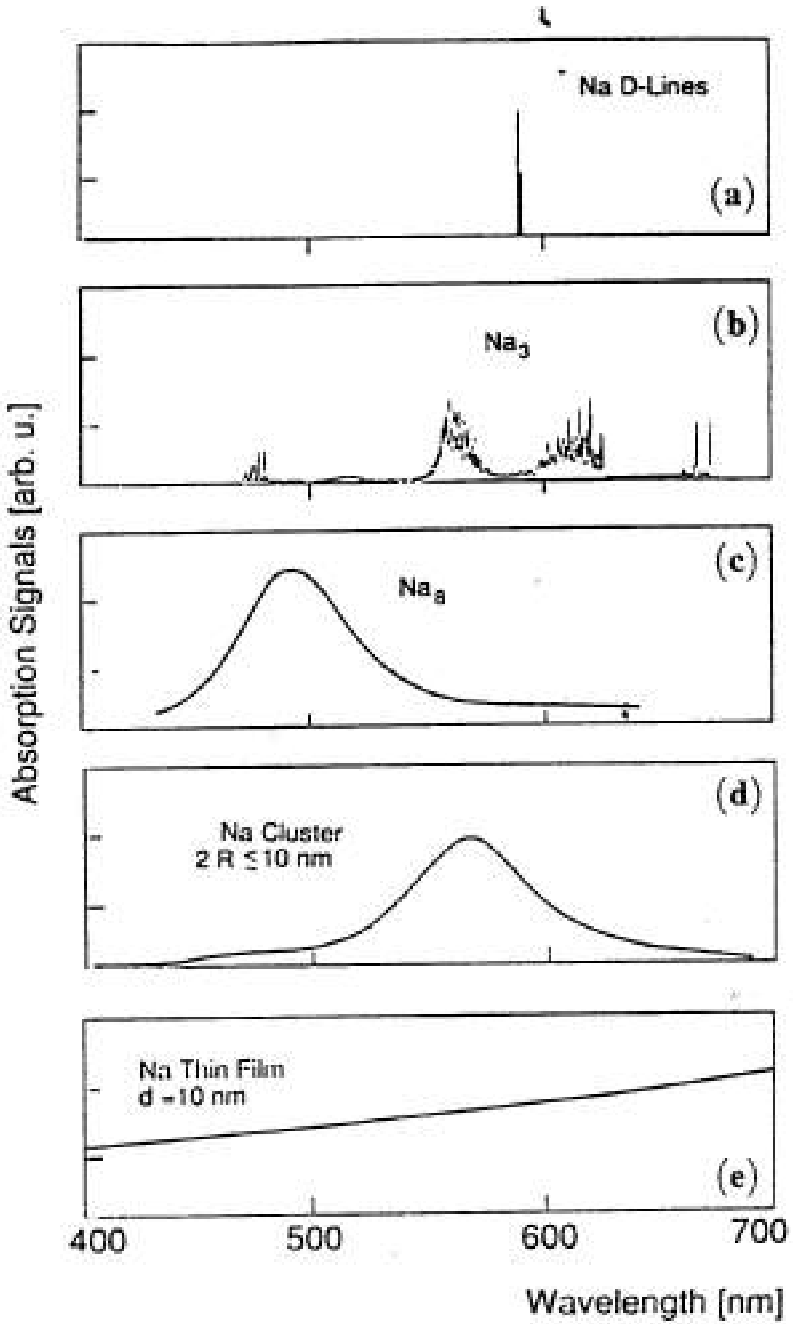

Fig. 1.4. Optical properties of sodium. From top to bottom:

- Spectrum of atomic sodium
- Two photon ionization spectrum of Na_3 [1.174]
- Beam depletion spectrum of Na_8 [1.155]
- Absorption of large Na clusters in NaCl [1.175]. The size was below the resolution of optical microscopes and supposedly ranges around 10 nm.
- Transmission of a thin film of bulk sodium (thickness 10 nm).

REALITY BEYOND MIE'S THEORY

NANO - EFFECTS

COMPARISON:

MIE THEORY <=> REALISTIC EXPERIMENT

Classical Mie - Theory: Electrodynamical Part
(propagation of light) :
exact in Maxwells theory, but
only under selected assumptions

Material Properties :
Mie : homogeneous dielectric
functions of bulk-like material

Experimental Reality : Not all electrodynamic assumptions
of Mie theory valid in nanoparticles

Material Properties of nanoparticles
differ from bulk-like material
("nano-size effects,
surface/interface-effects ect.)

=> Extensions and corrections required and performed since hundred years to adapt Mie theory better to reality.

=> EXTENDED MIE THEORY (EMT)

BEYOND MIE'S THEORY

(A) REALISTIC ELECTRODYNAMICS :

1) Incident wave is not plane
(e.g.focused laser beam, diffuse white light source: outgoing waves not plane)

2) The step-like Maxwell boundary conditions do not hold
(3-d particle surface/interface not included)

3) Additional boundary conditions (long. plasmons)

4) Inhomogeneous interface layer (traps, bonds)

4) Particle shapes are not spherical
(Polyhedra; edges; corners; surface roughness)

5) Heterogeneous particle structures
(core/shell; multigrain structures)

6) Atomic and molecular adsorbares (sensoric devices)

7) Embedding in liquid or solid matrices
(Chemical interface interactions)

8) Deposition on substrates (flattening by interface forces; substrate interferences; interface charges; image forces; chemical interactions)

9) Particles electrically charged (chemical potential; charge double layers at surface)

10) Many-particle systems
(sizes, shapes, local distributions not uniform)

11) Dense packing in many-particle systems
(electrodynamical particle-particle coupling)

(B) MATERIAL PROPERTIES :

12) Dielectric function of the particle material differs from bulk DF due to nano-size effects: $\varepsilon = \varepsilon(\omega, R)$
(quantum size effects; mean free path effect; band structure effects)

13) Tensorial dielectric function (e.g. carbon particles)

14) Nonlocal electrodynamic response

15) Surface dielectric function (polarizability)

16) Dielectric function of the particle material is not locally homogeneous due to surface properties: $\varepsilon = \varepsilon(\omega, r)$

17) Changes of ε due to static and dynamic charge transfer

18) D. F. of the matrix varies with frequency $\varepsilon_{matrix}(\omega)$

19) D. F. of the matrix is inhomogeneous/ unisotropic
(e.g. close to the particle interface)

20) D. F. of matrix is complex (absorbing matrix)

21) D. F. of the particle material is non-linear

23) Tunneling among neighboring particles in densely packed many-particle-systems

24) Agglomeration and Coalescence in densely packed many particle systems (formation of particle clusters, particle chains, larger, irregular aggregates)

25) etc.

Table 2.12. Plasma Peak Positions: theories for red and blue shifts.

	References	Shift with decreasing R
1) Maxwell theory;		
Drude dielectric function		
with free path limitation	2.82, 177	Red
with diffuse surface layer / spill-out	2.206	Red
with substrate interaction	2.120	Red
additional boundary condition (ABC)	2.175, 445	Blue
with dielectric core	2.446	Red ore Blue (depending on ε_{core})
with interband transitions		Red or Blue
2) Discrete energy levels;		
linear response	2.211, 447	Blue
with surface states and interband transitions	2.323	Blue or Red, depending on surface properties
3) Quantum box model;		
RPA	2.218	Blue
	2.211	Red
improved	2.448	Blue and oscillation
4) Thomas-Fermi approximation;		
sum rule	2.449	Blue
statistical method	2.234, 249	Red
5) Jellium; local density;		
self consistent	2.235, 239, 240, 242	Red
sum rules	2.238, 251, 259	Red
6) Hydrodynamical model;	2.217	
diffuse electron density profile	2.450	Red (smooth), Blue (step profile)
	2.207, 451	Red

Table 2.12 (continued)

	References	Shift with decreasing R
7) Nonlocal effects	2.163	
8) Lattice contraction; Influences on the conduction electron density	2.452–455	Blue-shift (Ag particles: volume contraction $\Delta V/V = 5\,\%$, shift $\approx 0.1\,\mathrm{eV}$)
9) Changes of the effective mass of the conduction electrons		Increase: red-shift Decrease: blue-shift
10) Size dependent changes of electronic band structure	Ag: 2.456, 457 Au: 2.458	
11) Size dependent changes of optical interband transitions	Au: 2.193, 459 Ag: 2.460	Blue-shift Blue-shift
12) Additional "molecular" absorption structures in samples with a distribution of particle sizes	Ag: 2.218, 461–464	Blue-shift, broadening
13) Deviations of the embedding medium-ε_m from the mean value near the particle interface (adsorption layers, ion enrichment, etc.)	2.75	Increase of ε_m: red-shift decrease of ε_m: blue-shift
14) Rough particle-matrix interface	2.191	Au: red-shift, broadening
15) Asymmetric plasma band shapes (R dependent)	2.191	Ag: blue-shift
16) Physisorption/chemisorption/chemical reactions at the interface	2.465, 466 (also 4.30)	Blue and red shifts

Table 2.14. Additional effects influencing widths and positions and splitting of plasmon bands.

A: Single cluster samples

1) Shape effects
   a) Irregular shape
   b) Ellipsoidal shape (orientation averaging!)
   c) Fluctuating shape (degeneracy of minima in Nilsson-Clemenger Model)
2) Volume (interior) effects
   a) Size dependent interband excitation contributions
   b) Extrinsic (electrodynamic) size effects
   c) Lattice defects (impurities, point defects, multidomain structures with grain boundaries)
3) Surface/Interface effects
   a) Nonlocal effects
   b) Physisorbed adsorbates
   c) Chemically reacting adsorbates (oxide layers, compound layers, organic ligands, etc.)
   d) Coatings
   e) Charge transfer between cluster and adsorbates/matrix
   f) Inhomogeneous/anisotropic embedding media (fluctuations of the local ε_m)

B: Many cluster samples

1) Noninteracting clusters
   a) Cluster size distributions
   b) Cluster shape distributions
2) Interactions between clusters
   a) Effective media
   b) Coagulation aggregates
   c) Coalescence aggregates
   d) Percolation, nanostructured matter
3) Interactions between cluster aggregates

EXAMPLE :

MAXWELLS BOUNDARY CONDITIONS

SOFT BOUNDARY CONDITIONS;
SPILL OUT OF THE ELECTRON DENSITY

Boundary conditions at $r = R$ ("sharp" boundary conditions)

$E_{\Theta}^{incident} = E_{\Theta}^{interior}$;

$E_{\Phi}^{incident} = E_{\Phi}^{interior}$;

$\varepsilon^{outside} \cdot E_r^{incident} = \varepsilon^{inside} \cdot E_r^{interior}$

Longitudinal fields :Current density: j_{total}^{normal} continuous at $r = R$ (Sauter-Forstmann condition).

Analog for H.

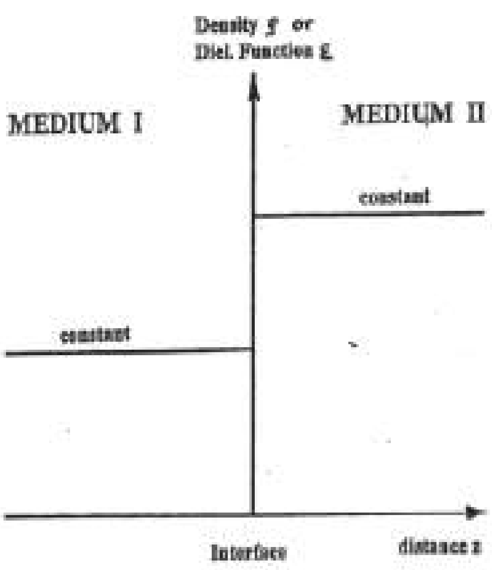

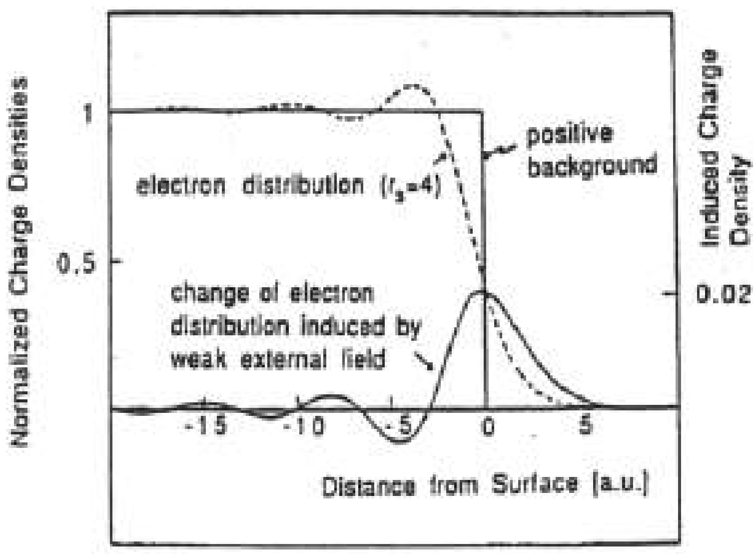

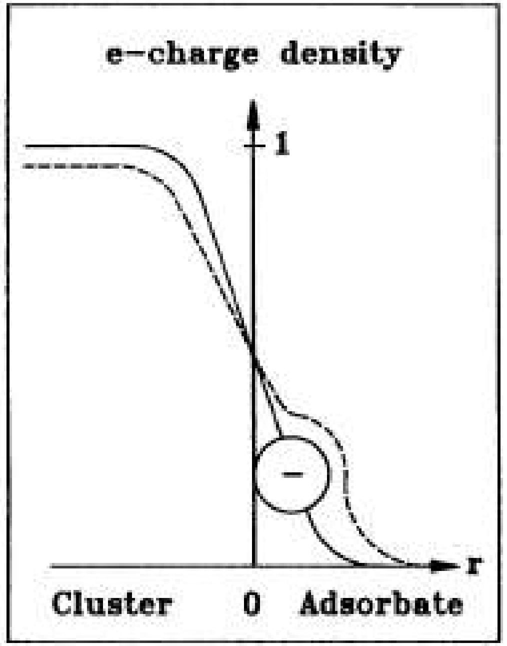

Interlayer charge transfer

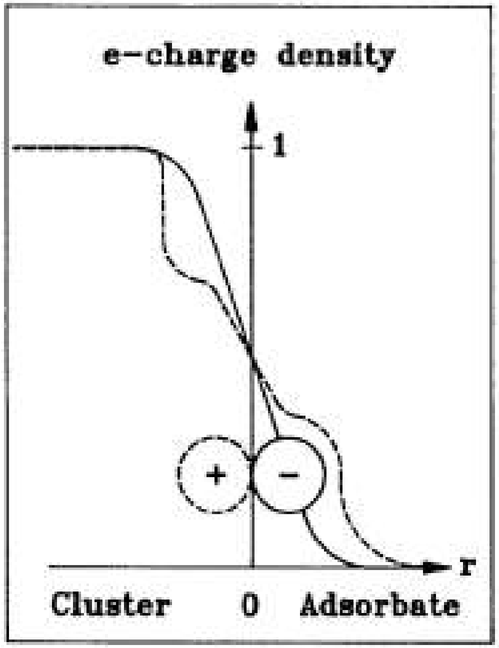

Surface double-layer

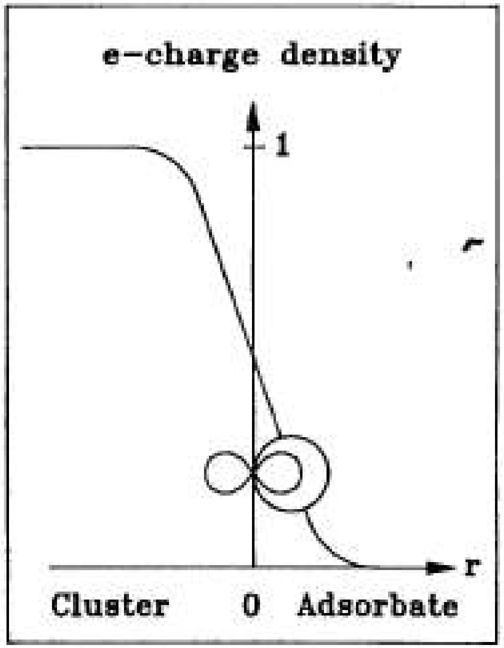

Covalent bonding

(Model extending Schultze & Rolle, Can.J. Chem.75 (1997))

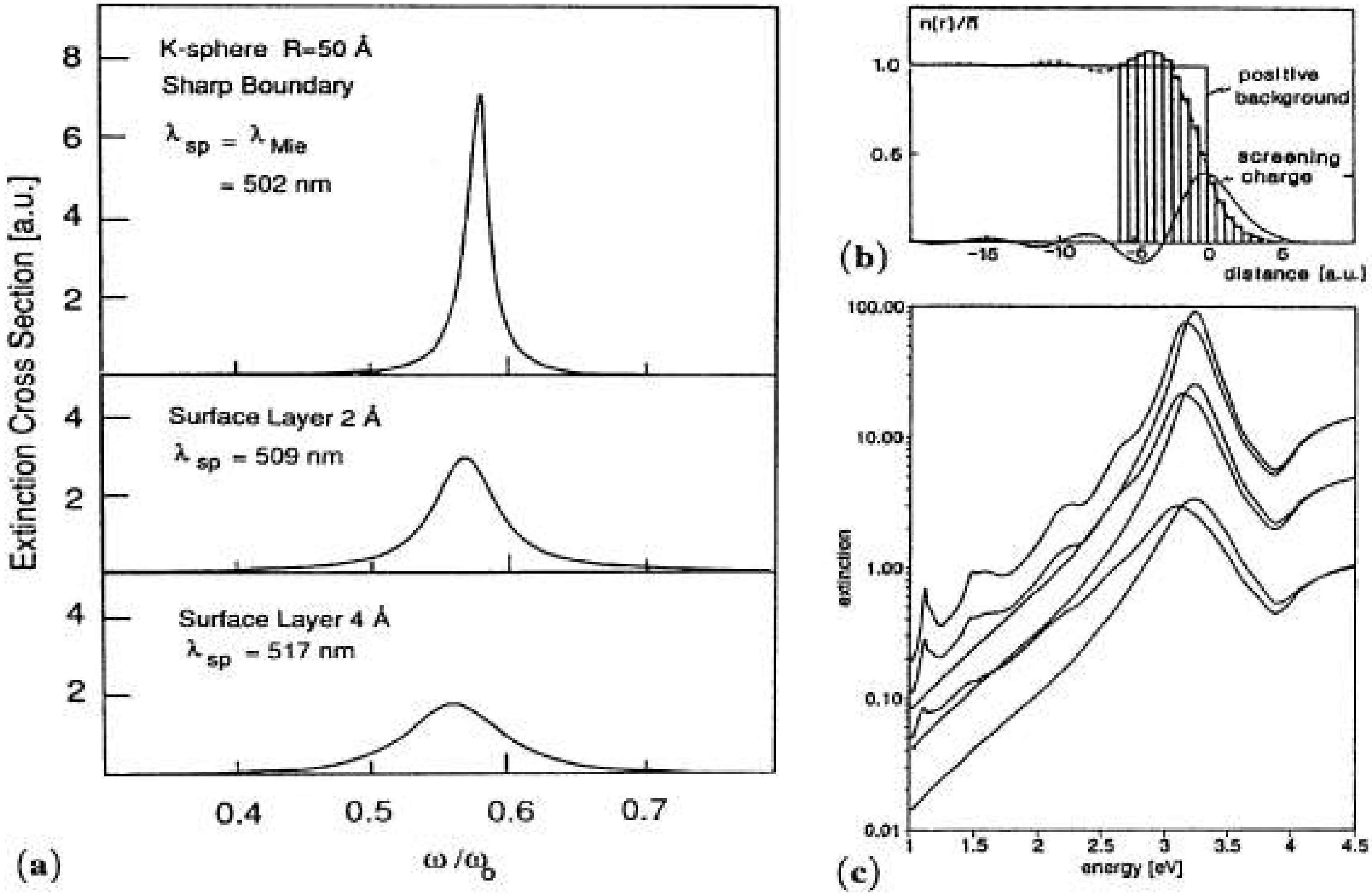

Fig. 2.44. (**a**) Theoretical extinction cross section for a potassium sphere with 5 nm radius (after [2.206]). The upper curve was calculated using classical Mie theory in the electrostatic approximation for a sphere with sharp boundary of the electron charge distribution. In the two lower curves a diffuse surface with linearly decreasing electron density in a transition layer of thickness 2 Å and 4 Å was assumed, leading to broadening and to a red shift of the surface plasmon resonance. (**b**) Modeling of the spill-out at the surface of free Na and Ag clusters. The s-electron densities as given by [2.201, 205] were approximated by discretization with multishell clusters. (**c**) Absorption spectrum with and without spill-out effect ($R = 1.5$, 2.5, and 3.5 nm) following from (**b**).

EXAMPLE

REALISTIC
OPTICAL DIELECTRIC FUNCTIONS

NANO – EFFECTS :

(1) Size – Effects :

> Physical and chemical properties depending on the atomic interactions in the sample volume
(binding forces, atomic structures, quantum size effects, band structure effects, etc.)

> Physical and chemical effects depending on "critical /characteristic lengths"
(volume transport properties).

(2) Surface – Effects :

> Physical and chemical properties depending on the atomic interactions changed at the surface
(atomic arrangements, atomic distances near the surface, 3-dim. surface layers).

> Physical and chemical properties depending on special surface structures.

(3) Interface – Effects :

> Special influences of adsorbed / chemisorbed foreign atoms, and surface shells of foreign materials, 3-dim. interface layers)

(4) Combined Size – and Surface/Interface – Effects:

> Limitations of "characteristic lengths" by electronic surface interactions (collisions)
(General 1/R – effects, mean free path effects etc.).

Example : spherical nanoparticle
surface : $S = 4 \pi R^2$ volume : $V = 4/3 \pi R^3$ —> $S / V \sim 1/ R$

DIELECTRIC FUNCTION OF A METAL OR SEMICONDUCTOR.

[Dielectric displacement $\vec{D}$]= $\varepsilon\cdot\left[\text{Field } \vec{E}\right]$

A basic expression was given by Bassani and Parravicini

$$\hat{\varepsilon}(\omega) = \varepsilon_1(\omega) + i\cdot\varepsilon_2(\omega) = 1 - \underbrace{\frac{\left(ne^2 / \varepsilon_0 m_{eff}\right)}{\omega^2 + i\gamma\,\omega}}_{\text{conduction electrons}} + \underbrace{\chi^{inter}}_{\text{interband transitions}}$$

with

$$\chi^{inter} = \frac{8\hbar^3\pi e^2}{m_{eff}^2}\sum_{f,i}\int_{B.Z}\frac{2d\vec{K}}{(2\pi)^3}\left|e\cdot M_{if}\left(\vec{k}\right)\right|^2 \left\{\frac{1}{\left[E_f\left(\vec{k}\right)-E_i\left(\vec{k}\right)\right]\left[\left(E_f\left(\vec{k}\right)-E_i\left(\vec{k}\right)\right)^2-\hbar^2\omega^2\right]}+i\frac{\pi}{\hbar^2\omega^2}\delta\left[E_f\left(\vec{k}\right)-E_i\left(\vec{k}\right)-\hbar\omega\right]\right\}$$

n = electron density

m_{eff} = effective mass

γ = relaxation frequency

M_{if} = transition matrix elements

E_i, E_f = initial and final energy band state

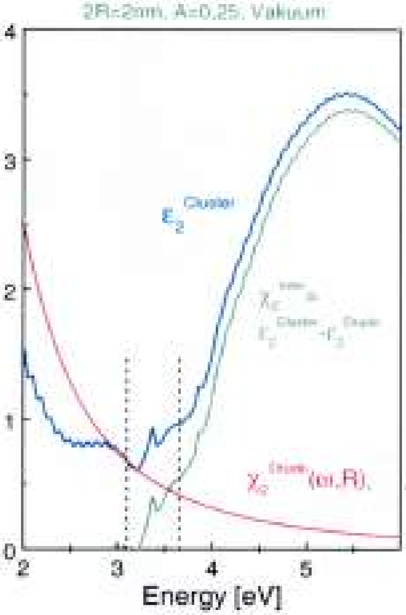

Abbildung 3.14: Imaginärteil von ε der Cluster im freien Strahl mit $\overline{2R}$=2nm (aus KKR) zusammen mit χ_2^{Inter} und $1+\chi_2^{Drude}$. Unter 3,1 eV verursacht die Dämpfung der freien Elektronen eine Verbreiterung der Mie-Resonanz. Darüber hinaus verändern die Interbandübergänge Lage und Breite der Resonanz. Die Markierungen geben die Resonanzlage des freien Strahles und die von in SiO_2 eingebetteten Cluster an.

EXPERIMENTAL EXAMPLE

OPTICAL PROPERTIES
OF
SCHMID - CLUSTERS
AND
- NANOPARTICLES

$Au_{55}(PPh_3)_{12}Cl_6$

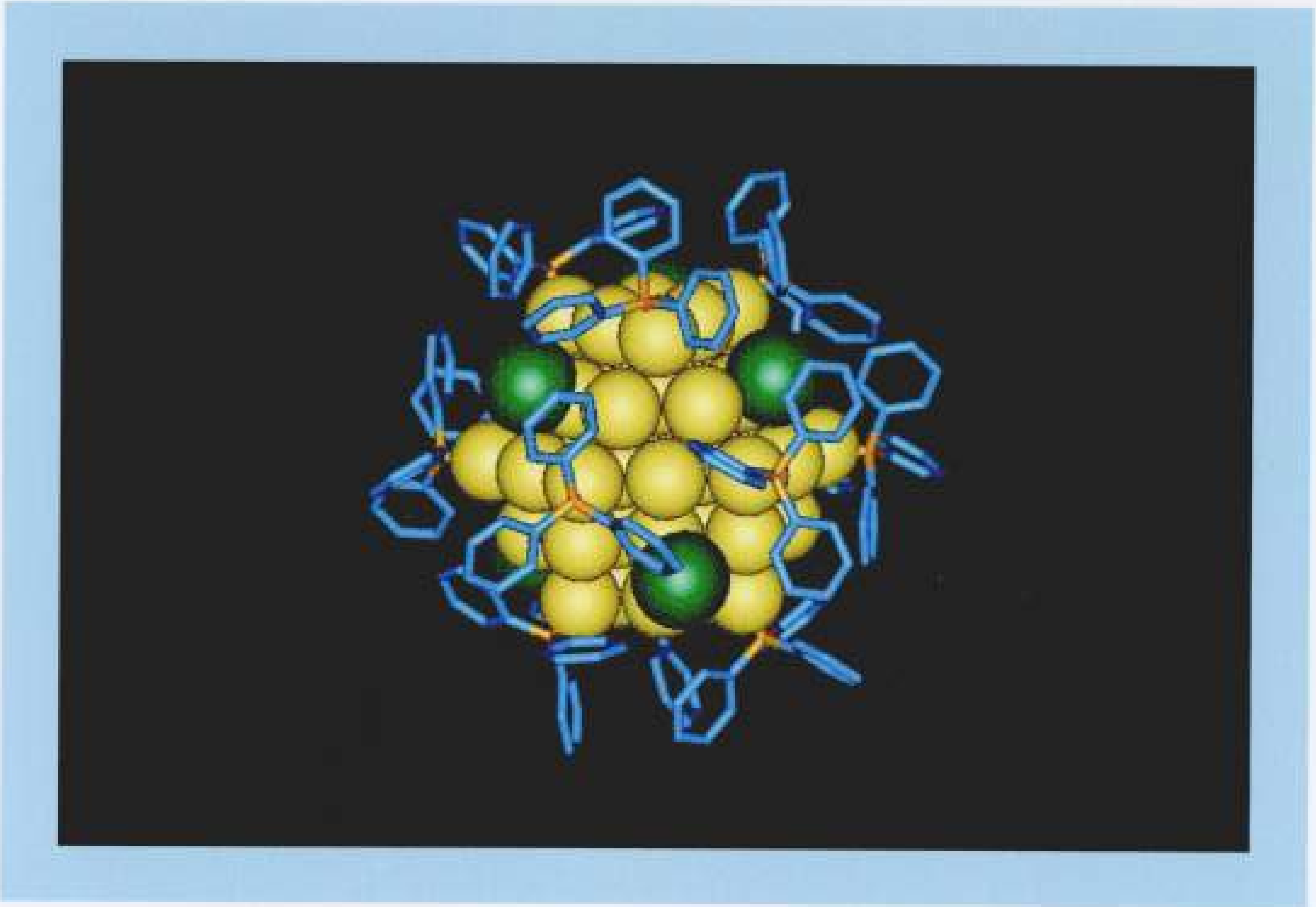

gelb: Au; grün: Cl; orange: P; blau: Phenyl

$Au_{55}(PPh_3)_{12}Cl_6$

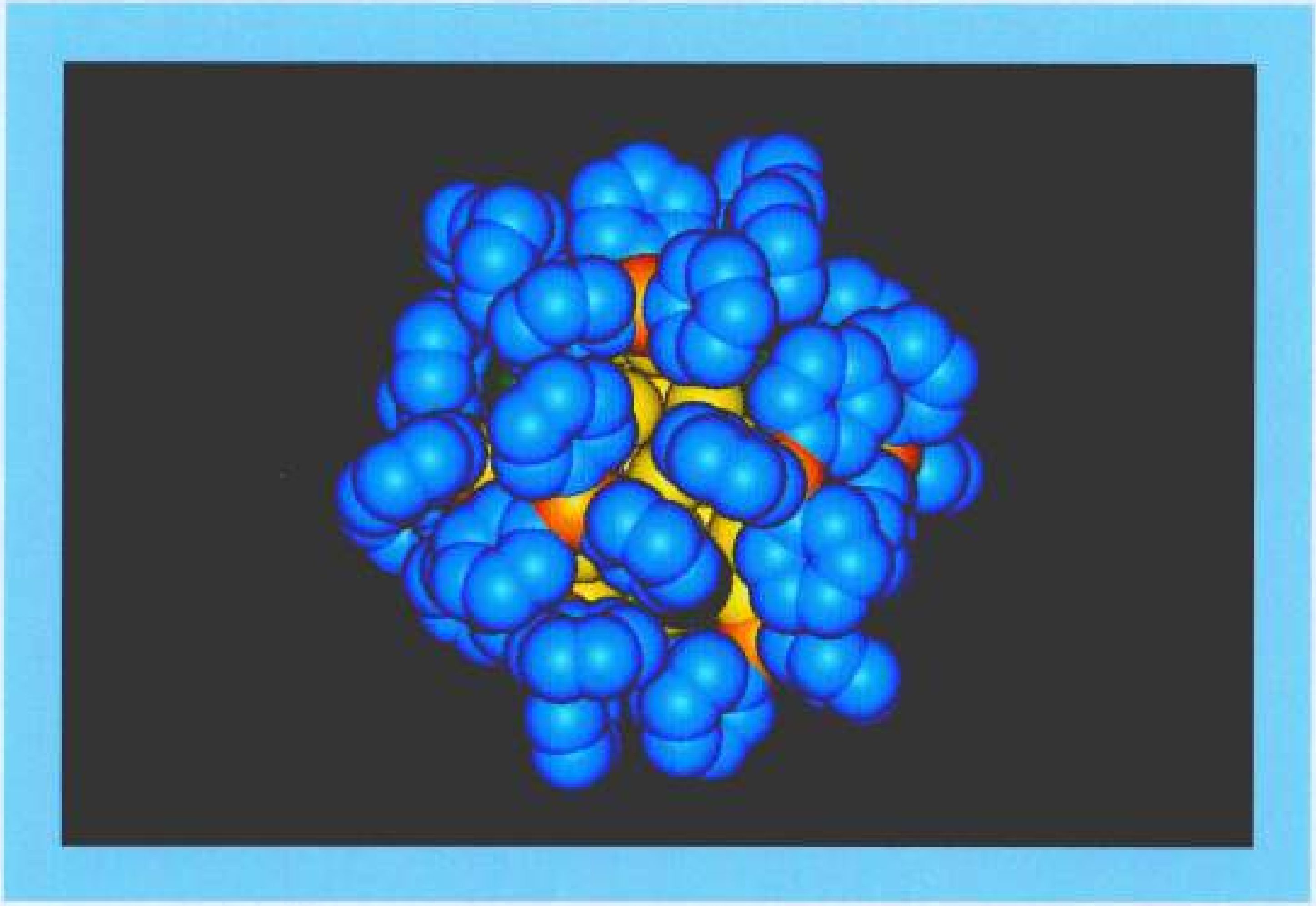

Simulation des Clustermodells: Dr. Hubert Kuhn und Maria Leis, Fachbereich Chemie, Universität Essen

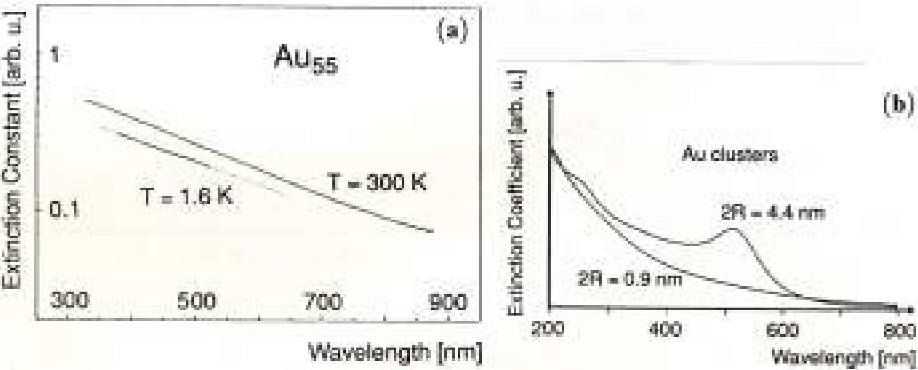

Fig. 4.58. (a) Optical extinction of ligand stabilized and matrix isolated Au_{55} clusters at different temperatures (after [4.90]). The respective dielectric functions are plotted in Fig. 4.22. (b) Extinction spectra of Au hydrosols (after [4.259a]). The lower curve corresponds to mean diameter of 0.9 nm (i.e. mean cluster size Au_{34}) the upper one to 4.4 nm (Au_{2800}).

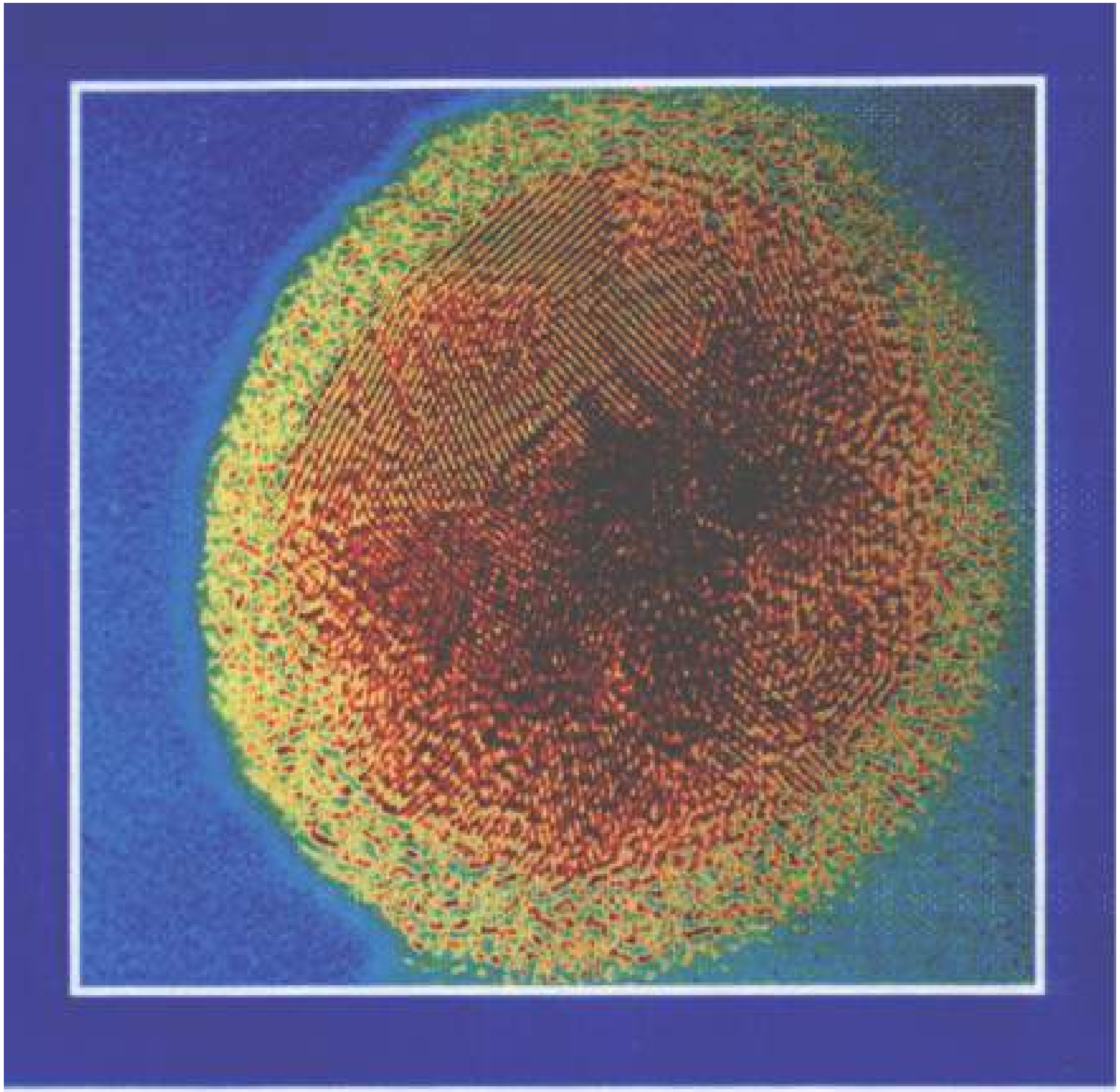

GOLD-NANOPARTICLE / TRIPHENYLPHOSPHINE SHELL
2 R = 15 nm

(Schmid(Essen) / Bovin (Lund) 1996)

GOLD - MOLEKÜL / Triphenylphosphin
(13 Atome)

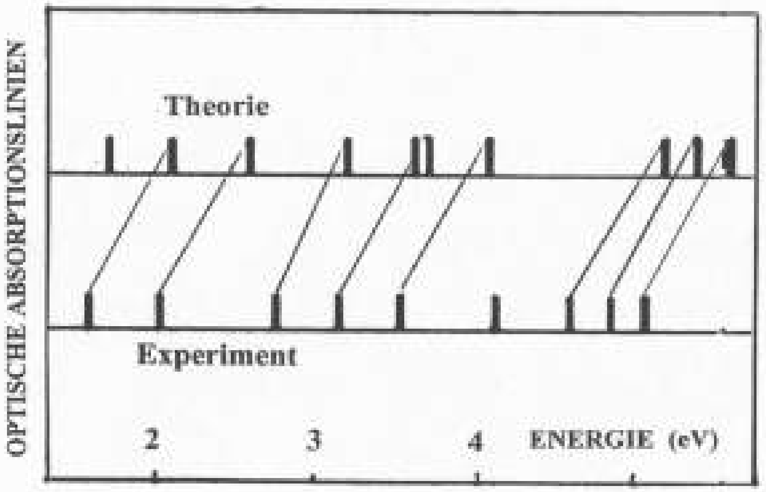

GOLD - CLUSTER / Triphenylphosphin
(55 Atome)

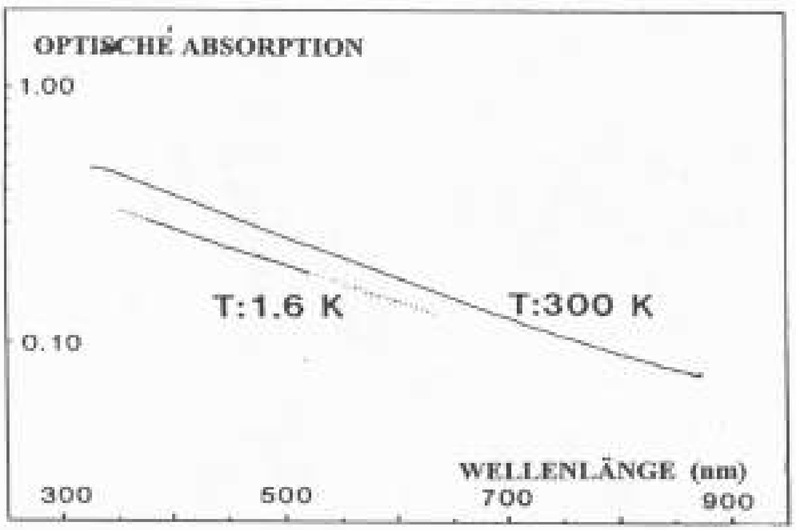

GOLD - CLUSTER / Glasmatrix
($10^3 \rightarrow 10^4$ Atome)

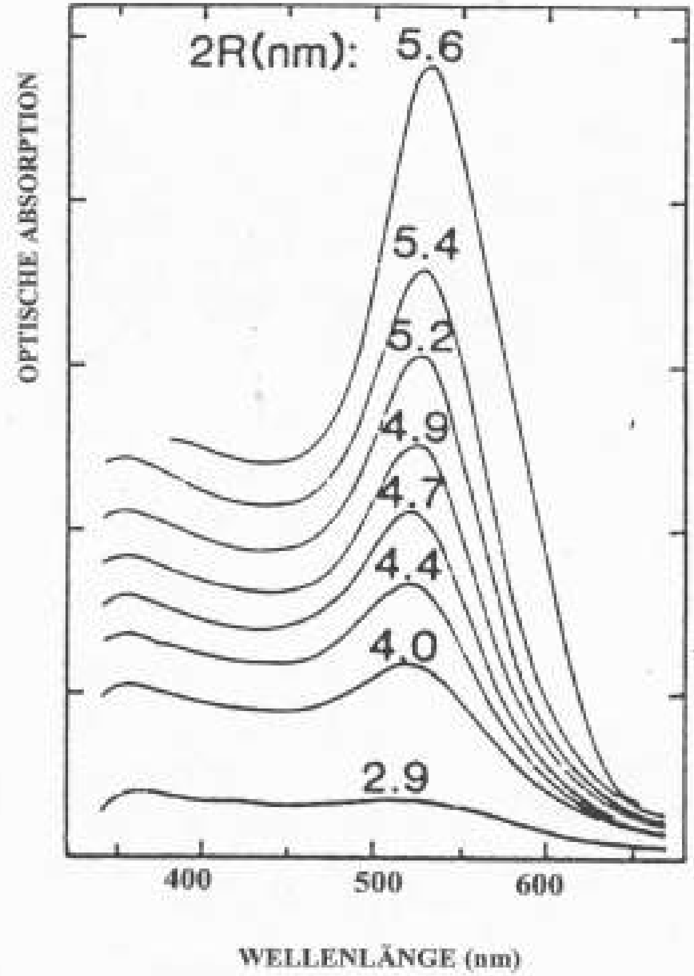

Au-particles in photosensitive glass
($\Gamma_{1/2}$: half halfwidth)

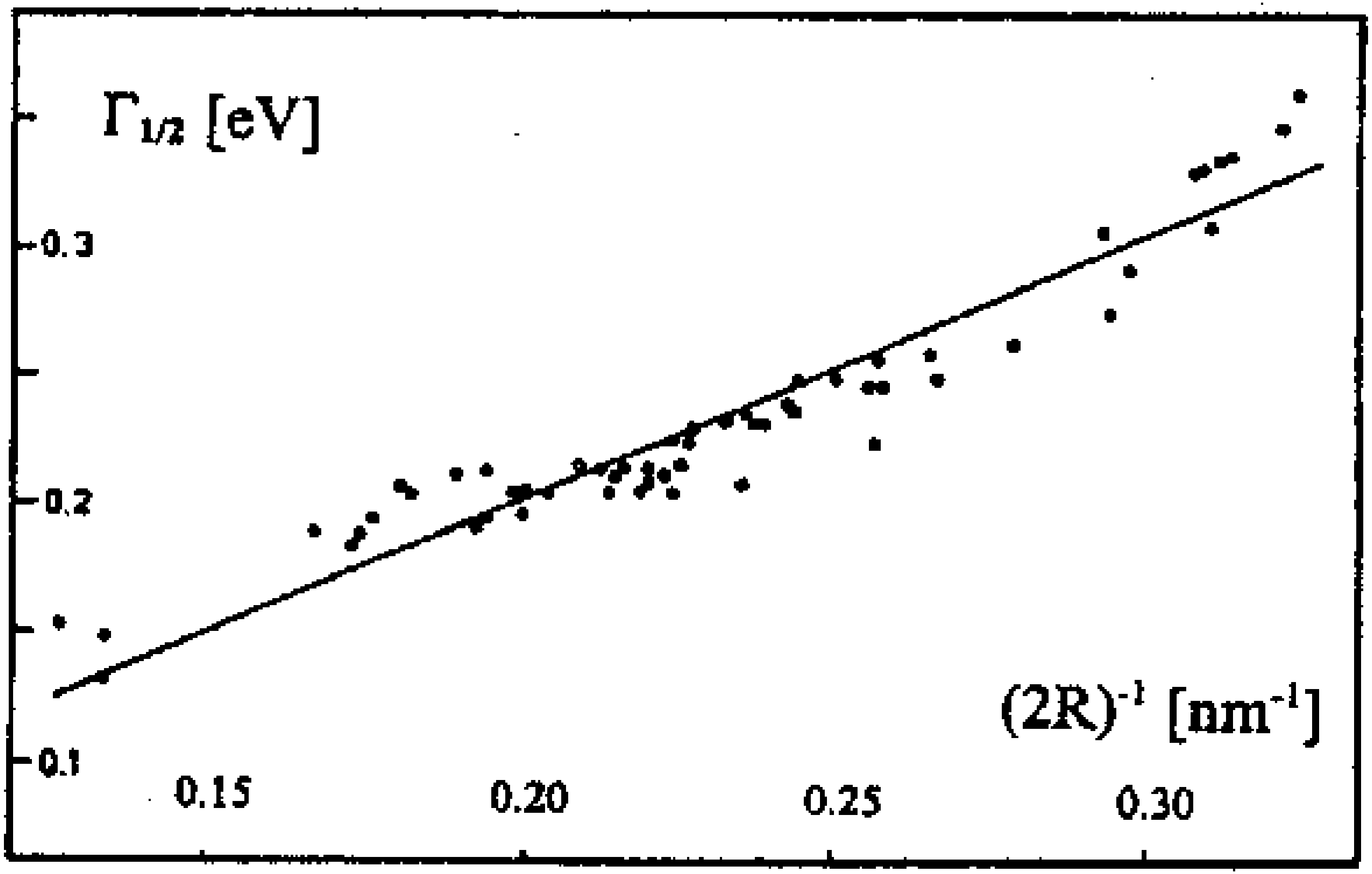

Cluster/Nanoparticle Size Effects

A wealth of cluster size corrections to the bulk-ε has been developed since half a century for metallic and semiconductor clusters.
They can be classified according to their theoretical basis:

- **Classical conductivity theory** (electronic mean free path limitation (*free path effects, FPE*); quasicontinuous electronic band structure, DRUDE electrons)

- **Quantum box models** (discrete electronic ground states in the otherwise empty box; vertical potential walls (*quantum size effects, QSE)*)

- **Linear response theories** (inclusion of ions; discrete electron energy levels (*quantum size effects)*)

- **Jellium models** (uniform positive background, free electrons, only; selfconsistent *smooth* potential; DFT; inclusion of exchange and correlation effects (*quantum size effects)*)

Both, the case of quasicontinuous bandstructure and of discrete*, quantized* electronic level structure can occur. This depends on the relation between the level spacings ΔE and energetic level widths δE including life-time effects : $\delta E > \Delta E$ means that the size quantization structure is smeared out and electrons may be continuously accelerated as presumed for classical conductivity, while for $\delta E < \Delta E$ separated levels exist.
While level spacings were introduced on various routes (roughly estimated, we have

$$\Delta E \approx E_{Fermi}/N \quad \text{(Assumption: no symmetry degenerations)}$$

N = number of involved electrons in the cluster), the level widths are still controversely discussed. In the case of metallic clusters, only few experimental hints have been published which point to a discrete level structure in clusters consisting of more than, say some ten atoms. The recent investigation of Sinzig et al. on ligand stabilized monosize Pd clusters gives first clear indications. Since magnetic and thermal properties were examined, only levels very close to E_{fermi} were involved with, probably, longer life-times, in contrast to the *hot metal electrons* usually excited by optical means which, up to now did not point clearly to level discretization in any experiment.

An interesting feature of the many cluster size effect theories is the high degree of formal (not quantitative !) correspondence concerning the resulting correction terms for the dielectric function.
While only few theories deal with the real part of the dielectric function, and mostly only small corrections of the bulk-ε were predicted, drastic changes of its imaginary part were found which, despite the different bases of the models, conformably are described by the famous general *1/R-law,* (which also appears as a surface/interface effect):

$$\varepsilon_2 (\omega, R) \approx \varepsilon_2^{bulk}(\omega) + \Delta\varepsilon_2 (\omega, R) \quad \text{with} \quad \Delta\varepsilon_2 (\omega, R) \propto \mathbf{A}_{size} / R$$

We have introduced here the **A**-*parameter* which, as we will show below, plays a key role for determining the quantitative amounts of size dependences and was extended to *interface* effects.

In the frame of the quantum size effects, the **A**/R - term is derived from the size dependence of the level spacing, while in the free path effect, this term is attributed to a reduction of the conduction electron mean free path due to collisions at the cluster surface.
These collisions contribute with an additional relaxation frequency :

$$1 / \tau = 1/\tau_{bulk} + 1/\tau_{surface} \quad \text{with} \quad 1/\tau_{surface} = \mathbf{A}_{size}\, v_{Fermi} / R ,$$

v_{Fermi} being the Fermi velocity of those electrons which are most effective for electron relaxation processes.

For this latter case the following explicit expression of the dielectric function was obtained, which holds , among other cluster materials, for silver clusters around the visible spectral region:

$$\varepsilon (\omega, R) \approx 1 + \chi_{interband} - \omega_p^2 / \omega^2 + i\ \omega_p^2 / \omega^3 \ (1/\tau_{bulk} + \mathbf{A}_{size}\, v_{Fermi} / R)$$

In this approximation, a small size dependence of the real part of ε was neglected and the main size dependence remains with the imaginary Drude part.

In fact, not only the optical response of the Drude electrons is influenced by the confinement, but also are the interband contributions. As has been shown however, these size dependences only become relevant at essentially smaller sizes, due to the closer localization of electron hole pair excitations. They will be discussed later.

EXPERIMENTAL EXAMPLE

SIZE - EFFECTS
AND THE
DIELECTRIC FUNCTION
OF
SILVER NANOS
IN
PHOTOSENSITIVE GLASS

PHOTOSENSITIVE GLASSES :

M A T E R I A L :

Metal Ion doped crown glass:
Metals (Ag, Au, Cu),
Photoreducing Ions (Ce),
Thermoreducing agents (Sb)

⇓

NUCLEATION :

UV-irradiation through a mask: ($Me^{+} \rightarrow Me^{0}$)
„latent image“
Homogeneous nucleation (Me^{0}) by annealing
„pre-development“

⇓

GROWTH :

Heterogeneous growth (Me^{+}) by annealing
„development“

⇓

TERMINATION OF GROWTH

Fixation by cooling down
Remaining Me* ions immobile by glass viscosity

⇓

I M A G E

Color: by particle size
Particle size : by local irradiation intensity

Noble Metal Particles in Photosensitive Glass

Among the nanoparticle preparation methods, Photosensitive Glass stands out for several reasons:

1) Particle nucleation and growth processes are separatedly to be varied, so from a given number of nuclei particles grow at a constant number. Thus the size distribution is extremely narrow, comparable with a mass filter of moderate quality.

2) Growth takes place at high temperatures (400 - 500^0 C) by Ag-ion diffusion
in the glass of high viscosity. So, growth is very slow and each adsorbed ion has time to find energetically optimal positions at the particle surface. So, the imperfection density of the metal lattice is extremely small.

3) The particles are embedded in a homogeneous glassy matrix, so the growth process is isotropic and the particles form energy minimal, i.e. almost spherical surfaces.

4) The growth process can be interrupted at any time, by taking the sample out of the furnace, so series of spectra can be recorded from ONE sample with aimedly varied sizes.

5) The particles are well protected by the glass matrix. So, the samples can easily be handled at air, e.g. by immersing directly into liquid Helium

6) Photosensitive glass can be doped alternatively with different noble metal ions and their mixtures, giving rise to alloy particles. It is not expected that constituent ions from the glass matrix are enclosed in the particle to essential amounts.

SILVER PARTICLES IN PHOTOSENSITIVE GLASS
(2R = 12 ± 0.2 nm)

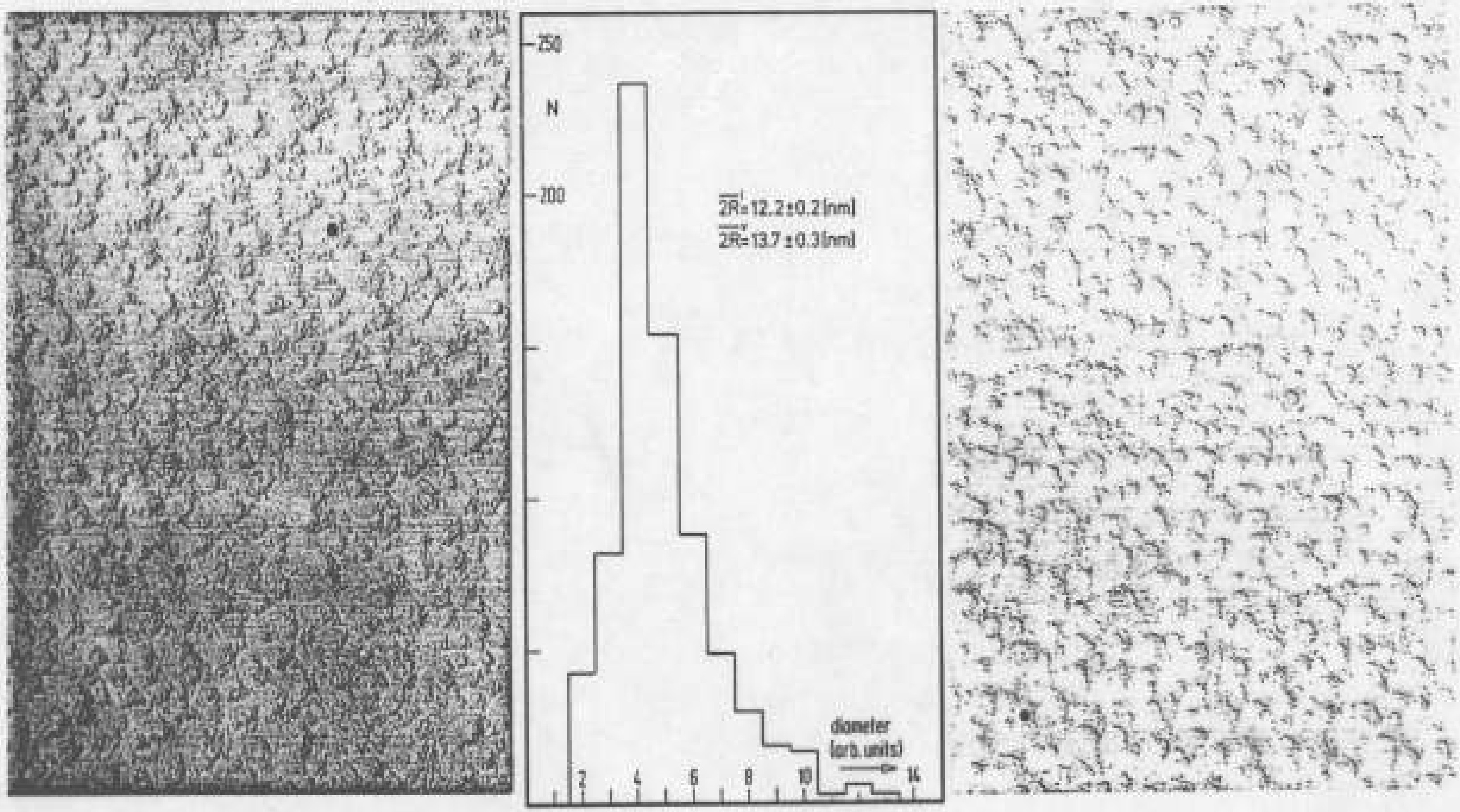

TEM-Preparation: C-adhesive double film replica extraction technique / fresh surface of fracture

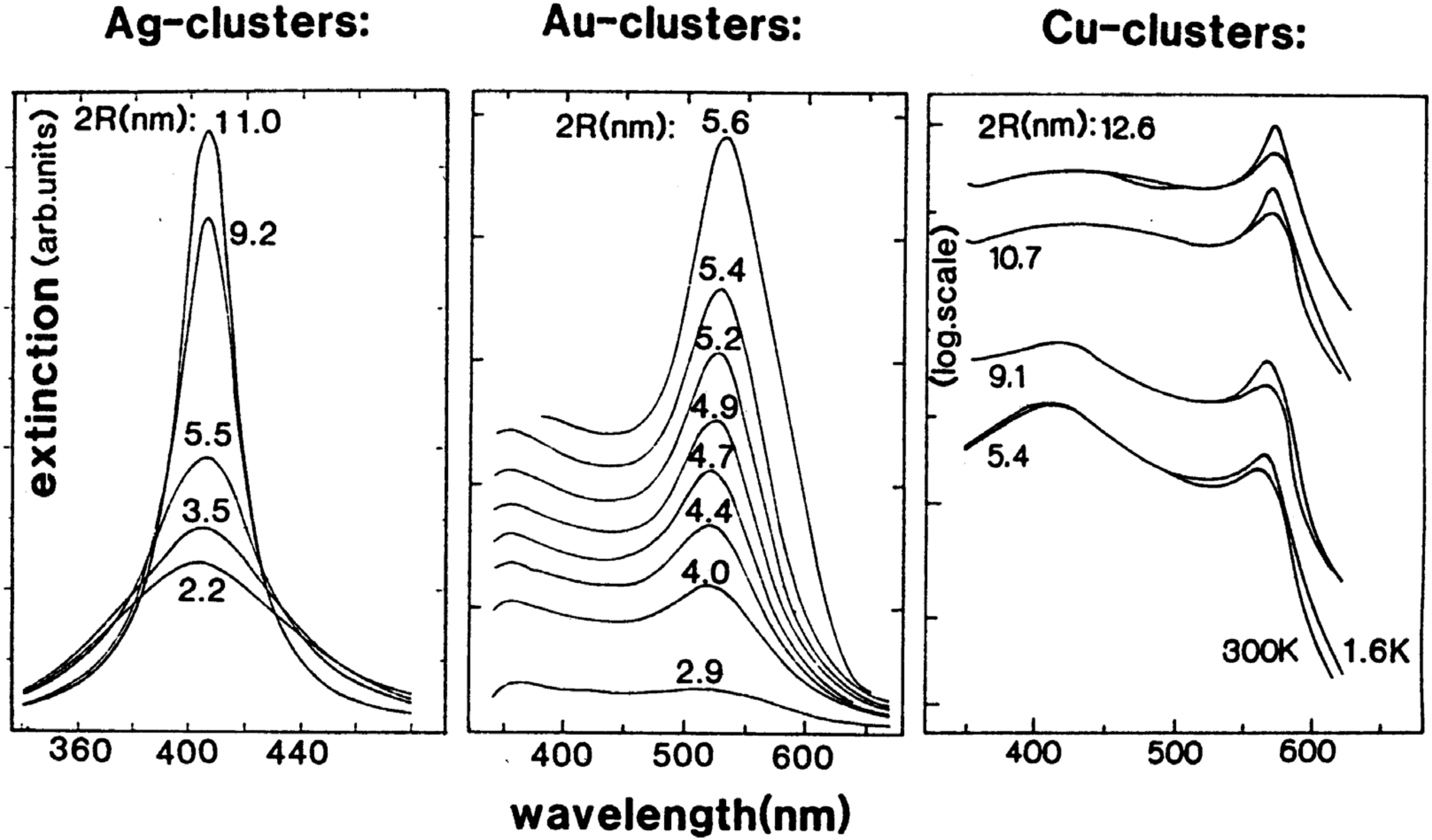

Fig. 4.12. Measured extinction spectra of Ag, Cu and Au clusters of various sizes in a glass matrix (after [4.66, 115, 131]). The spectra of Cu and Au are clearly resolved due to the high value of ε_m which shifts the resonances away from the interband transition threshold.

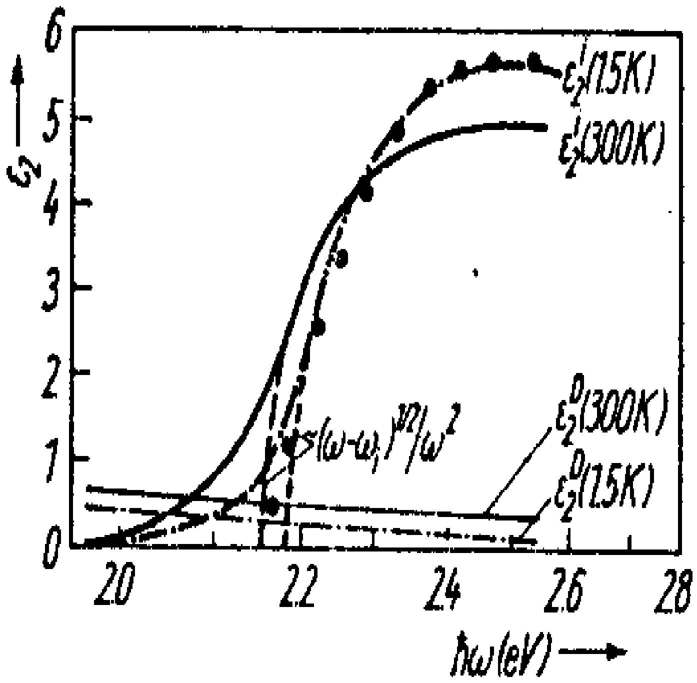

Fig. 7

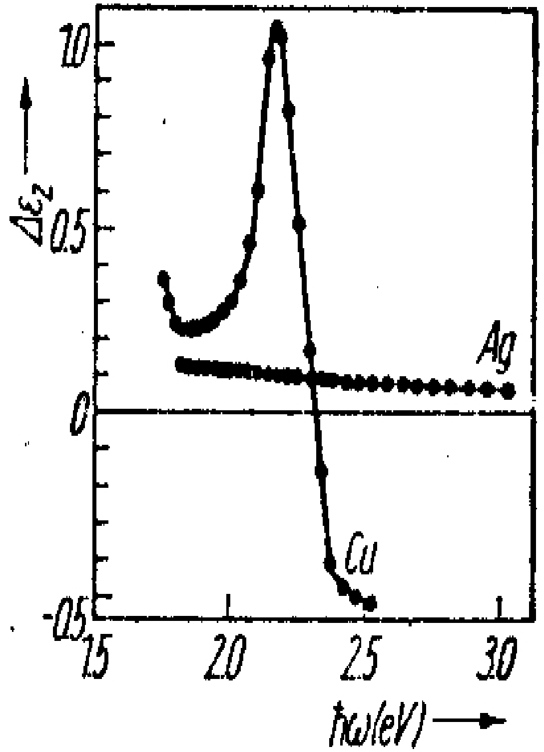

Fig. 8

Fig. 7. ε_2 spectra of Cu at 300 and 1.5 K, decomposed into contributions by conduction electrons, $\varepsilon_2^{\mathrm{D}}$, and interband transitions, $\varepsilon_2^{\mathrm{i}}$. The dashed extrapolation curves were used to determine the threshold energies. Points: calculated by Williams et al. [23] for $T = 0$ K

Fig. 8. Variation of $\varepsilon_2(\hbar\omega)$ with temperature, $\Delta\varepsilon_2 = \varepsilon_2$ (300 K) $-$ ε_2 (1.5 K) for Cu and Ag

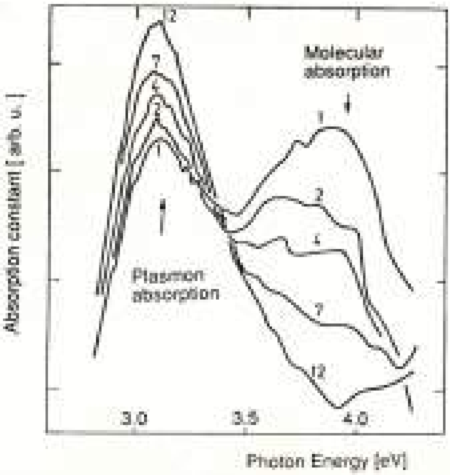

Fig. 4.64. Experimental absorption spectra of silver clusters in photosensitive glass (after [4.266]). Mean cluster sizes increase from $\overline{N} \lesssim 30$ (1) to $\overline{N} \approx 400$ (12). Molecular absorption features of smaller clusters within the size distribution disappear while the plasmon peak of larger clusters builds up.

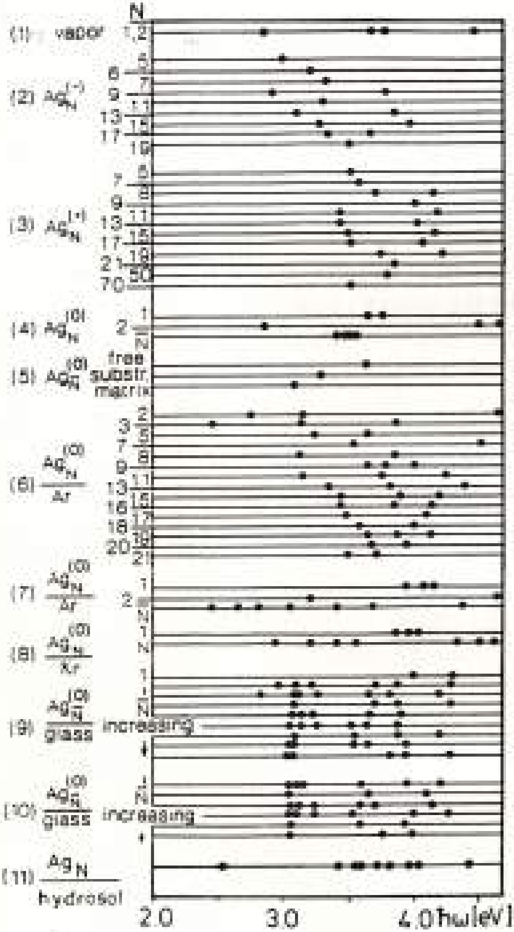

Fig. 4.65. Compilation of peak positions, irrespective of their height, observed for very small and small Ag clusters. N denotes the size, $\overline{N}$ the average size of the clusters. (1) optical absorption of vapor containing atoms and dimers. (2) photofragmentation of mass selected Ag_N^- cluster beam [4.221, 222]. (3) photofragmentation of mass selected Ag_N^+ cluster beam [4.40, 219, 221]. (4) optical absorption of Ag cluster smoke [4.26, 27]. (5) optical absorption of Ag clusters ($\overline{N} \approx 250$) in a beam, deposited on SiO_2 substrates or embedded in SiO_2 matrices [4.30]. (6) optical absorption of neutral mass selected Ag_N clusters in solid Ar [4.287–289]. (7) optical absorption of distribution of neutral Ag_N clusters in solid Ar [4.113]. (8) optical absorption of distribution of neutral Ag_N clusters in solid Kr [4.268]. (9) and (10) optical absorption of two samples with distributions of neutral Ag_N clusters in photosensitive glass, recorded during their growth between $N = 1$ and $N \leq 250$ (see text) [4.115, 266]. (11) Oligomeric Ag clusters in hydrosol [4.87, 336, 337].

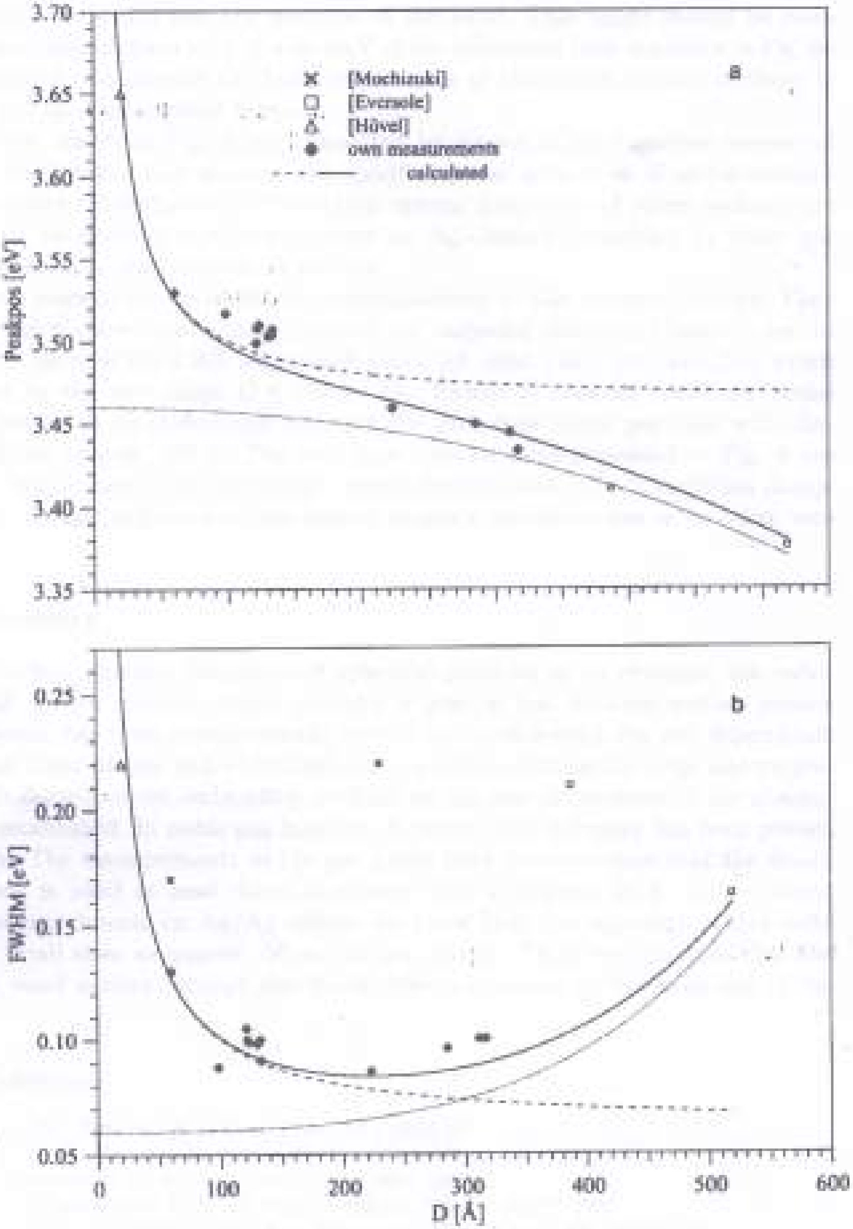

Fig. 6. Surface plasmon resonance of free Ag-clusters. a: peak position, b: full width at half maximum. The symbols represent experimental results. The lines are calculated. dotted: with retardation, no surface contribution, dashed: no retardation, with surface contribution, solid: retardation and surface contribution

Evaluation of the Absorption Spectra by Kramers Kronig Analysis to obtain the realistic, Size dependent Dielectric Function of the Particle Material

The absorption spectra of Silver nanos were recorded in limited spectral regions around the Mie resonance.
Measurements were also performed at 1.6 K by immersing the samples in suprafluid Helium (below the Lambda-point).

The Kramers Kronig Analysis (KKR) requires the absorption spectrum from $\omega = 0$ to $\omega = \infty$. So, far away from the pole of the Kramers-Kronig Function the spectra had to be replaced by estimated values.
1) Toward low frequencies the absorption decreases toward zero following the DRUDE DF.
2) Toward high frequencies the absorption has been measured up to several hundred eV quantum energy, For the range above, a constant additive contribution was obtained by a self consistent calculation of the spectra.
So, the L-spectra of Gans-Happel theory were evaluated, and from K(ω) and L(ω) the data of $\boldsymbol{\varepsilon} = \varepsilon_1(\omega,R) + i\,\varepsilon_2(\omega,R)$ were obtained for all members of a particle size series.

The results are shown in the Figure.
Obviously, the Real Part, i.e. the polarizability only changes weakly, while the Imaginary Part, i.e. the relaxation, varies for a factor of 10 between $2R^{average} = 2.5$ and 21 nm.

There are several models for interpretation:
(1) The mean free path effect is based upon classical single electron dynamics. Conduction electrons in the band structure can absorb only if their energies are close to E_{Fermi} . Their trajectories through the particles are assumed to be straight forward, interrupted by momentaneous scattering processes as known from classical conductivity theory. Depending on different assumptions for the surface scattering,

the resulting mean free path $l^{surface}$ is of the order of particle radius R. In nanoparticles which are smaller than the mean free electron path of the bulk metal l^{bulk}, the additional SURFACE scattering process is important: Its time of free flight $\tau^{surface}$ is included into the total relaxation time τ^{total} according to Matthiessen's rule :

$(\tau^{total})^{-1} = \sum (\tau^{i})^{-1}$, where i stands for the contributions of
point defect-,
dislocation-,
grain boundary-,
phonon- and
electron-electron scattering.
In nanoparticles the surface scattering contribution $(\tau^{surface})^{-1}$ is added. The according contribution to the relaxation frequency Γ which is contained in the DRUDE - DF amounts to

$$\Gamma^{surface} = A^{size}\, v^{Fermi} / R,$$

where the A^{Size}-parameter encloses the details of the scattering process.

(2) The Quantum Size Effect: The simple quantum box model yields discrete electron eigenfunctions and. accordingly, discrete electron energy levels with , in rough approximation, an average level spacing of the order of $\Delta E \approx E^{Band} / N^{2/3}$ where E^{Band} is the width of the conduction band and N the number of atoms in the box (i.e. the particle). In the following we assume the level width to be smaller than ΔE.
Now the "conduction electrons" can no longer be treated as classical electrons, instead they perform level transitions under the influence of an incident electromagnetic field.
Kawabata and Kubo stated that the particle surface does not act as a scatterer but determines the level spacing.
The transitions give rise to "Landau damping" which, surprisingly, results in a relaxation time of roughly the same formal structure as in the case of the FPE.

$$\Gamma^{QSE} = A^{size*}\, v^{Fermi} / R,$$

So, the 1/R - law appears to be almost universal.

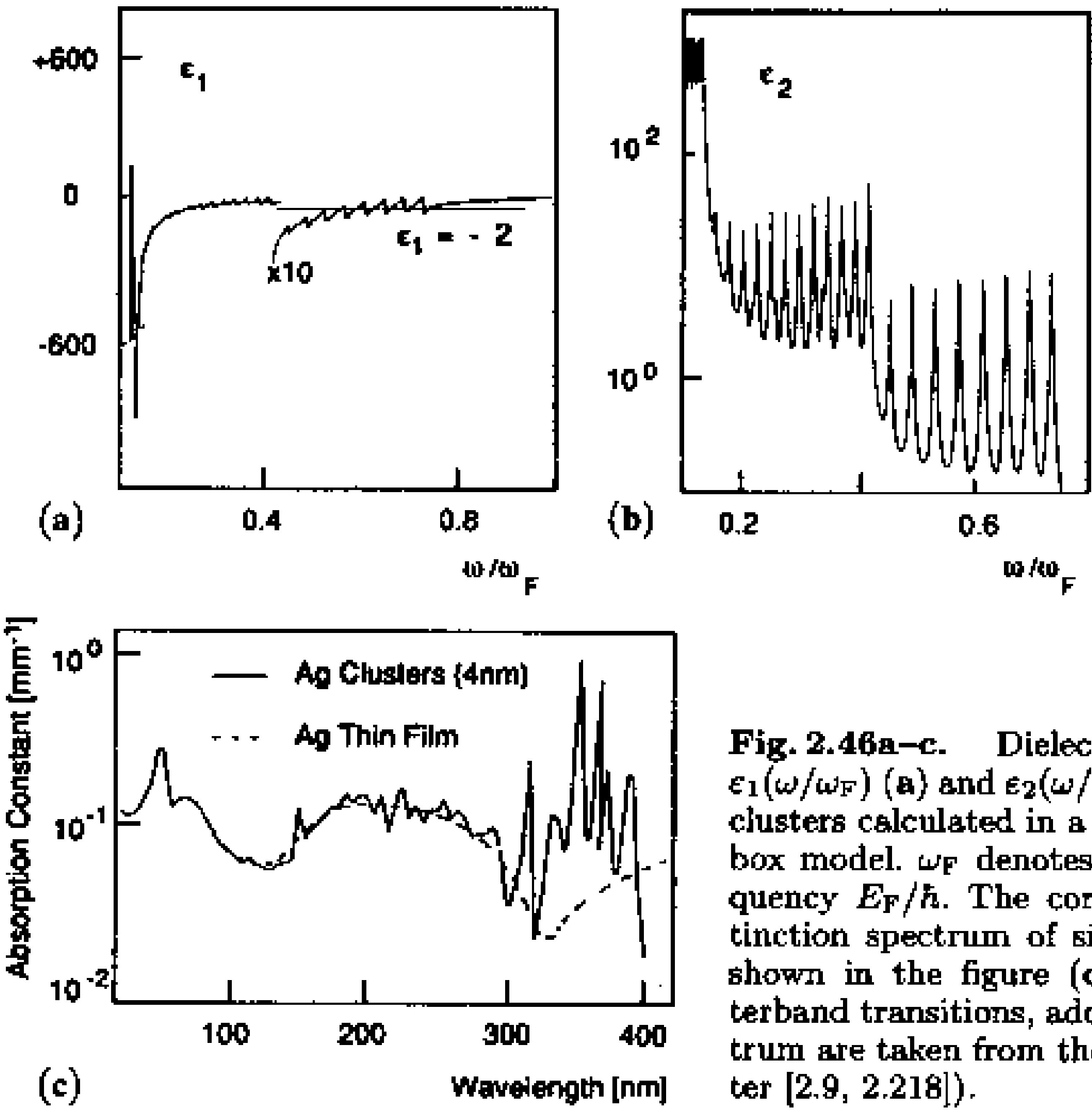

Fig. 2.46a–c. Dielectric functions $\varepsilon_1(\omega/\omega_F)$ (**a**) and $\varepsilon_2(\omega/\omega_F)$ (**b**) of 4 nm clusters calculated in a cubic potential box model. ω_F denotes the Fermi frequency $E_F/\hbar$. The corresponding extinction spectrum of silver clusters is shown in the figure (**c**). The Ag interband transitions, added in the spectrum are taken from the literature (after [2.9, 2.218]).

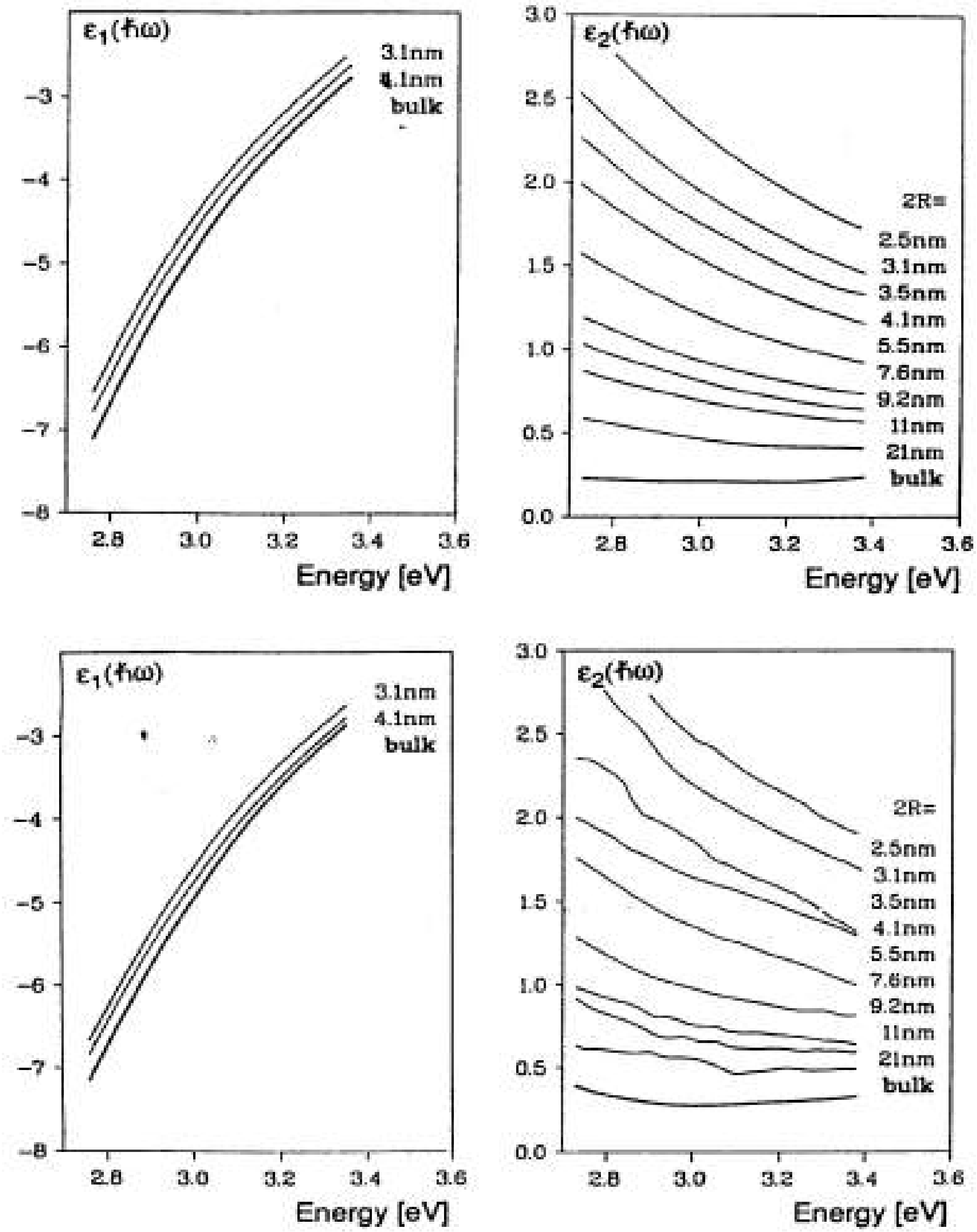

Fig. 4.21. Experimental size dependence of dielectric functions $\varepsilon_1(\hbar\omega)$ and $\varepsilon_2(\hbar\omega)$ for Ag clusters obtained by Kramers-Kronig analysis (Fig. 2.3) of absorption spectra like in Fig. 4.11 (bottom) (after [4.66]). These results compare well to the theoretical functions (top, from Fig. 2.41). The "bulk" curves were obtained by subtracting the calculated free path contributions of (2.53) (i.e. by extrapolating to $R \to \infty$).

UNIVERSITÄT DES SAARLANDES

Photosensitive glass : Silver-cluster-picture
Cluster sizes : 2nm (pale) to 10 nm (yellow)

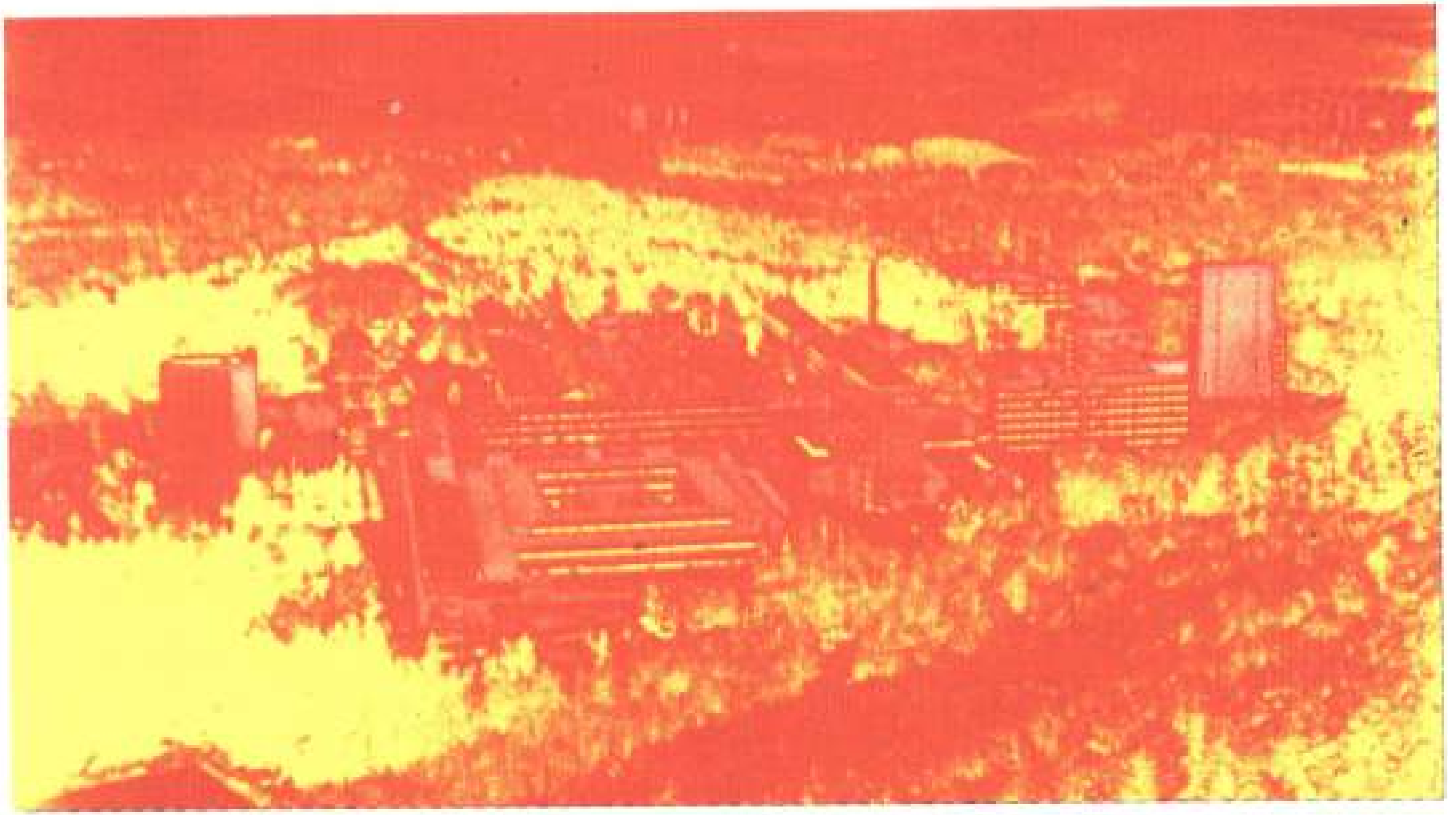

Only the A-parameters differ. For free particles without embedding medium we have $A \approx 1$ (MFP-effect), $A = 0.25$ (Persson), $A \approx 0.5$ Kawabata, Kubo) etc. (For a detailed description see given Literature).

In the Figures the DF of the Ag particle is plotted as following by introducing this contribution into the dielectric function of bulk silver. There is almost quantitative correspondence with the experimental data, if we choose $A = 1$.
Also, the formal extrapolation to infinitely large particles (i.e. bulk) fully agrees with the bulk data for silver from Literature.

We will later see, that in the case of an embedding medium, the A-parameter changes drastically. For glass as medium then the QSE-theory of Persson yields $A = 1$.
Notwithstanding our experiments give $A = 1$, this is no confirmation of the MFP but points to the validity of the QSE of Persson.

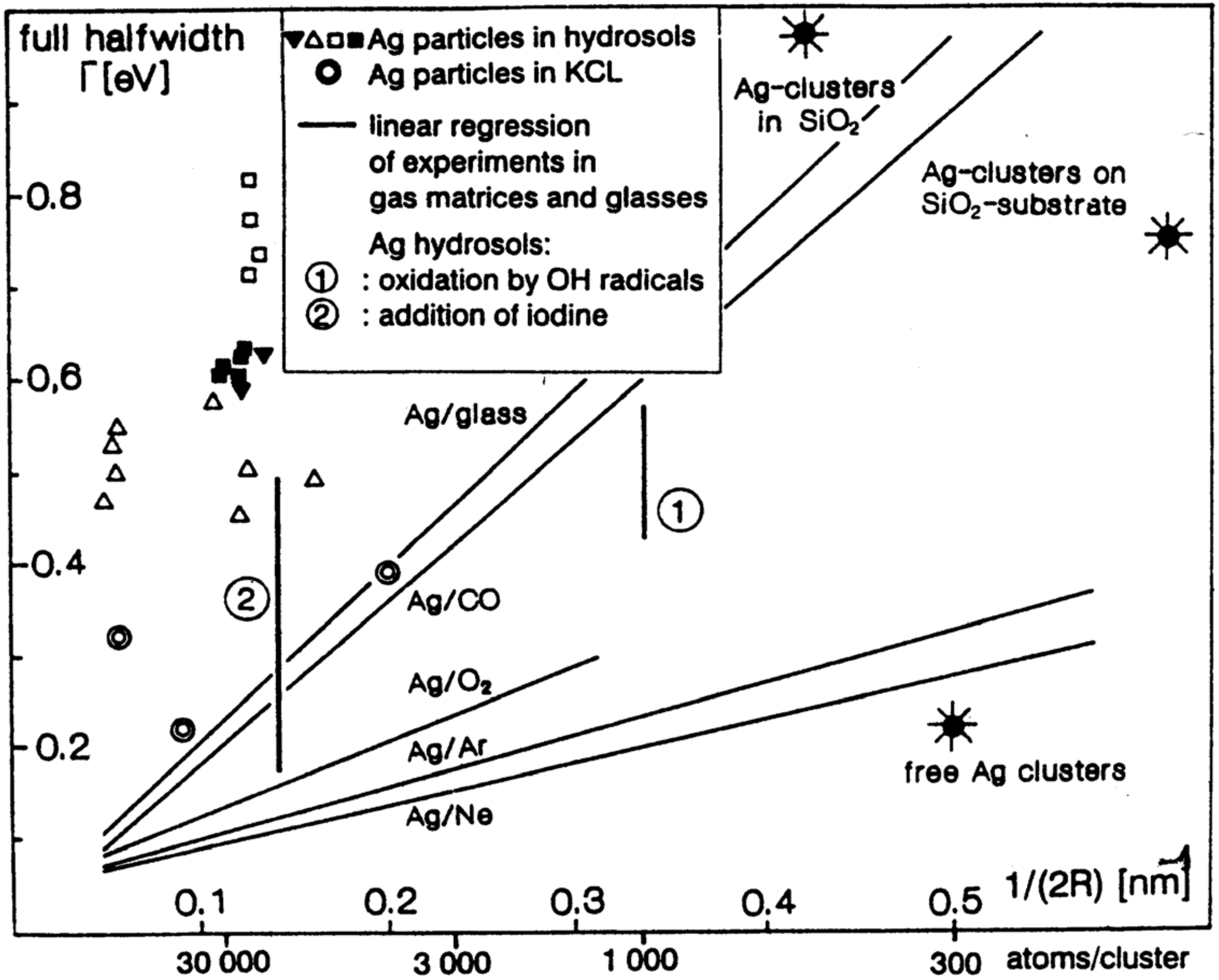

(b)

Fig. 4.14. Influence of surrounding media on peak position (**a**) [4.10] and width (**b**) [4.30] of surface plasmon resonances of Ag clusters of various sizes. For hydrosols and alkali halide matrices, the $1/R$ law obviously does not hold.

EXPERIMENTAL EXAMPLE

SIZE - EFFECTS
IN THE
INTERBAND - TRANSITION EDGE
OF
NOBLE METAL NANOS

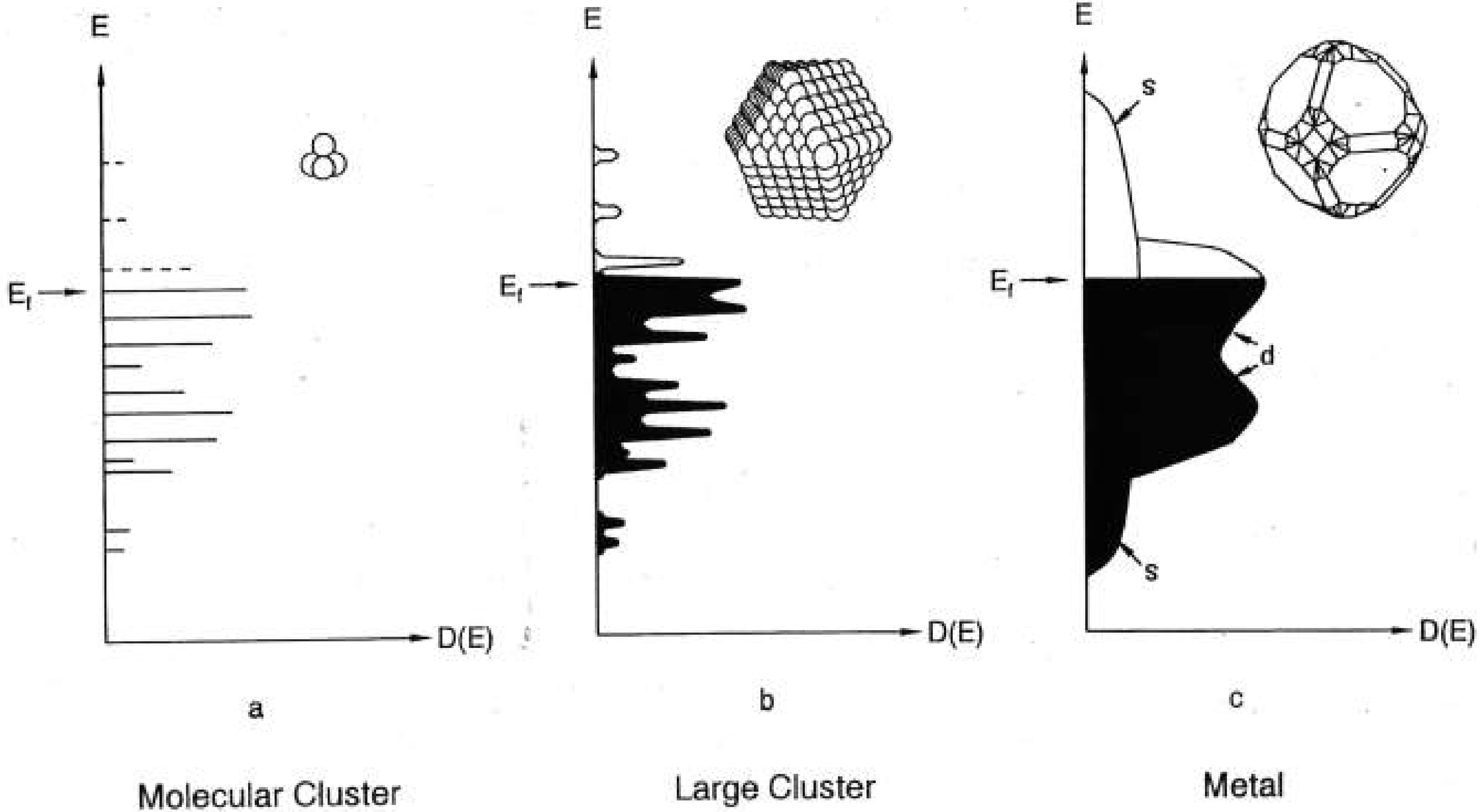

(G.Schmid - Uni Essen - 1999)

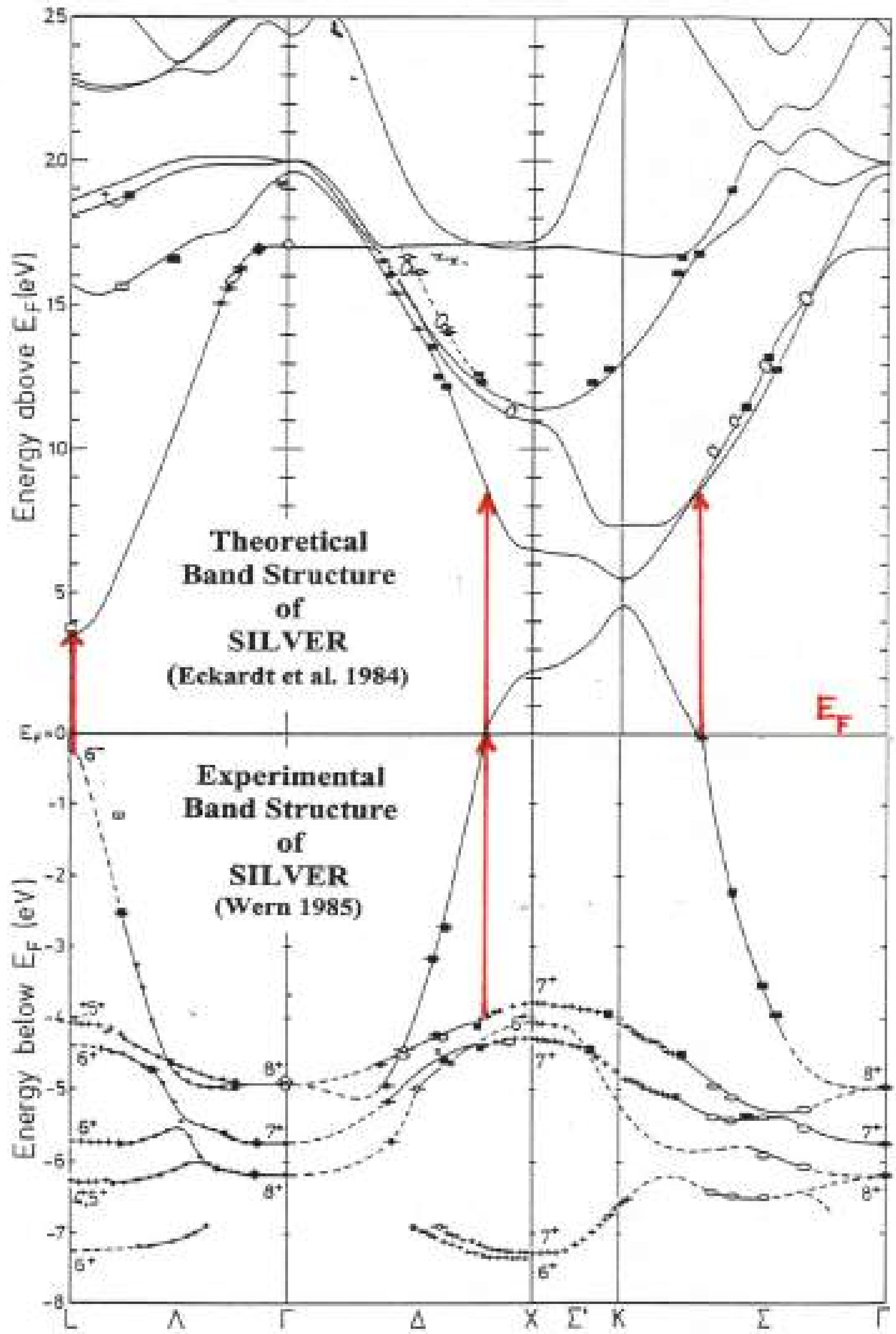

Theoretical
Band Structure
of
SILVER
(Eckardt et al. 1984)
Experimental
Band Structure
of
SILVER
(Wern 1985)
Energy above E_F (eV)
Energy below E_F (eV)
E_F
L
Λ
Γ
Δ
X
Σ'
K
Σ
Γ

Christensen, Seraphin

Au

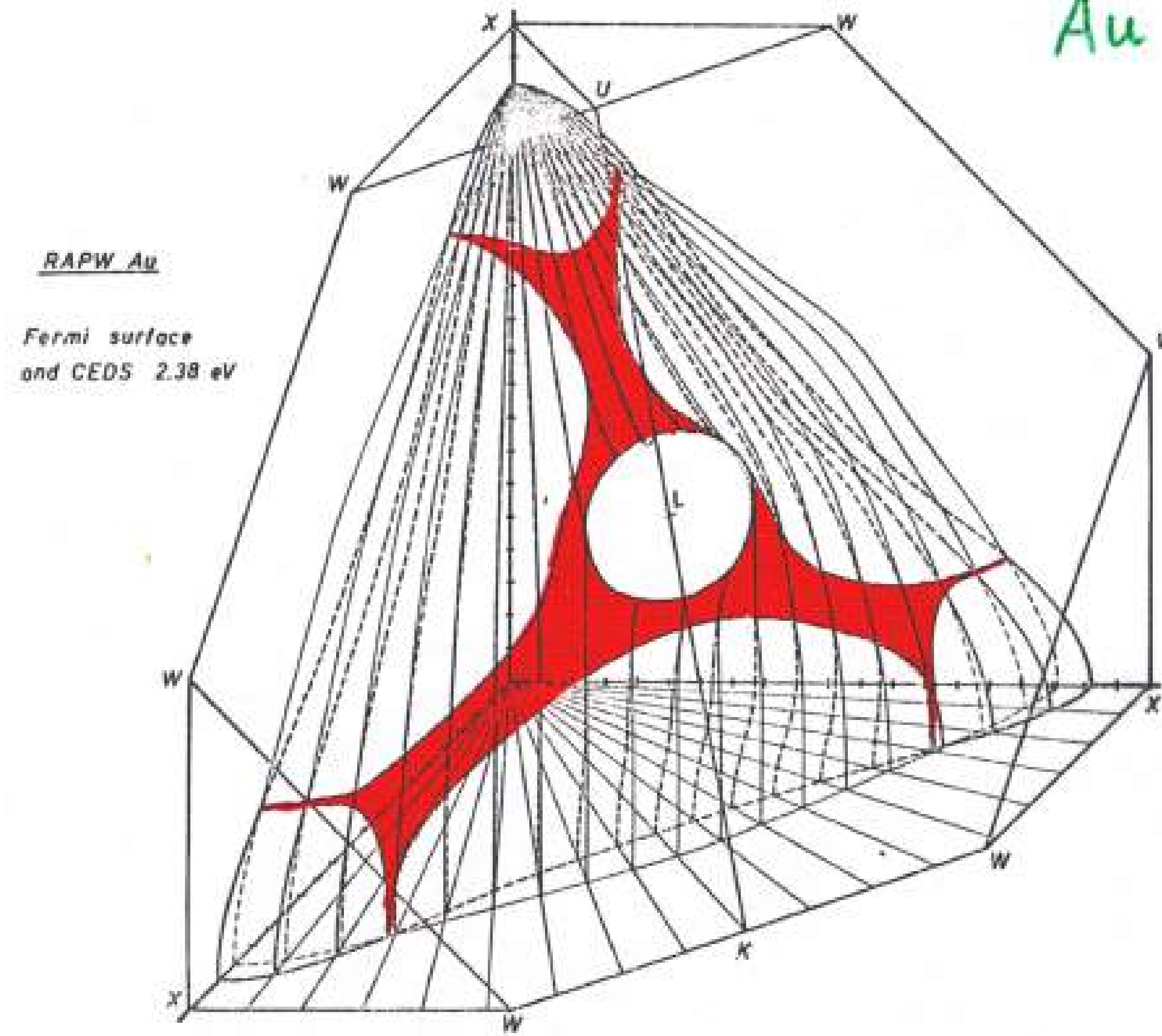

FIG. 23. Axiometric plot of sections of the Fermi surface (fine lines) and the CEDS corresponding to $E_F - E_i = \hbar\omega_t = 2.38$ eV (heavy lines) for constant azimuthal angles. In the hatched area, the two surfaces coincide. $\vec{k}$ vectors in this region correspond to the states giving the steep increase of the absorption at the interband edge $\hbar\omega_t = 2.38$ eV.

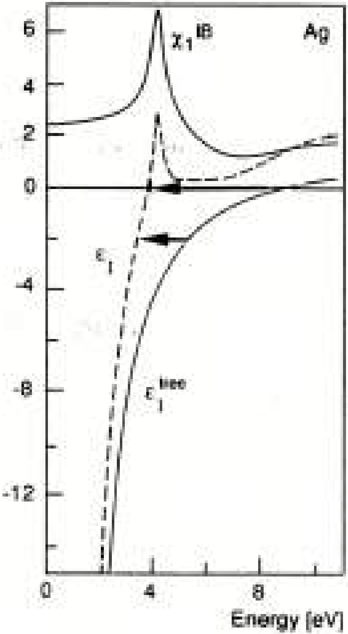

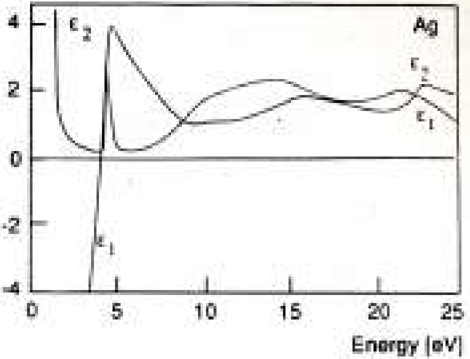

Fig. 2.1. Right: Dielectric functions $\varepsilon_1(\hbar\omega)$ and $\varepsilon_2(\hbar\omega)$ for bulk solid silver (after [2.26]). Below about 4 eV $\varepsilon(\hbar\omega)$ is dominated by free electron behavior, above 4 eV by interband transitions. Left: Decomposition of measured $\varepsilon_1(\hbar\omega)$ into the free electron contribution $\varepsilon_1^{\text{free}}$ (Drude) and the interband transition contribution χ_1^{IB}. Due to χ_1^{IB}, the energy for $\varepsilon_1(\hbar\omega) = 0$ is redshifted by about 5 eV from the free electron value.

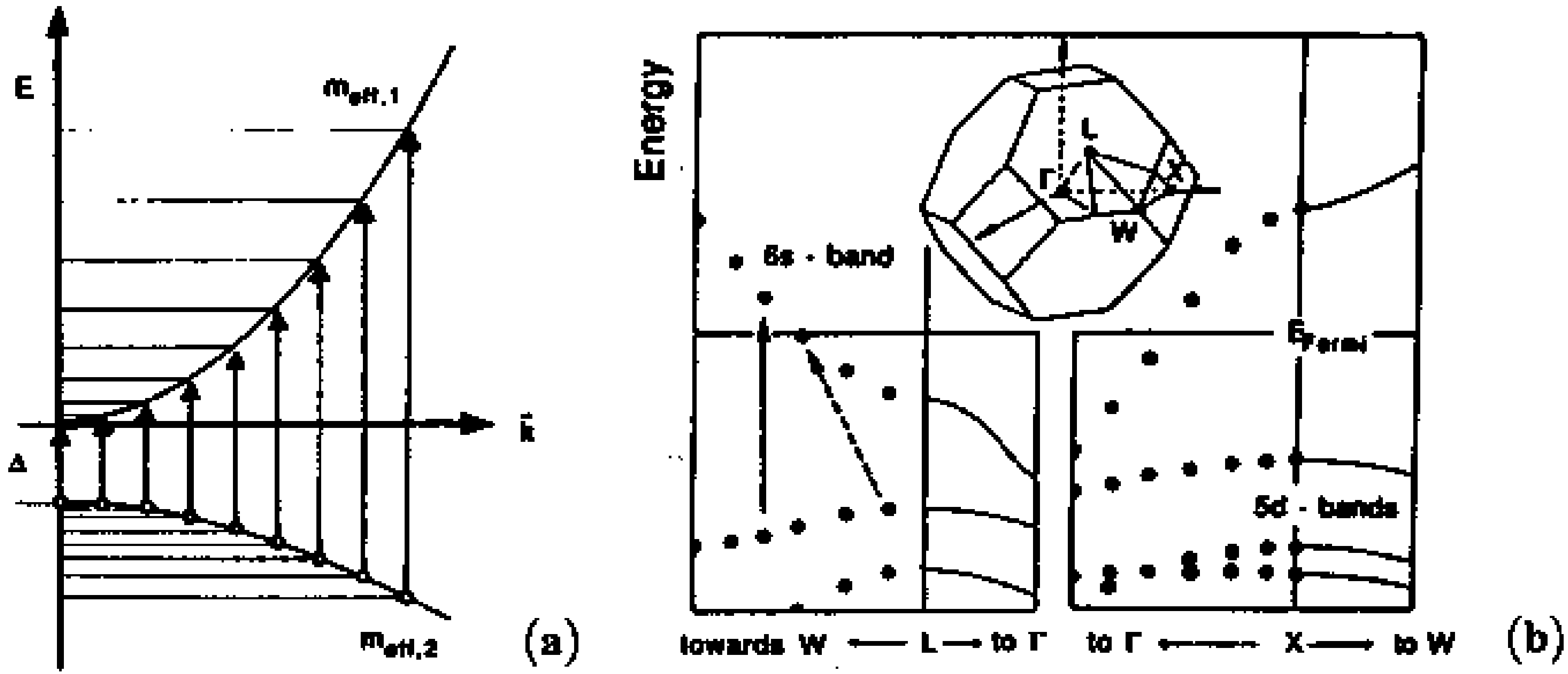

Fig. 2.53. **(a)** Two band energy scheme of the cubic box model. The arrows mark "direct interband" transitions. **(b)** Interband transition edge in Au clusters. Two relevant sections of the $E(\boldsymbol{k})$ Au band-structure according to the bulk Brillouin zone are shown [2.35]. In the left parts, only those energy levels are indicated which are permitted by $\boldsymbol{k}$-quantization due to the finite size of the cluster whereas in the right parts, the unmodified band structure of the bulk is shown. The arrows indicate direct (solid line) and indirect (broken line) transitions, contributing to band edge absorption.

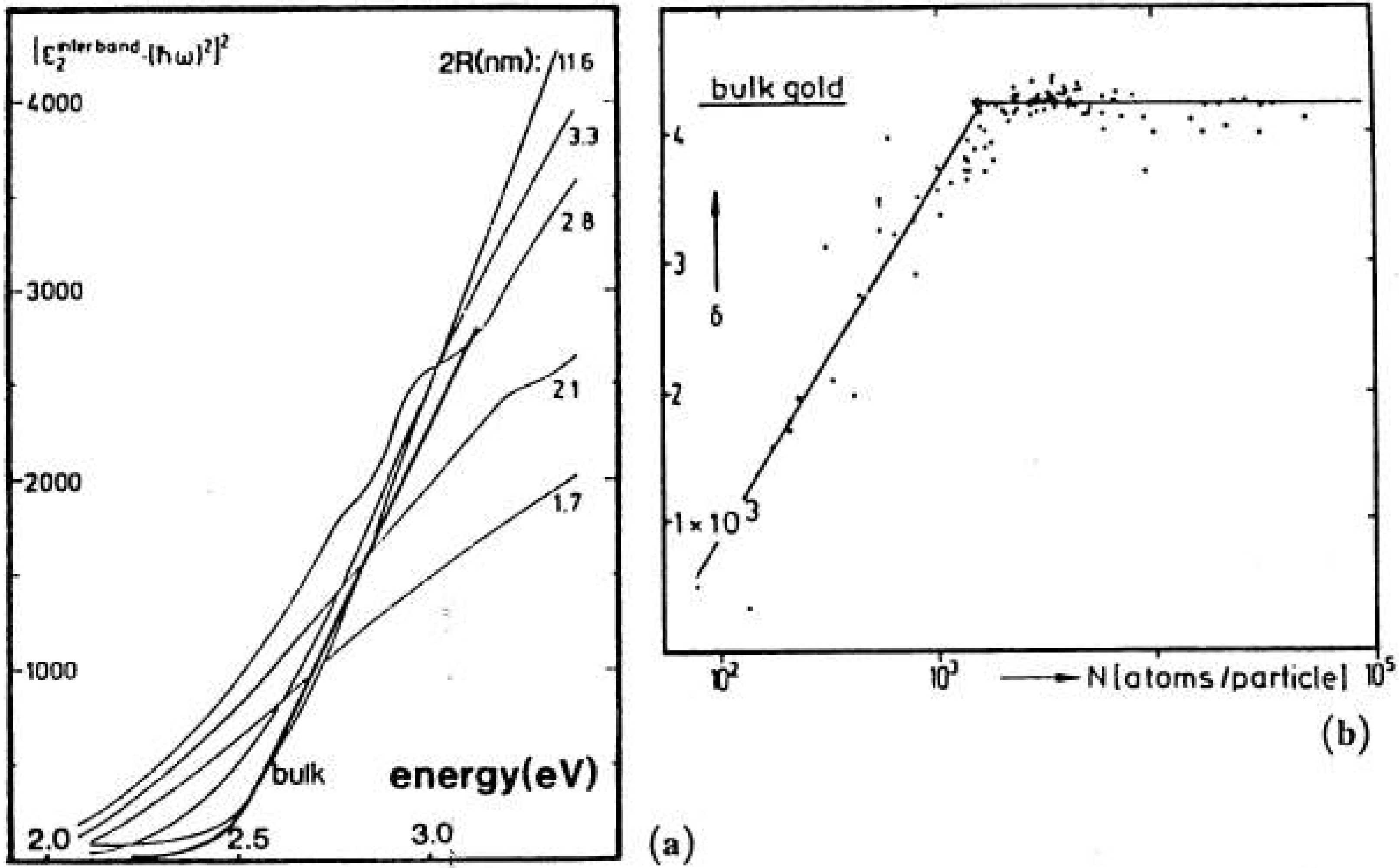

Au-clusters in Photosensitive glass: dependence of the optical interband transition edge on cluster size.

***left*: spectra; *right*: mean slope of the interband edge from about 100 samples.**

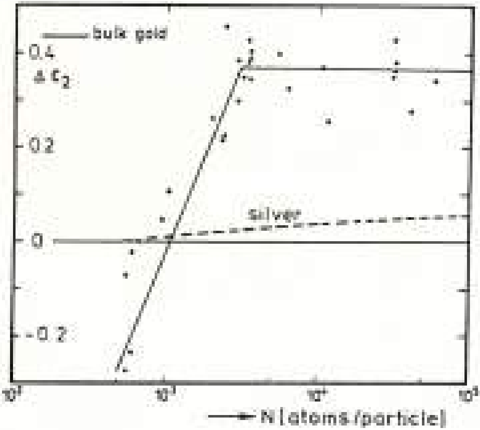

Fig. 4.28. $\Delta\varepsilon_2(\lambda = 510\,\mathrm{nm}) = \varepsilon_2(300\,\mathrm{K}) - \varepsilon_2(1.6\,\mathrm{K})$ for Au clusters (dots), and averaged experimental data of $\Delta\varepsilon_2(\lambda = 405\,\mathrm{nm}) = \varepsilon_2(300\,\mathrm{K}) - \varepsilon_2(1.6\,\mathrm{K})$ for Ag clusters (dashed line) as a function of the mean cluster size (after [4.119a]). The wavelengths correspond to the respective plasmon resonance maxima for embedding in glass.

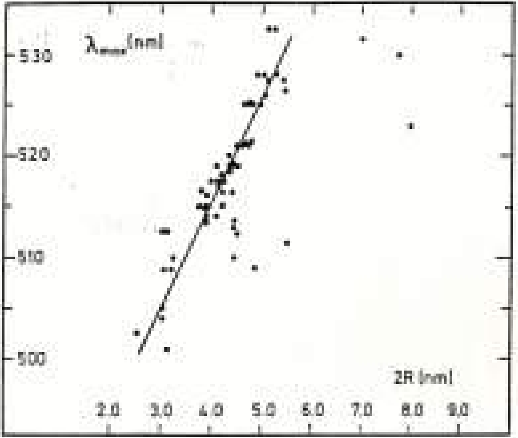

Fig. 4.23. Plasmon peak positons of Au clusters in photosensitive glass [4.117] versus cluster size. For extremely small clusters with $2R \leq 2.5\,\text{nm}$, the band position could not be determined because of extreme damping.

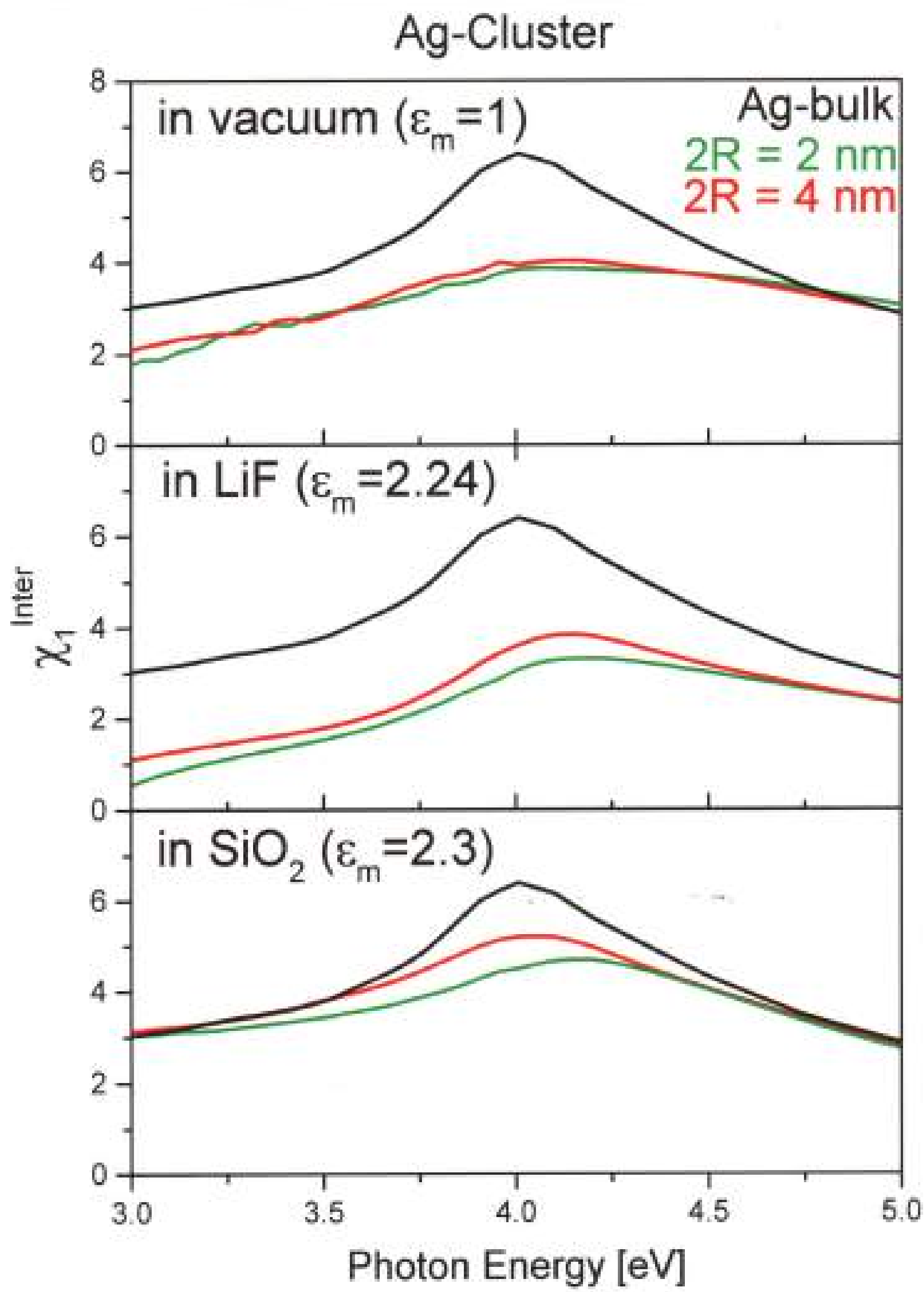

Ag-Cluster
in vacuum (ε_m=1)
Ag-bulk
2R = 2 nm
2R = 4 nm
in LiF (ε_m=2.24)
in SiO_2 (ε_m=2.3)
χ_1^{Inter}
0
2
4
6
8
3.0
3.5
4.0
4.5
5.0
Photon Energy [eV]

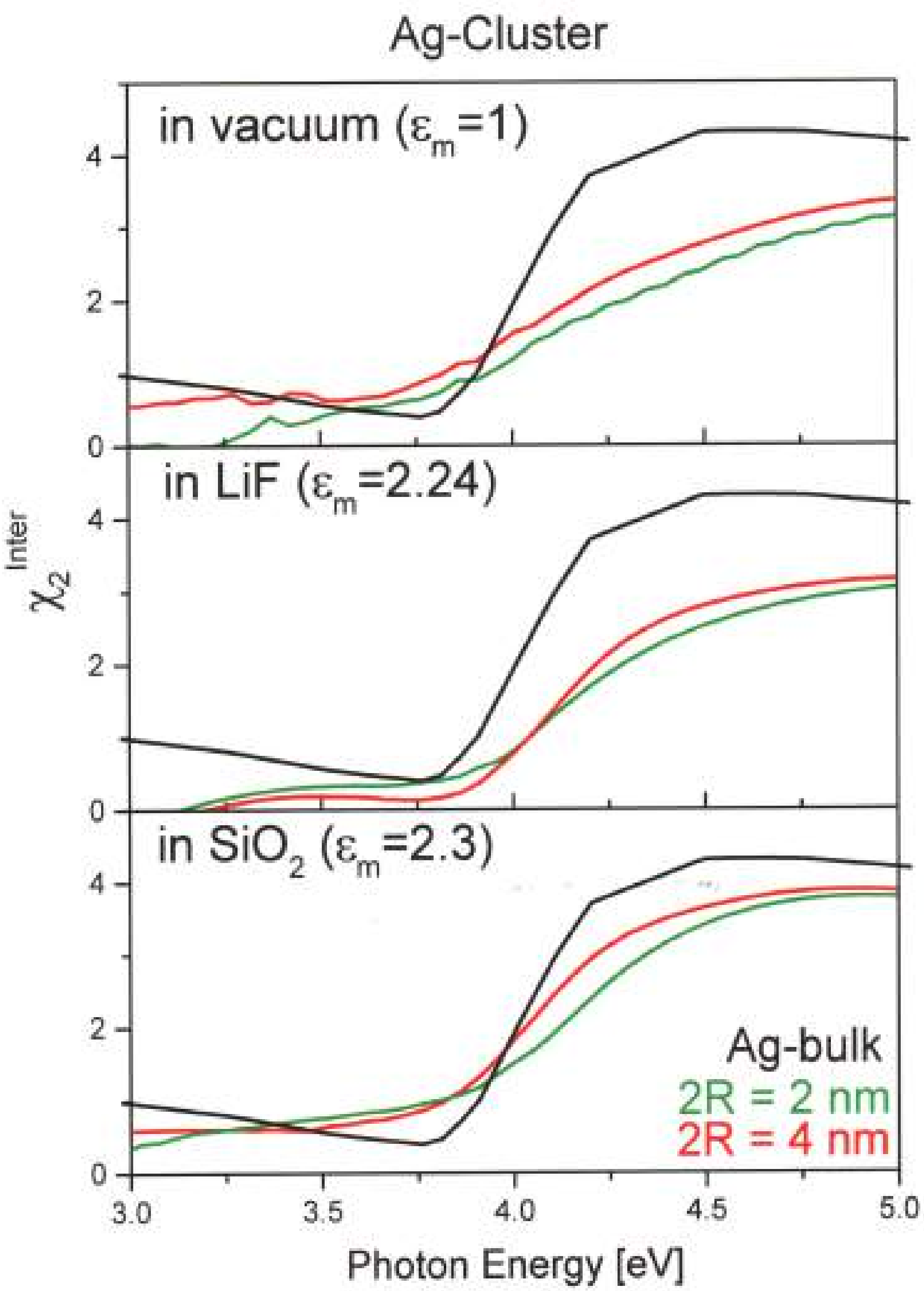

Ag-Cluster
in vacuum (εm=1)
in LiF (εm=2.24)
in SiO2 (εm=2.3)
χ2 Inter
Ag-bulk
2R = 2 nm
2R = 4 nm
Photon Energy [eV]
0
2
4
3.0
3.5
4.0
4.5
5.0

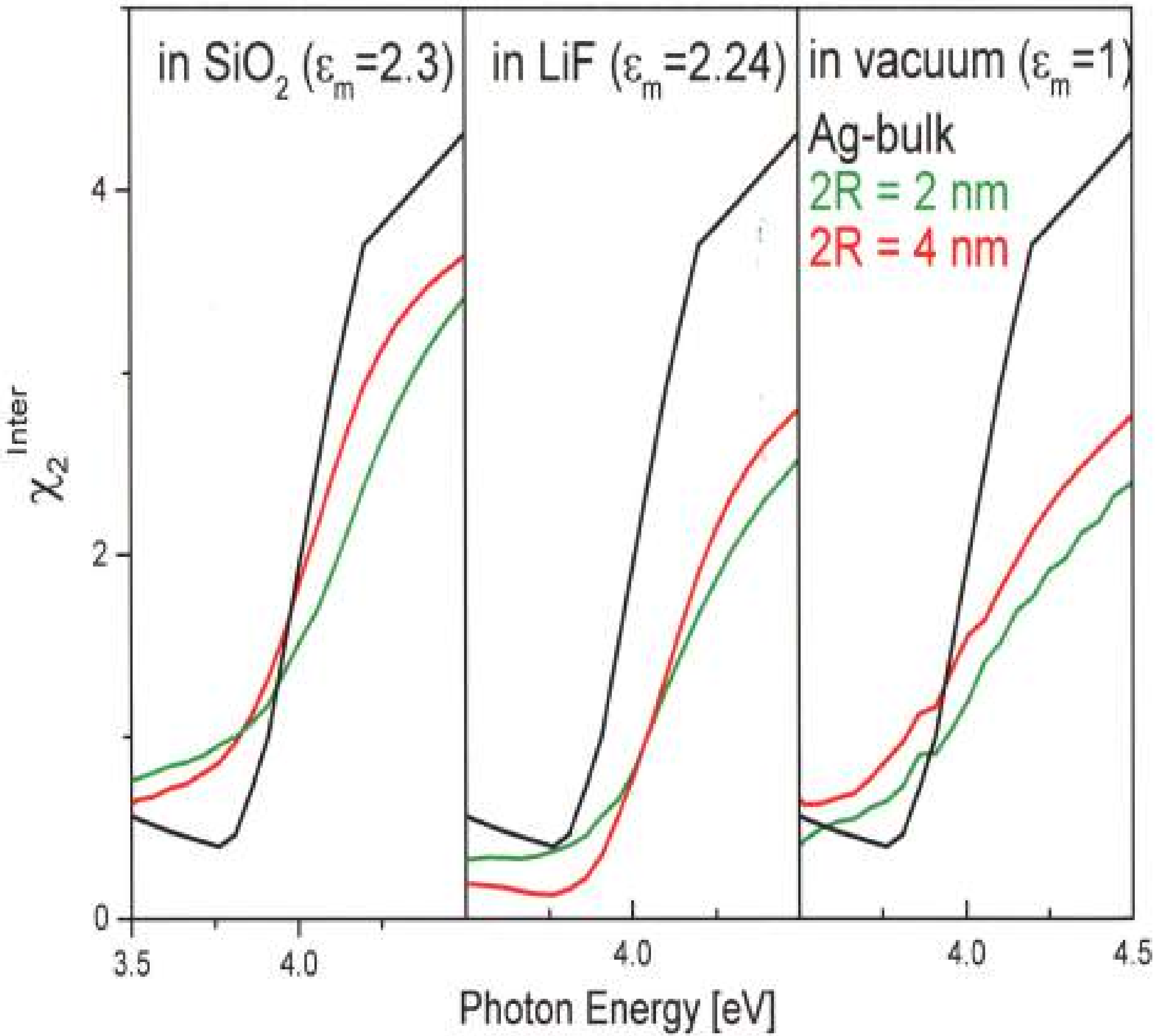

in SiO$_2$ (ε_m=2.3)
in LiF (ε_m=2.24)
in vacuum (ε_m=1)
Ag-bulk
2R = 2 nm
2R = 4 nm
χ_2^{Inter}
0
2
4
3.5
4.0
4.0
4.0
4.5
Photon Energy [eV]

EXAMPLES:

HETEROGENEOUS AND NON-SPHERICAL NANOPARTICLES

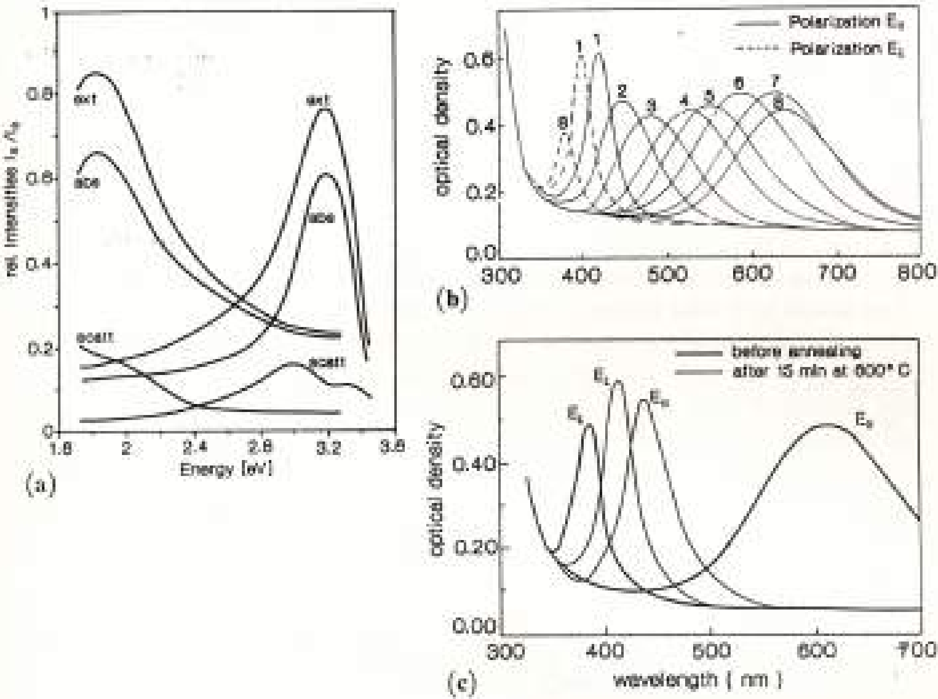

Fig. 4.18. Measured extinction spectra of oriented prolate Ag spheroids (**a**) created by applying external stress to spherical clusters in glass (after [4.71]). The spectra were recorded with polarization parallel and normal to the long axis giving rise to two separate peaks. Their positions depend on the axial ratio of the ellipsoids (**b**). Annealing at elevated temperatures reduces the eccentricity, i.e. leads back to more spherical shapes (**c**). An according sample is shown in Fig. 3.20.

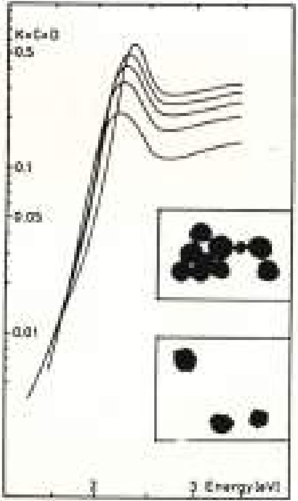

Fig. 4.16. Au hydrosol ($2R \approx 40$ nm) with different surface roughnesses between 1 and 5 nm (from top to bottom). The TEM's correspond to the top and bottom spectrum, respectively (after [4.10, 300]).

Nickel

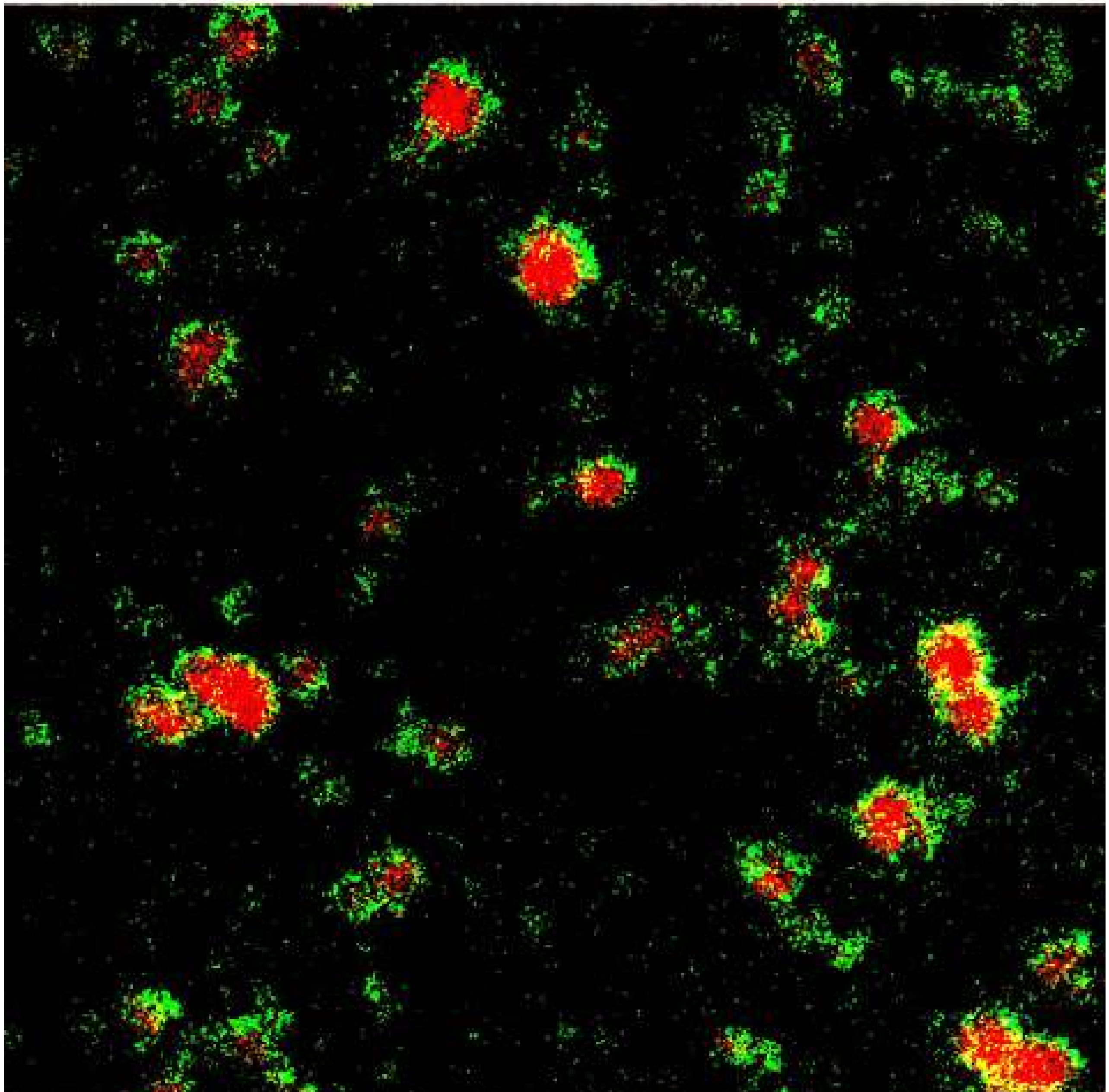

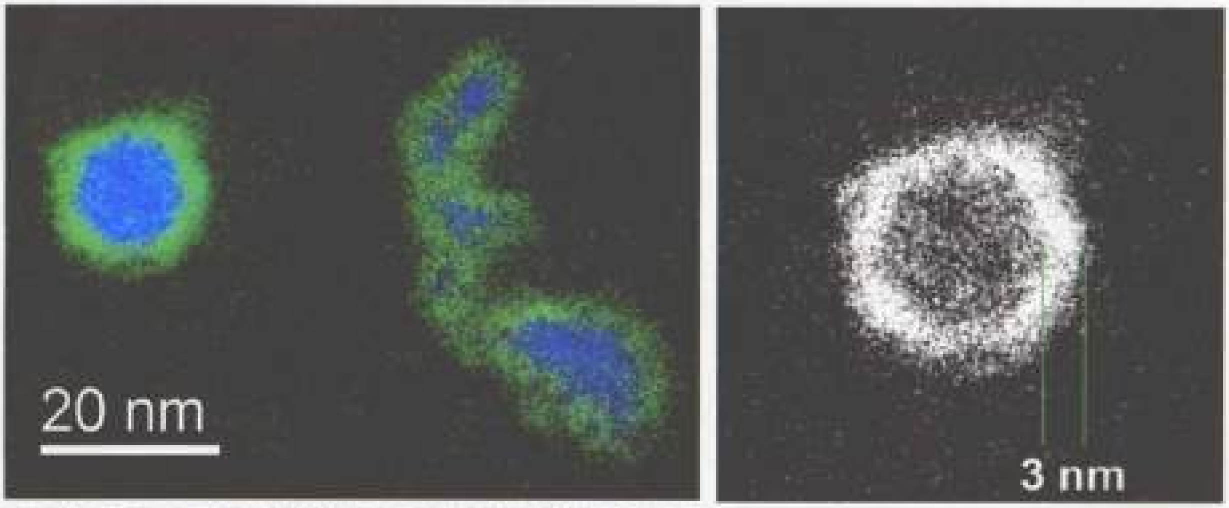

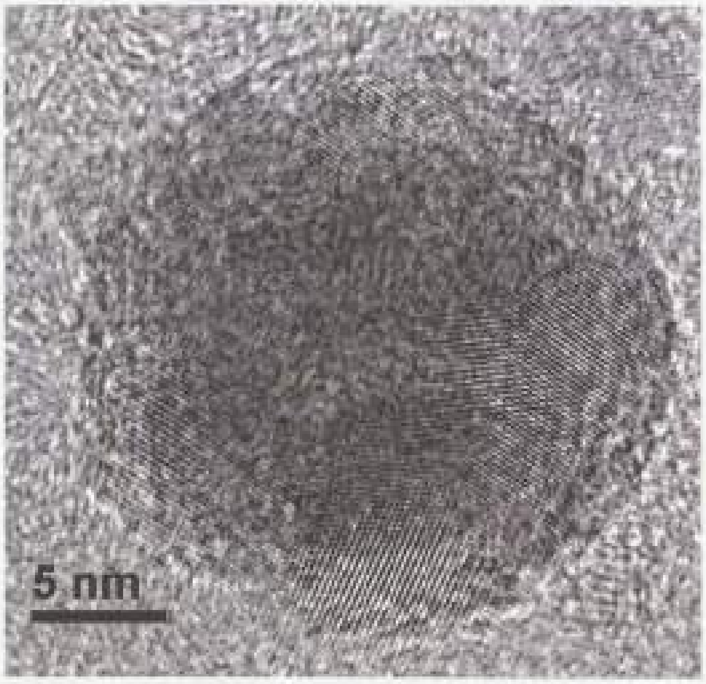

Co/CoO: High-resolution TEM (left image) proves the crystalline state of the CoO shell. The ESI elemental map in the middle displays the core-shell structure of the particles (Co - blue; oxygen - green). The right image shows the oxygen distribution for the spherical particle on the left. The latter allows directly to determine the thickness of the CoO shell.

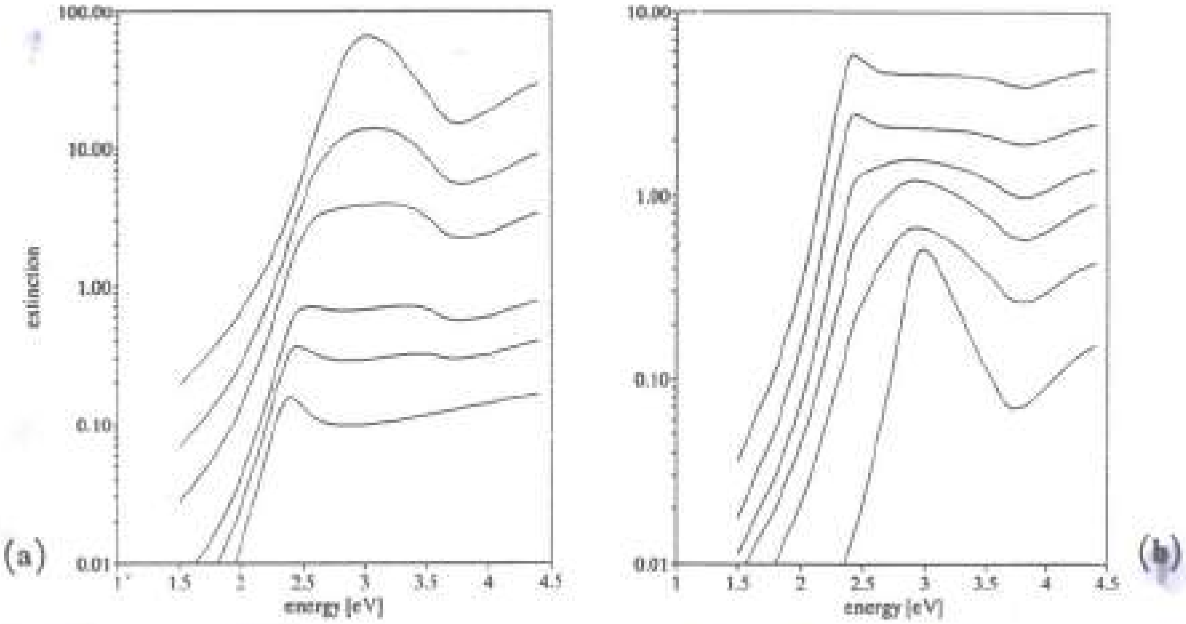

Spherical Heterogeneous Nanoparticles: Core/Shell Nanos

Upper spectra calculated; Left: Au core with R = 8 nm and one Ag shell with d = 0.5 to 8 nm. Right: Ag core with R = 8 nm and one Au shell with d = o.5 to 8 nm.

Lower spectra measured; Left: Au core with R = 6 nm and one Ag shell with d = 0 to 6.5 nm. Right: Ag core with R = 13.6 nm and one Au shell with d = 0 to 9 nm.

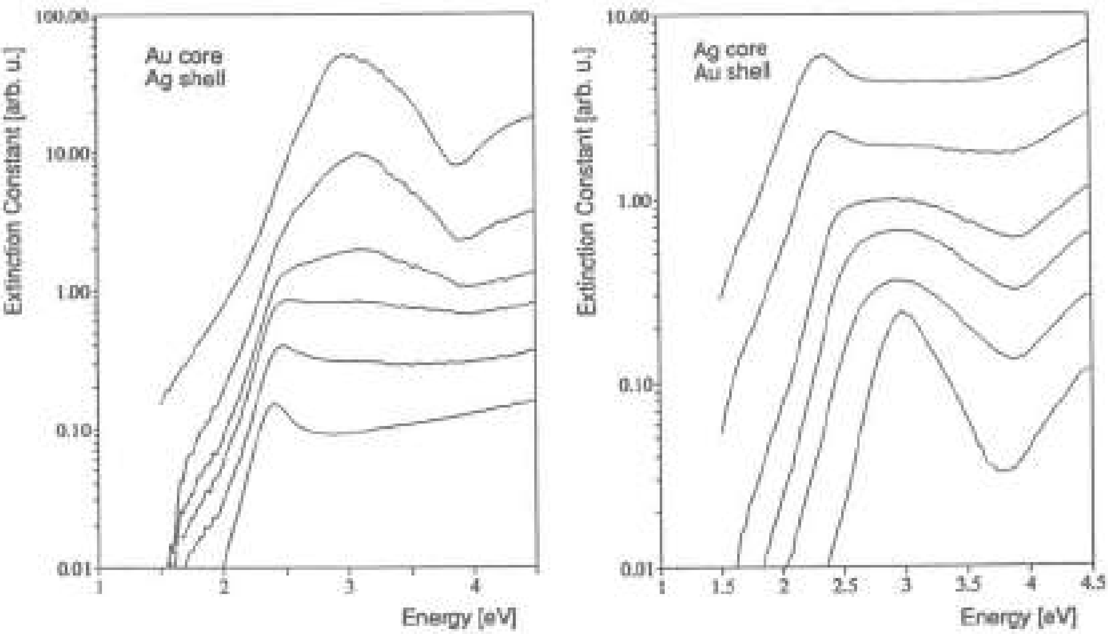

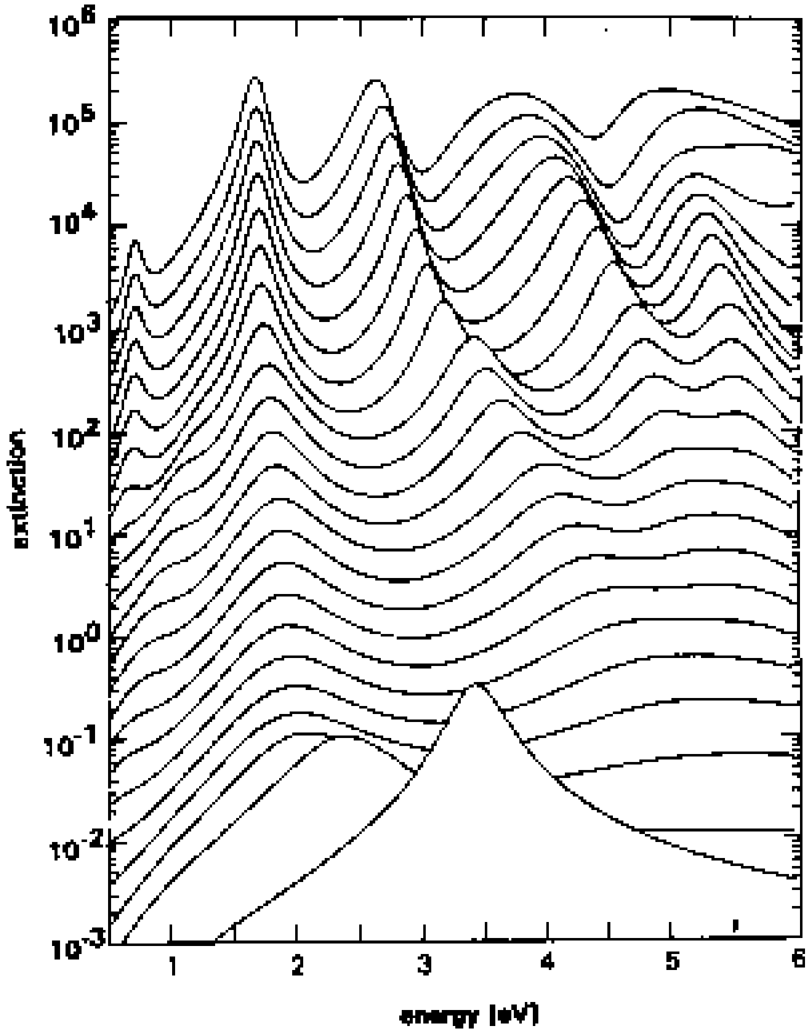

Figure 10 Extinction spectra of spherical heterostructures. Around a sodium core (R = 2 nm) there are six shells of alternating dielectric and sodium material. Total shell thickness: increasing from bottom to top between 0 and 10 nm. (From Sinzig, J. 1993.)

SURFACES AND INTERFACES

OF

NANOPARTICLES

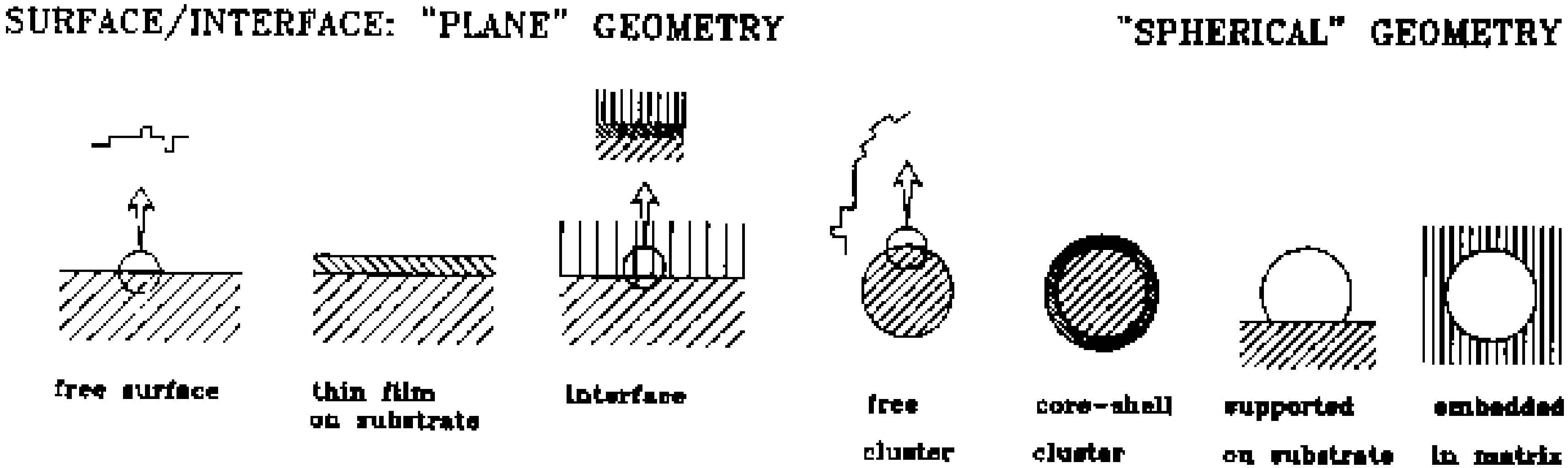

Topologies of Surfaces and Interfaces of planar and spherical symmetry

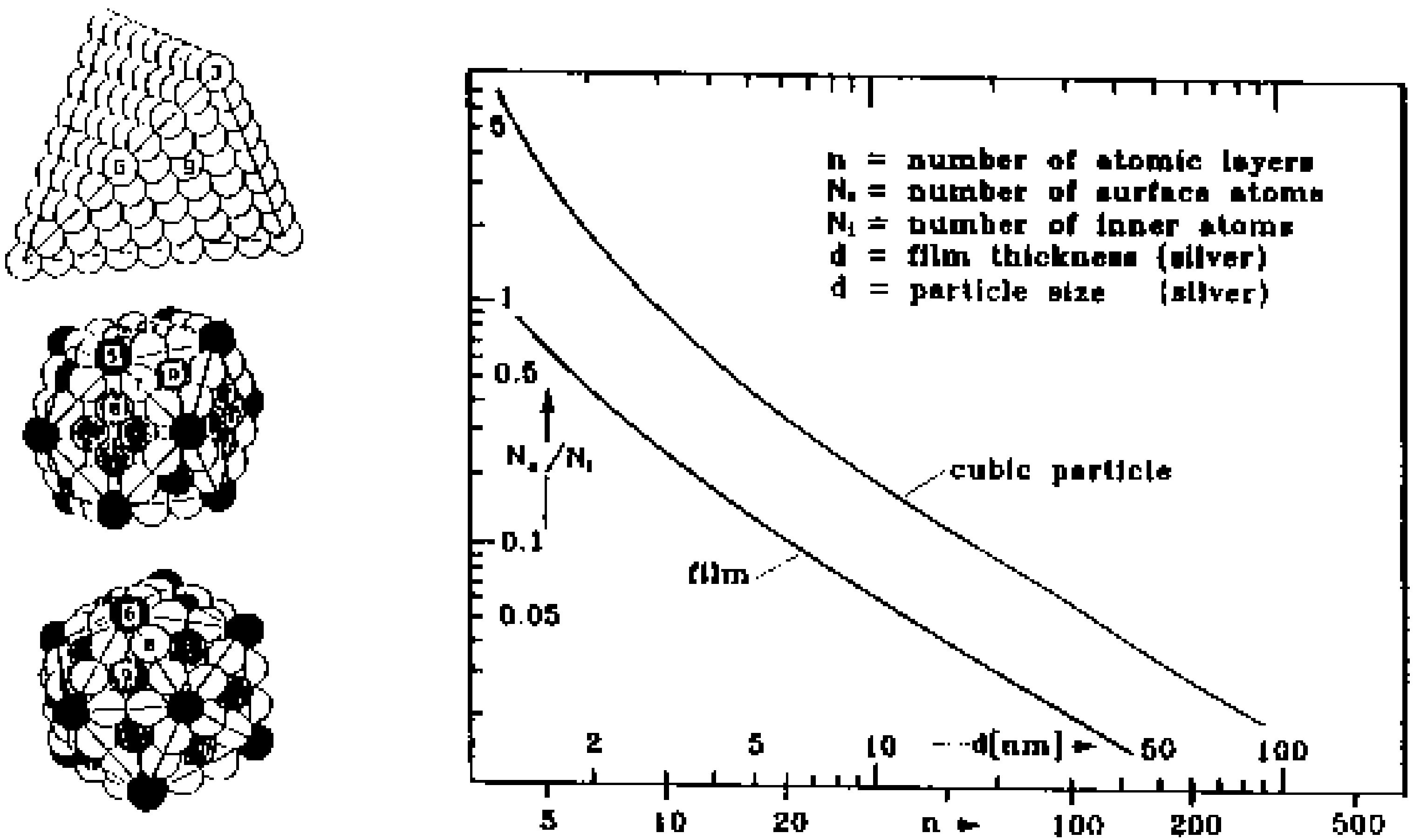

(a)Coordination numbers of surface atoms of a tetrahedral cluster (3,6,9), an icosahedral cluster (5,7,8,9) and a cuboctahedron (6,8,9). (after Fritsche et al (8))

(b)Ratio of numbers of surface and inner atoms in a planar film compared to a cubic cluster.

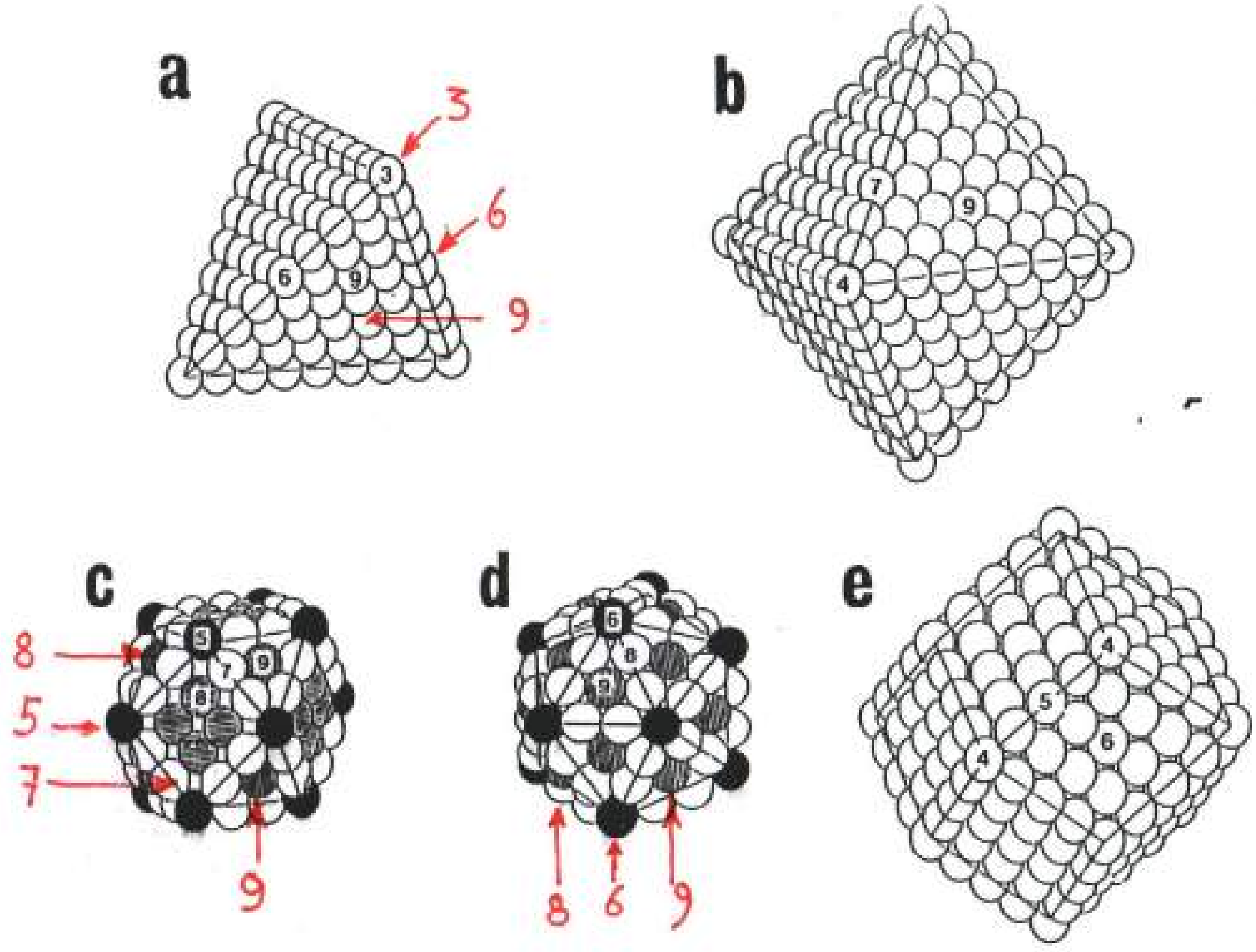

Figure 1

Surface atom sites and their coordination numbers in different polyhedra.

(a) tetrahedron (m = 9; 165 atoms); (b) octahedron (m = 9; 489 atoms); (**d**) icosahedron (m = 4; 147 atoms); (**c**) cuboctahedron (m = 4; 147 atoms); (e) bcc rhombic dodecahedron (m = 5; 369 atoms).

(after Fritsche et al. (1993))

SURFACE ENERGIES:

Nanoparticle :

Silver, spherical : $2R = 10$ nm; Surface : $O = 314\ nm^2$

Spezific surface energy $\varepsilon = 2.5\ Joule/m^2 = 16\ eV/nm^2$

Surface energy of the single, free nanoparticle:

$$E_C = 5.0\ k\,eV$$

Cluster-matter sample :

Volume : 1 mm^3 ; filling factor: 10^{-4}; 10^{13} particles

(a) without matrix : $E_P = 5\ 10^{16}\ eV = 8\ m\,J$

(b) with matrix : ?

CLUSTER - SIZE / SURFACE EFFECTS

SURFACE:

- BOUNDARY FOR ELECTRON WAVES
- DISCRETE EIGENSTATES
- STANDING WAVES
- SHELL MODEL
- SURFACE RESONANCES
- SURFACE STATES
- EVANESCENT WAVES
- REDUCED SCREENING
- INELASTIC SURFACES SCATTERING
- INCREASED ELECTRON - PHONON - COUPLING
- SURFACE INDUCED POLARIZABILITIES
- MULTIPOLAR ELEMENTARY EXCITATIONS
- SURFACE PLASMONS / POLARITONS
- SURFACE PHONONS / POLARITONS
- SURFACE MELTING

VOLUME:

- ATOMIC STRUCTURES
- STRUCTURE FLUCTUATIONS
- ATOMIC DISTANCES
- SUPPRESSION OF EXCITONS, MAGNETIC ORDER ETC.
- DISCRETE ATOMIC VIBRATION MODES

INTERFACE:
(COATINGS, MATRIX)

- ADSORPTION
- CHEMICAL BINDING
- EFFECTS ON EVANESCENT WAVES
- ELECTRICAL DOUBLE LAYERS
- STABILIZATION OF SPECIAL STRUCTURES
- SELECTIVE GROWTH

Properties of Nanoparticle Surfaces and Interfaces

FREE PARTICLE SURFACE

- Surface atomic structure
- Reconstruction
- Electronic surface states
- Electronic surface resonances
- Electronic „spill out"

PARTICLE INTERFACE

- Induced surface structure changes
- Changes of surface states
- Changes of surface resonances
- Changes of the „spill out"
- Electric charging of the cluster (*Static charge transfer)*
- Electric double layers (e.g. in colloidal systems)
- Surface pinned metal electrons
- Chemical interface reactions at different sites
- Electron transfer through interface Tunneling into/from adatom states *(Dynamic charge transfer)*
- Chemical Interface Damping of Mie plasmon polaritons

OPTICAL EFFECTS

AT

INTERFACES

BY

CHARGE TRANSFER

Optical Properties of Nanoparticle/ Surrounding Medium Systems

The Role of Charge Transfer Effects at the Interface

If free, uncontaminated nanos are deposited on some substrate or embedded in some surrounding medium, the free surface is converted into an interface. Each adatom from the surrounding medium may be bound by physi- or chemisorption at different stable positions on edges, corners or surface planes of the surface. So, the adatom levels of a dense surface coverage have, in general, broad energy spectra, some below, some above the Fermi energy of the particle.
On the nanometer scale, thus, interfaces, consisting of up to several layers of mixed particle and matrix atoms are 3-dimensional and inhomogeneous.They may contain special electronic INTERFACE STATES (adsorbate states) which differ from the states of, both, particle and matrix.
Due to the different chemical potentials (Fermi levels) of metal and matrix, charge transfer takes place into and through the interface with the aim of equilibrating them. So, metal particles in contact to surrounding foreign media are electrically charged at a whole.
In the most common case of {metal particles/dielectric matrix} systems, electrons leave the particles and are arrested in traps and in interface states causing a charge double layer which adds to the "spill-out" layer of the free particle surface.

This charge transfer has dramatic effects upon nanooptical properties:
(1) Since the plasmon frequency depends on the charge density of "free electrons" in the particle, the plasmon polariton frequency is red (or blue) shifted from the free particle value.
This is the STATIC CHARGE TRANSFER effect.
To measure this (tiny) peak shift, the precise position of the peak of the uncontaminated, free surface must be known, and this puts high demands on experiments.

(2) If there are empty electron interface states slightly above the Fermi energy in the particle, metal electrons can tunnel and occupy them. Vice versa such electrons can, after a statistical "residence time", tunnel back to the particle. This appears to be "normal" electron dynamics at the interface. This DYNAMIC CHARGE TRANSFER has, however, drastic consequences in the time window, where a plasmon polariton is excited. These electrons are lost from the particle for the life time of the occupied interface state, and after returning back to the particle, the electrons are out of phase of the collective resonance motion of the electron plasma. So they do no longer contribute to but disturb the collective, coherent plasma excitation, thus reducing its life time and increasing the plasma relaxation. (Therefore, this charge transfer effect, discovered 1993, was initially called "chemical interface damping".)
The number of transferring electrons per time can, in a simple model, be related to the number of surface collisions per time, so, compared to the total number of electrons, the general 1 / R -law should hold for the damping effect.
The dynamic charge transfer effect can, thus, be taken into account by an additive term to the relaxation frequency in the Drude part of the DF of the particle material (which also depends on 1/R).
The most straightforward way is to add an interface term $A^{Interface}$ to the A^{Size} parameter :

$$A^{total} = A^{Size} + A^{Interface}$$

What is important: $A^{Interface}$ depends on the chemical and topological composition of the interface, in particular the interface states.
Vice versa: we can learn about nano-interfaces from the numerical values of $A^{Interface}$ for chemically and structurally different kinds of embedding media.
To summarize : While the static charge transfer results in (tiny) peak shifts, the dynamic one increases (drastically) the relaxation of the plasmon peak, i.e. its width. So, in systems of nanoparticles with surrounding media (substrates or matrices), the particles cannot be treated as isolated, but as "dressed" particles, and the system {particle + medium} has to be considered as a whole.

J. Rostalski, M. Quinten :
Effect of a surface charge on the halfwidth and peak position of cluster plasmons in colloidal metal particles
Colloid Polym.Sci 274,648(1996)

---

(1) **Free charges** on the surface of metal clusters: surface layer; extra Maxwell boundary condition.Extra surface dielectric function.
Size dependent SPP blue shifts for neg. charges.

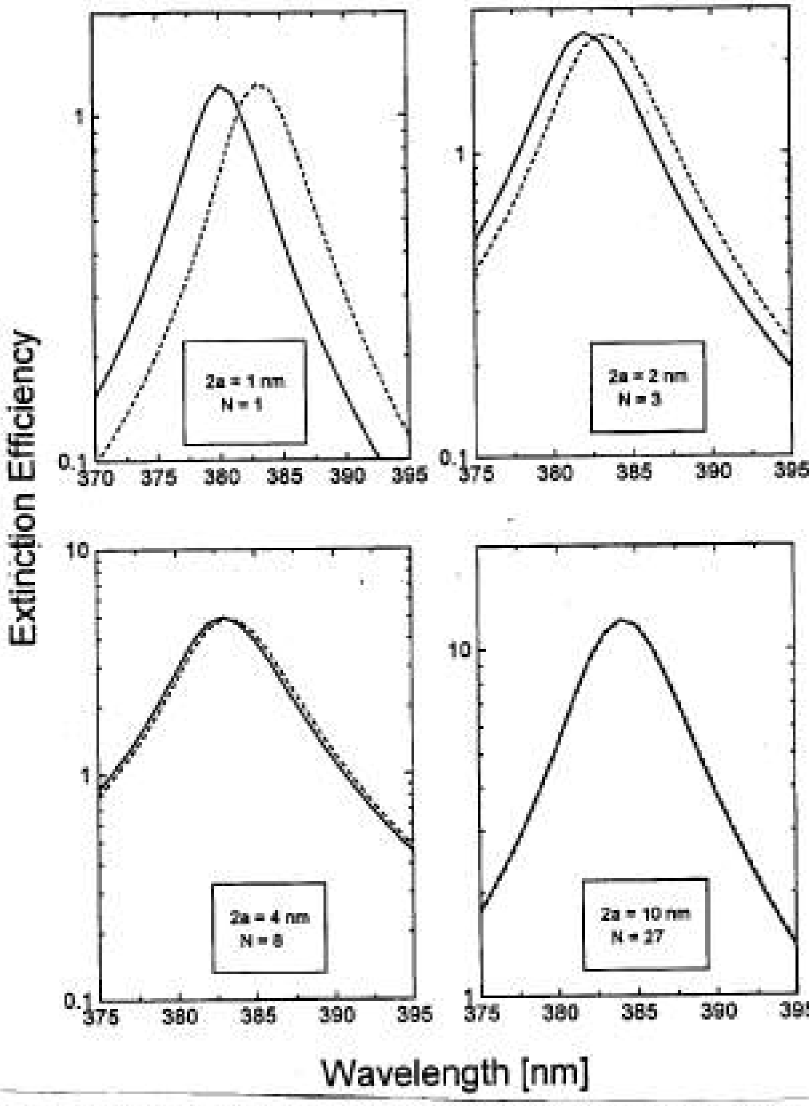

Fig. 1 Optical extinction efficiency spectra of charged silver clusters (solid lines) and uncharged silver clusters (dashed lines) with diameters $2a = 1$ nm, 2 nm, 4 nm and 10 nm. The maximum number N of elementary charges is given in the plots

(2)**Bound charges** on the surface of metal clusters : contribution to the free electron density in the clustervolume; change of the plasma frequency.
Size dependent SPP blue shifts.
for neg. charges

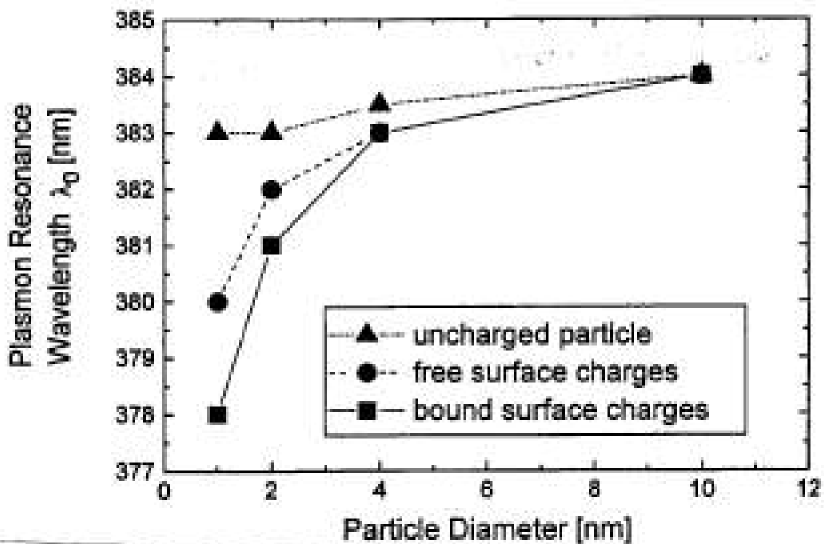

Fig. 2 Resonance wavelength λ_0 of charged silver clusters with diameters $2a = 1$ nm, 2 nm, 4 nm and 10 nm in the model of bound charges (full squares). For comparison, the results from the model of free surface charges (full circles) and for uncharged clusters (full triangles) are also plotted

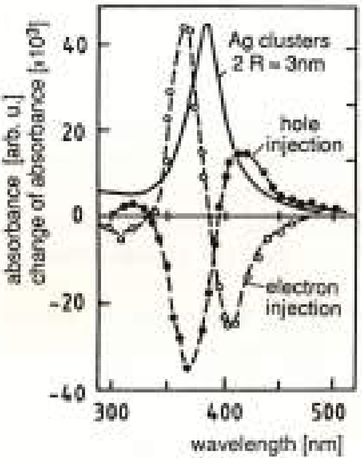

Fig. 4.74. Dipolar Mie resonance of Ag hydrosol clusters and its changes upon electron donation and hole injection (after [4.87]).

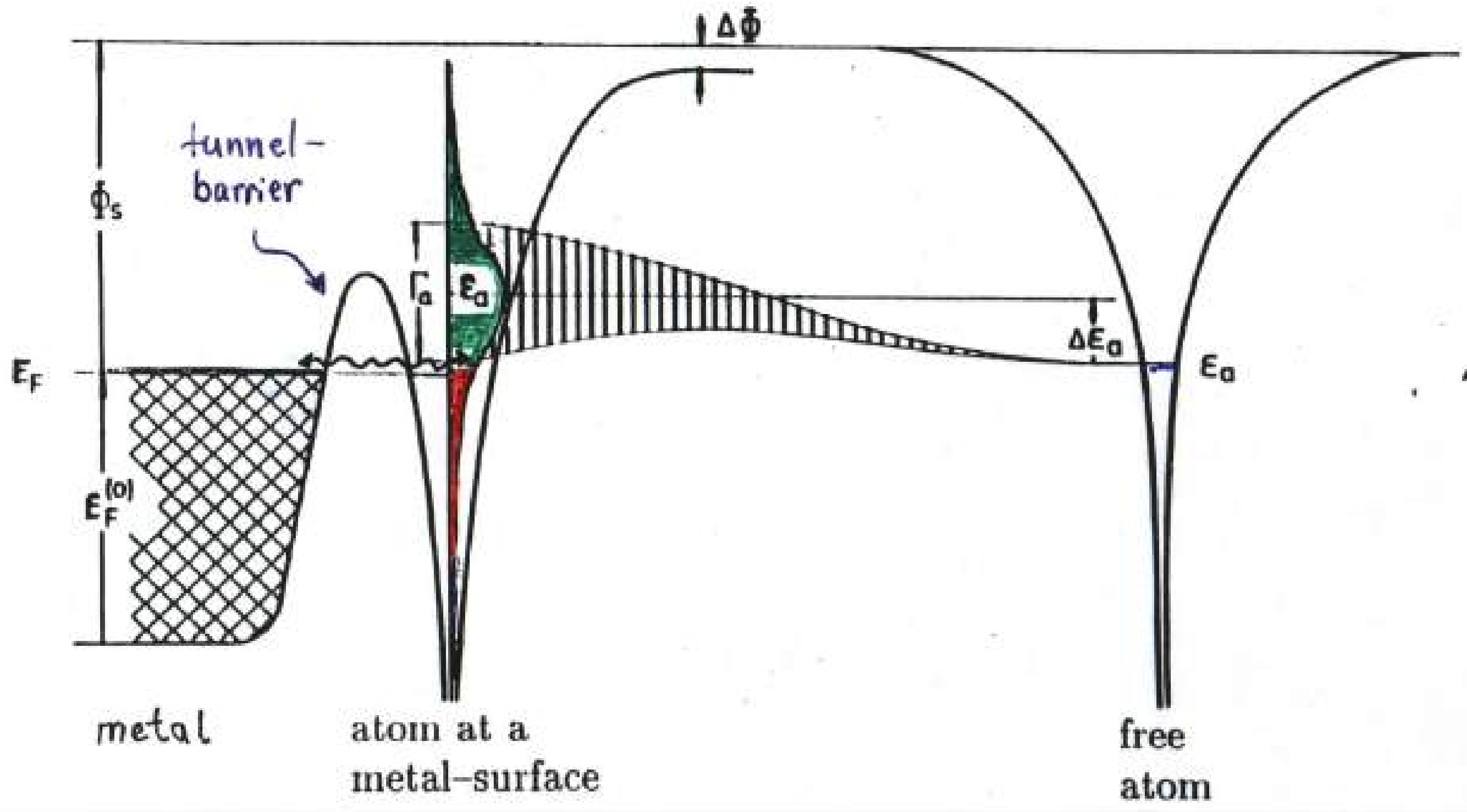

ΔΦ
tunnel-
barrier
Φ_s
Γ_a
ε_a
$\Delta\varepsilon_a$
ε_a
E_F
$E_F^{(0)}$
metal
atom at a
metal–surface
free
atom

STATIC CHARGE TRANSFER :

Mie plasmon resonance: peak position changes:

$$\Delta\omega_{resonance} \approx \{(n_1)^{1/2} - (n_2)^{1/2}\} \cdot (e^2/\varepsilon_0 \, m_{eff})^{1/2} \cdot (2\varepsilon_{matrix} + 1 + \chi_{1,\, interband})^{-1/2}$$

n_1 : conduction electron density in the ***free*** cluster

n_2 : density after contact with foreign material (adsorbate, substrate, matrix)

$$\Delta\omega^{experimental} = \Delta\omega^{dielectric} + \Delta\omega^{resonance}$$

$\Delta\omega^{dielectric}$: dielectric shift; calc. from Mie theory

MIE - PLASMON POLARITON : DIELECTRIC SHIFT

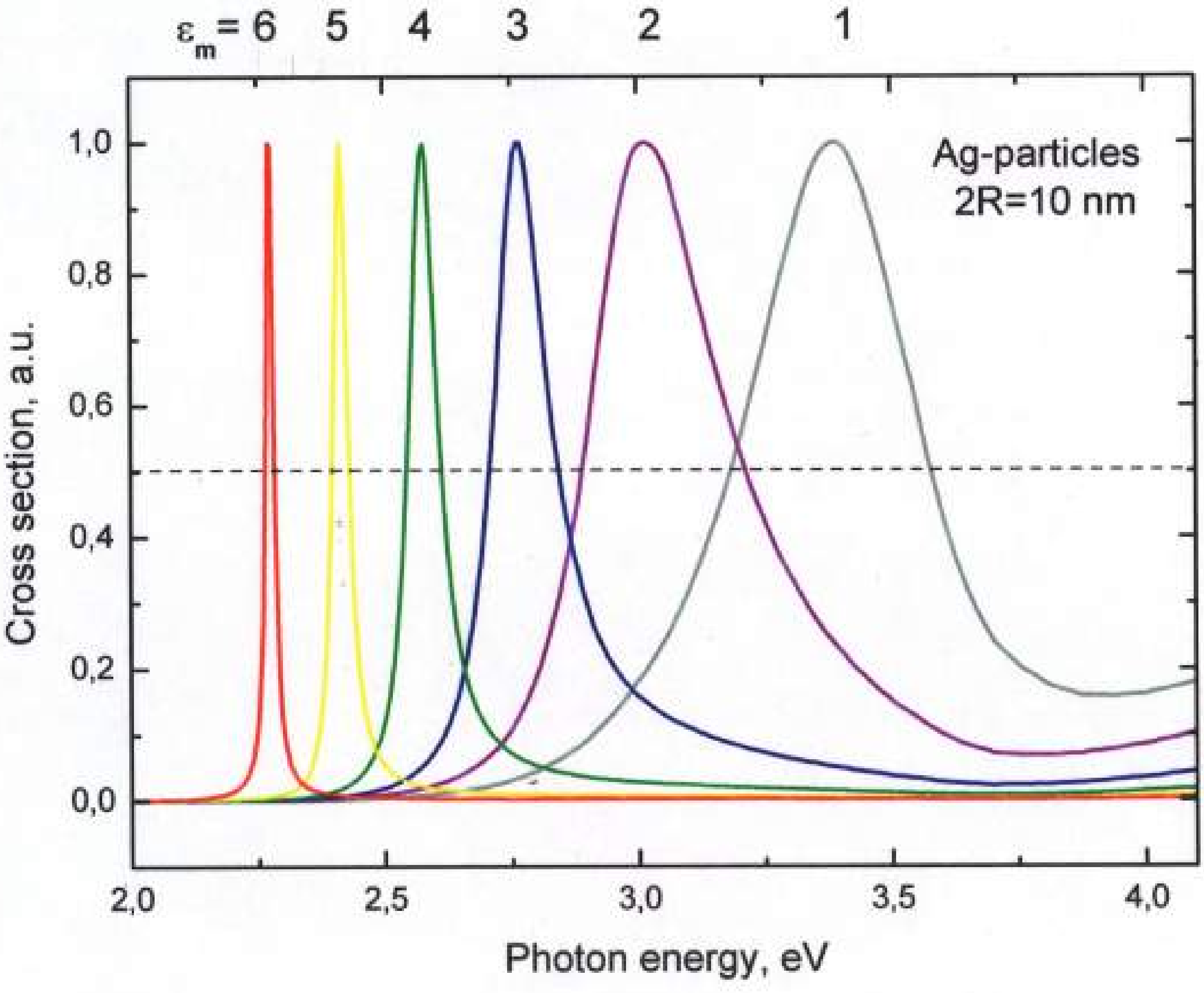

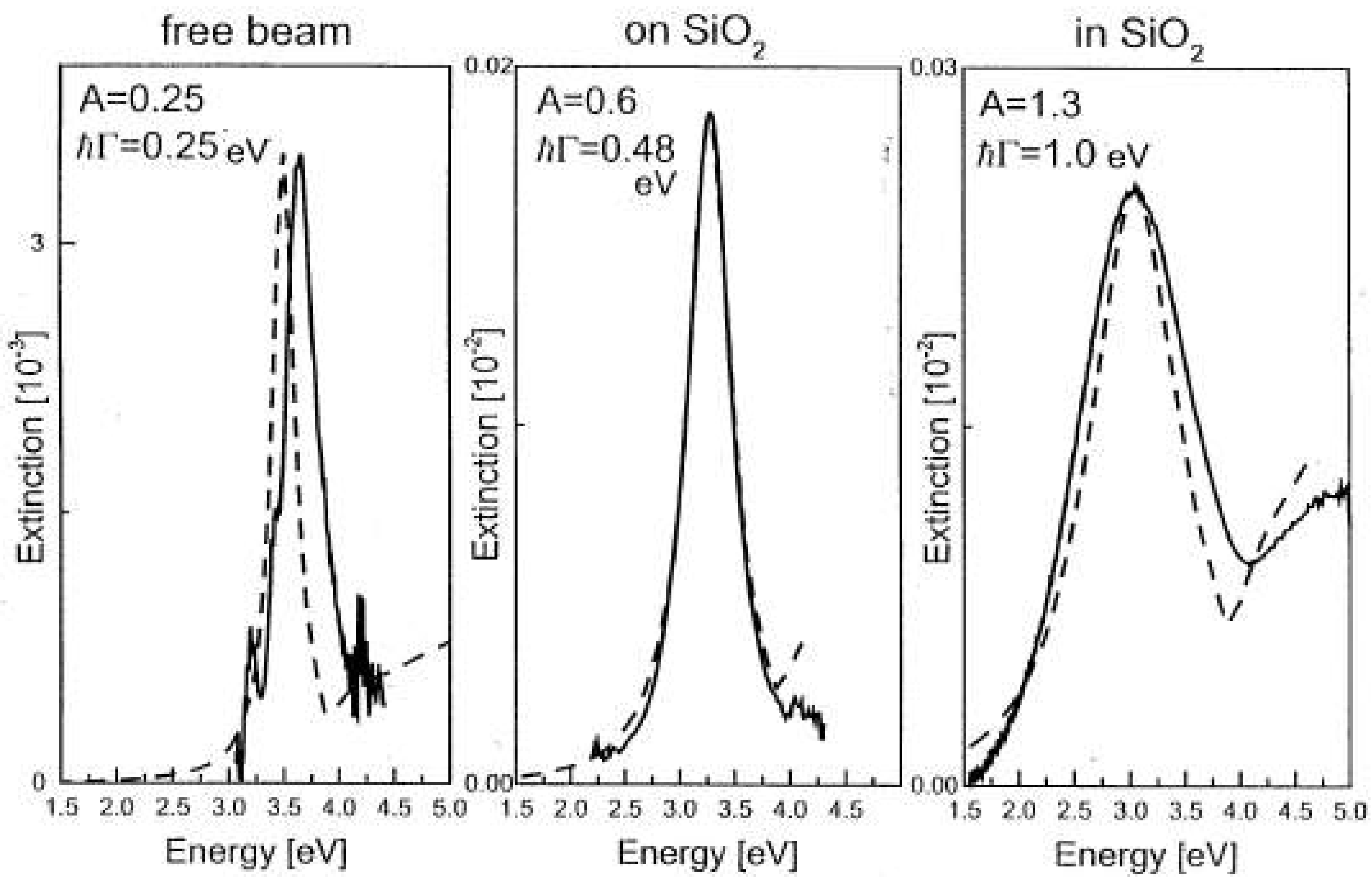
free beam
A=0.25
ħΓ=0.25 eV
Extinction [10⁻³]
3
0
1.5 2.0 2.5 3.0 3.5 4.0 4.5 5.0
Energy [eV]
on SiO₂
A=0.6
ħΓ=0.48 eV
Extinction [10⁻²]
0.02
0.00
1.5 2.0 2.5 3.0 3.5 4.0 4.5
Energy [eV]
in SiO₂
A=1.3
ħΓ=1.0 eV
Extinction [10⁻²]
0.03
0.00
1.5 2.0 2.5 3.0 3.5 4.0 4.5 5.0
Energy [eV]

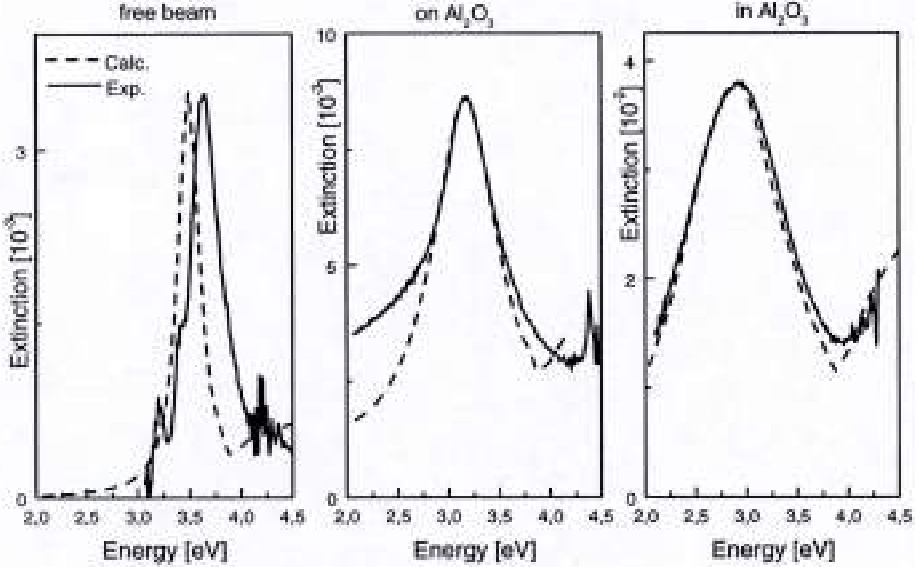

Abbildung 4.1: Silbercluster ($\overline{2R} = 2nm$) im freien Strahl, auf und in Al_2O_3 Matrix. Das Resonanzmaximum liegt bei $\hbar\omega_{max}$=3,03 eV und 2,91 eV, was der Mie-Rechnung für Al_2O_3 entspricht. Um die Breite wiederzugeben muß ein A-Parameter von A=0,6 und 1,6 gewählt werden. Die optischen Konstante der Matrix ist ε_m=3,0, wobei der Anteil des Substrates bei deponierten Clustern mit einem Achsenverhältnis c/a=0,88 54% beträgt.

STATIC CHARGE TRANSFER:

BAND STRUCTURE EFFECTS

(1) Changes of level occupation

- Change of Fermi-energy, Fermi-velocity
- Change of optical interband transition edge
- Change of effective mass
- Change of surface „spill out“
- Additional adsorbate levels, surface states

(2) Changes of band structure

- Change of atomic distances, lattice structure, surface structure

DYNAMIC CHARGE TRANSFER :

Mie plasmon resonance
Band half width:

$$\Gamma(\mathbf{A},R) \approx \Gamma_0 + (2\omega_p^2/\omega^3)\cdot[(d\varepsilon_1/d\omega)^2 + (d\varepsilon_2/d\omega)^2]^{-1/2}\cdot(v_{Fermi}\cdot\mathbf{A}/R)$$

(Kreibig Appl.Phys.1976)

(1) $\mathbf{A} = \mathbf{A}_{size}$: size parameter
(Quantum size effects : $\mathbf{A}_{size} = \mathbf{0.29}$ [Persson et al. 1993])

(2) Extension to electron transfer in the cluster/matrix interlayer:

$$\mathbf{A} = \mathbf{A}_{size} + \mathbf{A}_{interface}$$

Γ_0 : half width of Mie theory
$\mathbf{A}_{size}$: cluster size parameter (Kreibig et al.1970)
$\mathbf{A}_{interlayer}$: interlayer parameter (exp.:Schulze et al.1984) (theor.:Persson et al. 1993)

1. PHYSIKALISCHES INSTITUT
RWTH

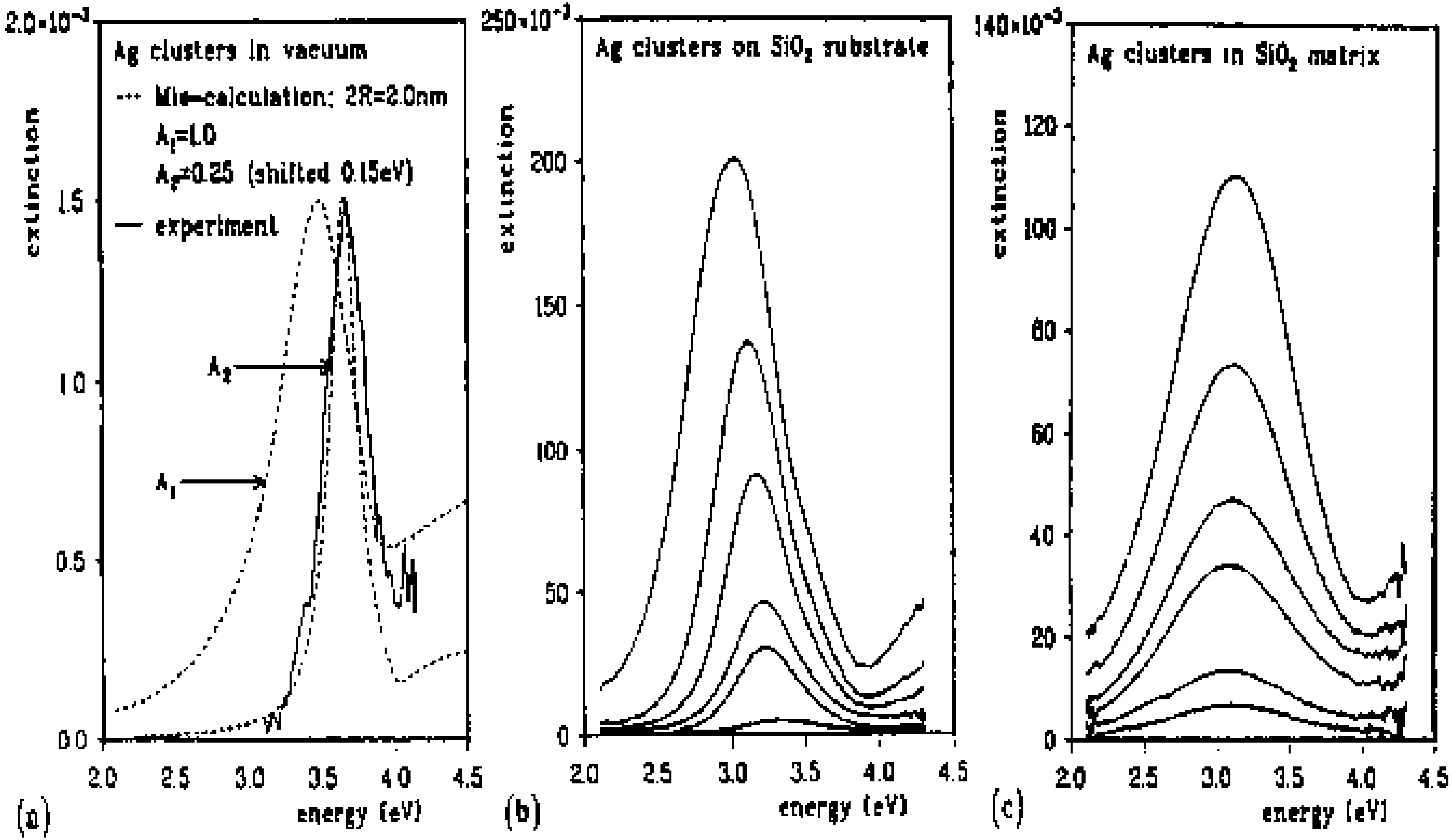

Ag clusters in vacuum
Mie-calculation; 2R=2.0nm
A_1=1.0
A_2=0.25 (shifted 0.15eV)
experiment
A_2
A_1
extinction
energy (eV)
(a)
Ag clusters on SiO_2 substrate
extinction
energy (eV)
(b)
Ag clusters in SiO_2 matrix
extinction
energy (eV)
(c)

Electronic Interactions in the Nanoparticle-Matrix Interface:

(1) Static Charge Transfer (Shift of Mie Peak) :

a) Ag particle - vacuum : $\Delta\hbar\omega = 0$
b) Ag particle - LiF matrix : $\Delta\hbar\omega = + 0.2$ eV
c) Ag particle - SiO_2 matrix : $\Delta\hbar\omega = - 0.17$ eV

(2) Dynamic Charge Transfer (Width of Mie Peak) :

a) Ag particle - vacuum : $A = 0.29$
b) Ag particle - LiF matrix : $A = 0.72$
c) Ag particle - SiO_2 matrix : $A = 1.3$

EXPERIMENTAL EXAMPLE

SILVER PARTICLES EMBEDDED IN FULLERITE

(Mean Particle Size : N = 5 10^2 Atoms)

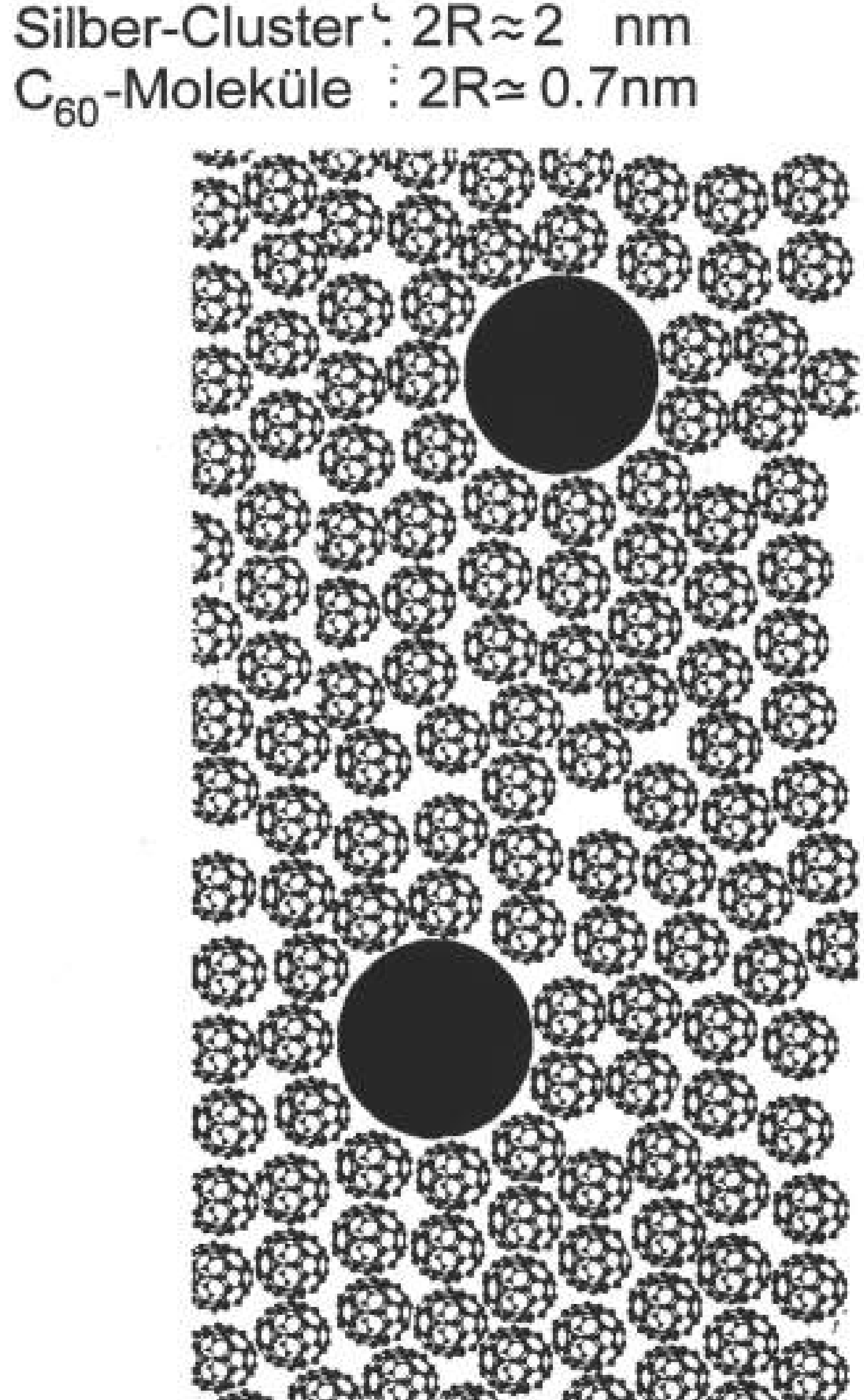
Silber-Cluster : 2R≈2 nm
C_{60}-Moleküle : 2R≃0.7nm

INTERFACE CHARGE TRANSFER (CHEMISORPTION) BETWEEN FULLERITE AND SILVER-CLUSTER

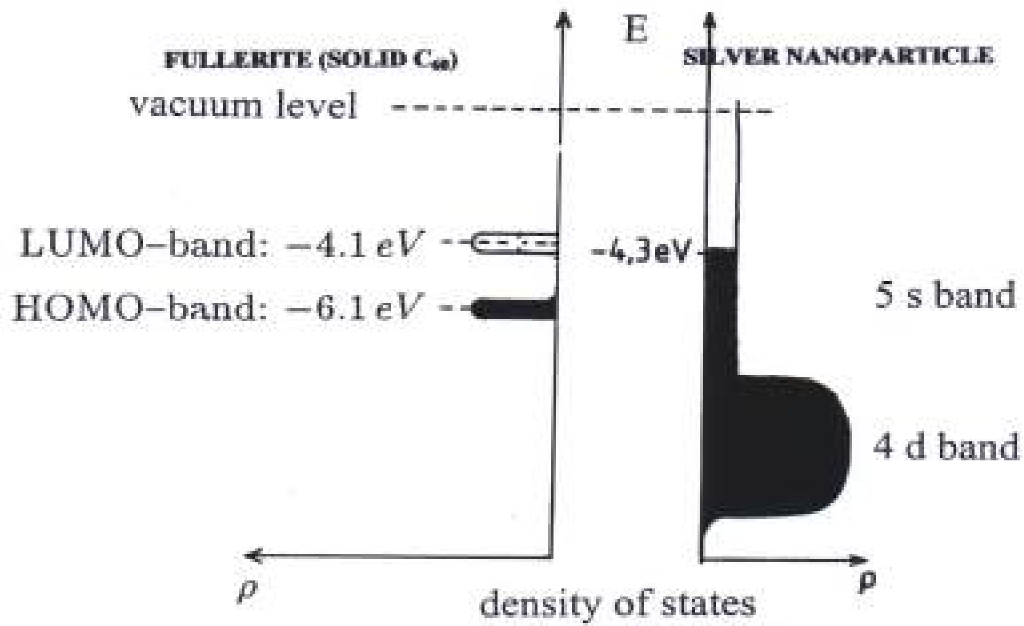

SCHEMATIC: after B. Persson (1992)

EXPERIMENTAL: ≈ 1 electron per interface-C_{60}

- Planar interface, UPS (Wertheim, Buchanan (1994)
- Spherical clusters, optical Mie-spectroscopy Gartz, Hilger, Kreibig (1994)
- Planar interface, EELS, LEED Hunt, Modesti, Rudolf, Palmer (1995)

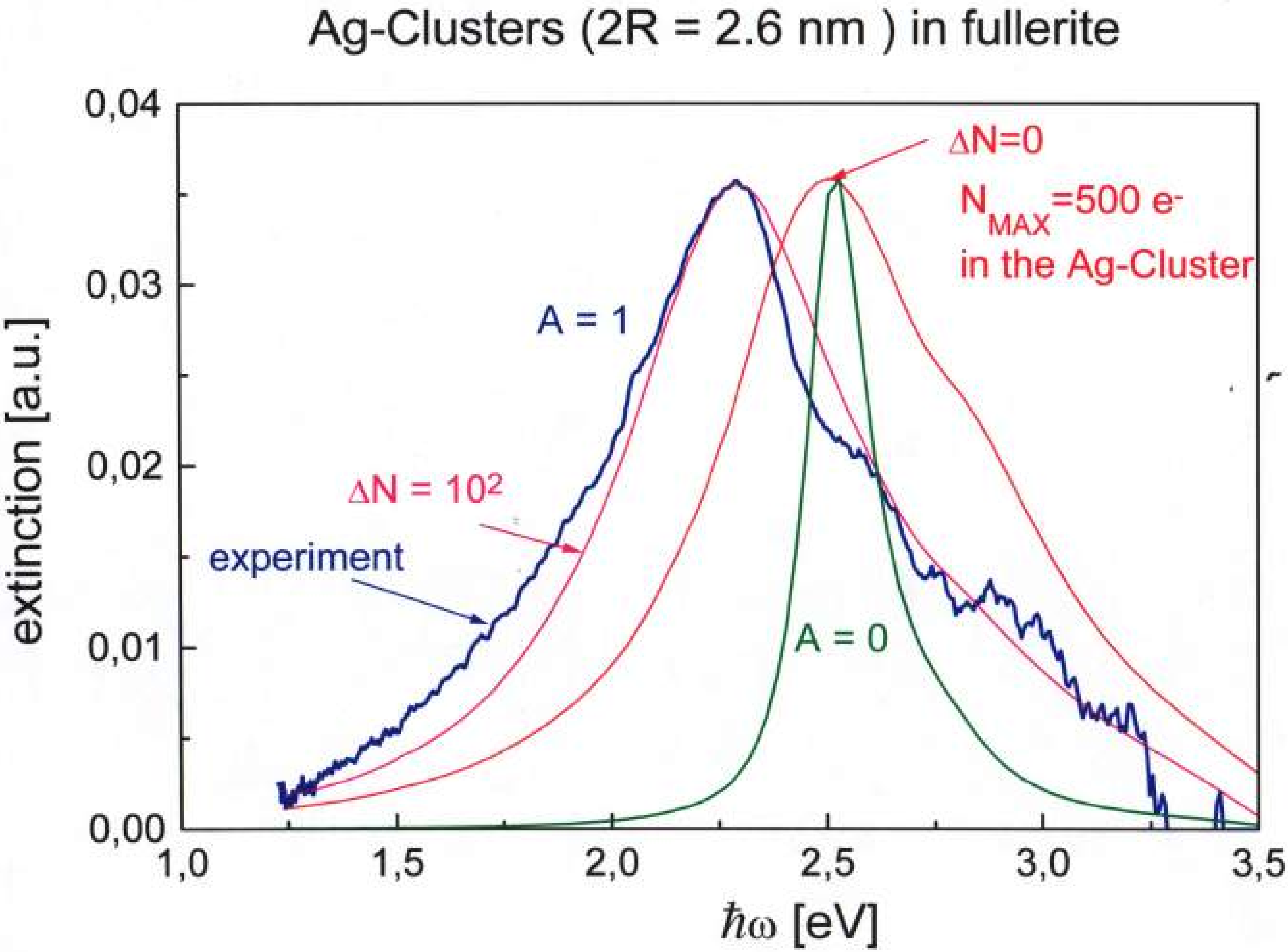

Ag-Clusters (2R = 2.6 nm) in fullerite
extinction [a.u.]
ħω [eV]
0,00
0,01
0,02
0,03
0,04
1,0
1,5
2,0
2,5
3,0
3,5
ΔN=0
N_MAX=500 e-
in the Ag-Cluster
A = 1
ΔN = 10^2
experiment
A = 0

fullerite - layer

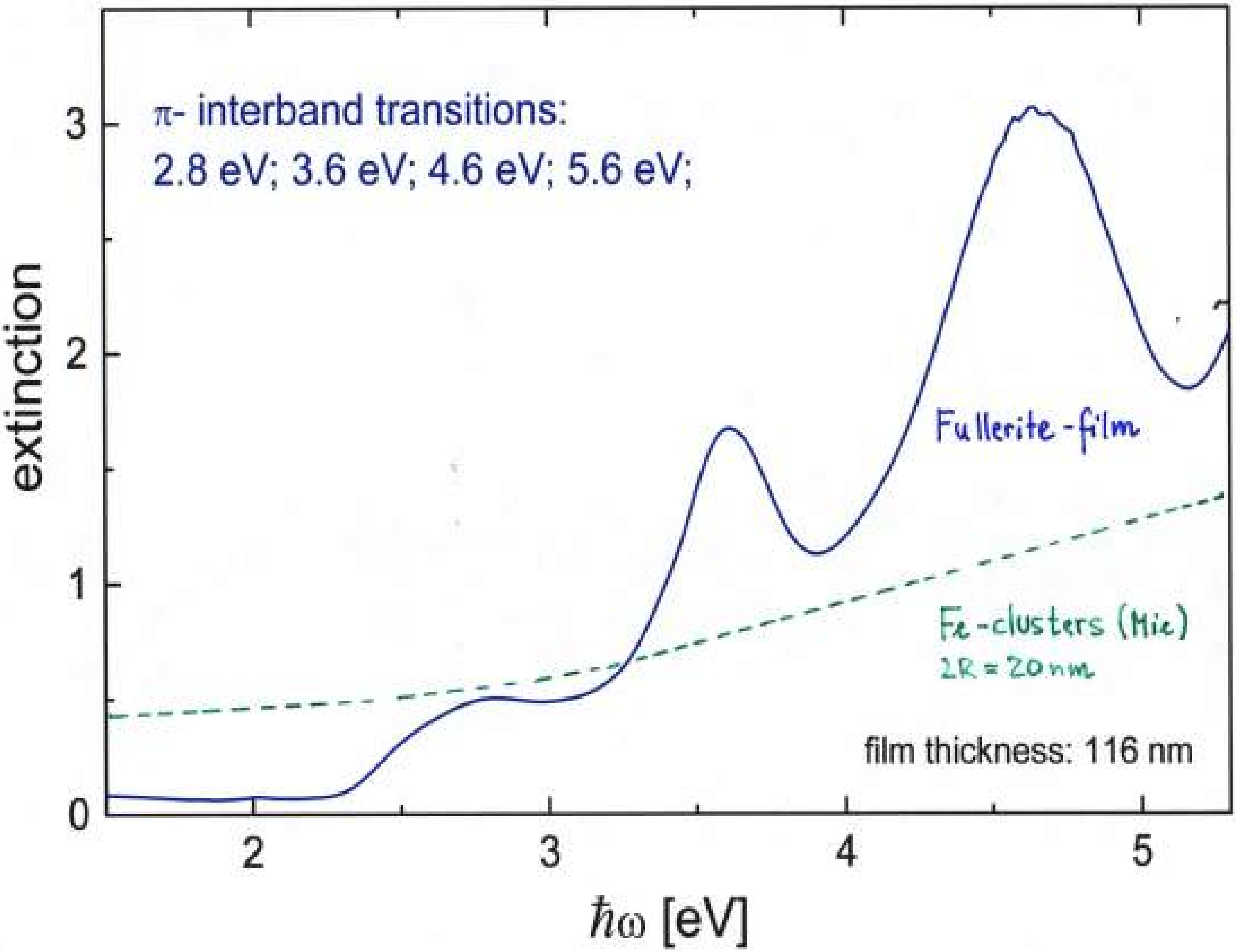

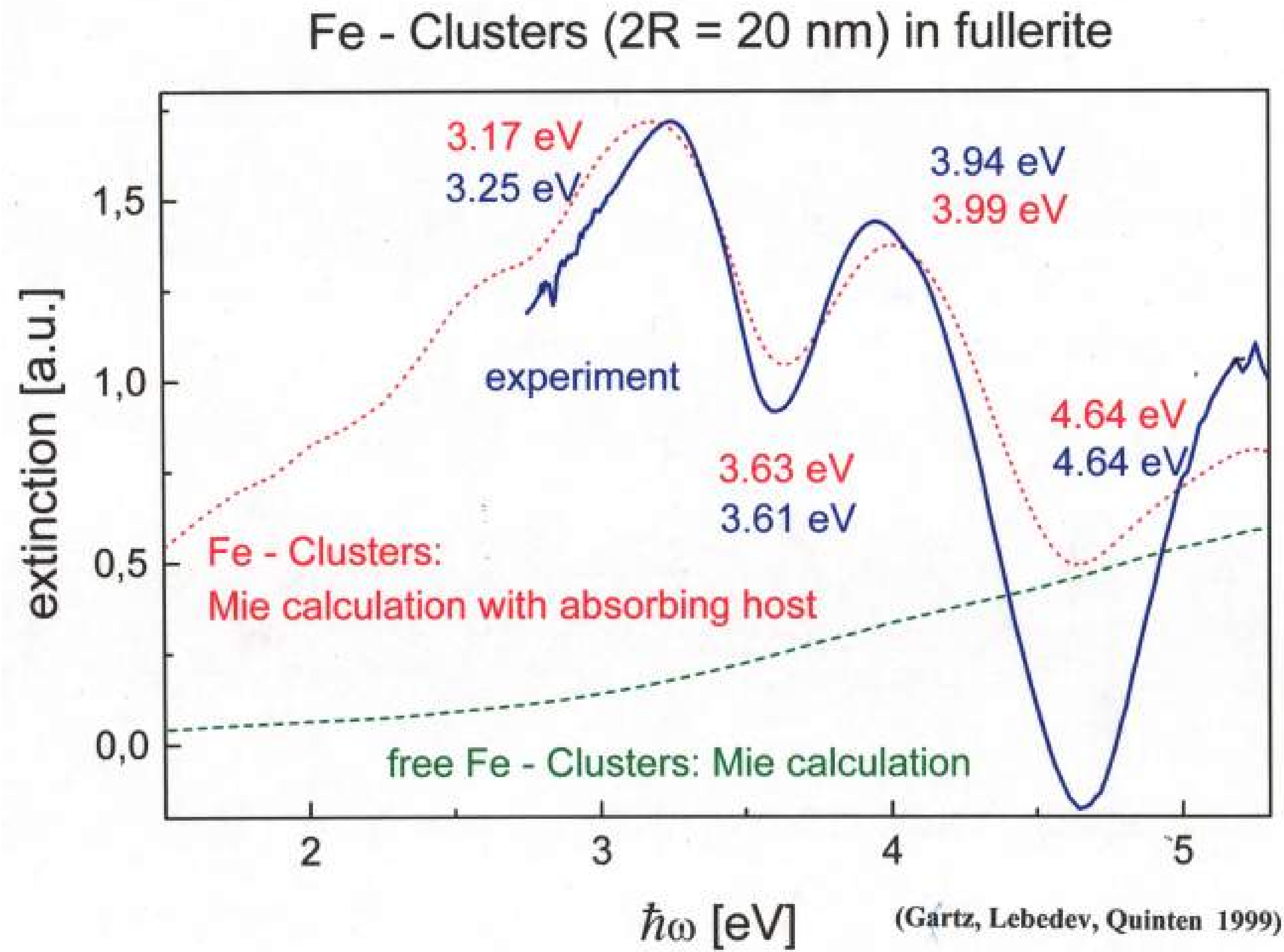
Fe - Clusters (2R = 20 nm) in fullerite
3.17 eV
3.25 eV
3.94 eV
3.99 eV
experiment
4.64 eV
4.64 eV
3.63 eV
3.61 eV
Fe - Clusters:
Mie calculation with absorbing host
free Fe - Clusters: Mie calculation
extinction [a.u.]
1,5
1,0
0,5
0,0
2
3
4
5
ħω [eV]
(Gartz, Lebedev, Quinten 1999)

EXPERIMENTS

ON

2 nm AG-NANOPARTICLES

IN UHV

)

THECLA:

Thermal Cluster Apparatus

(D.Schönauer, H. Hövel, A. Hilger)

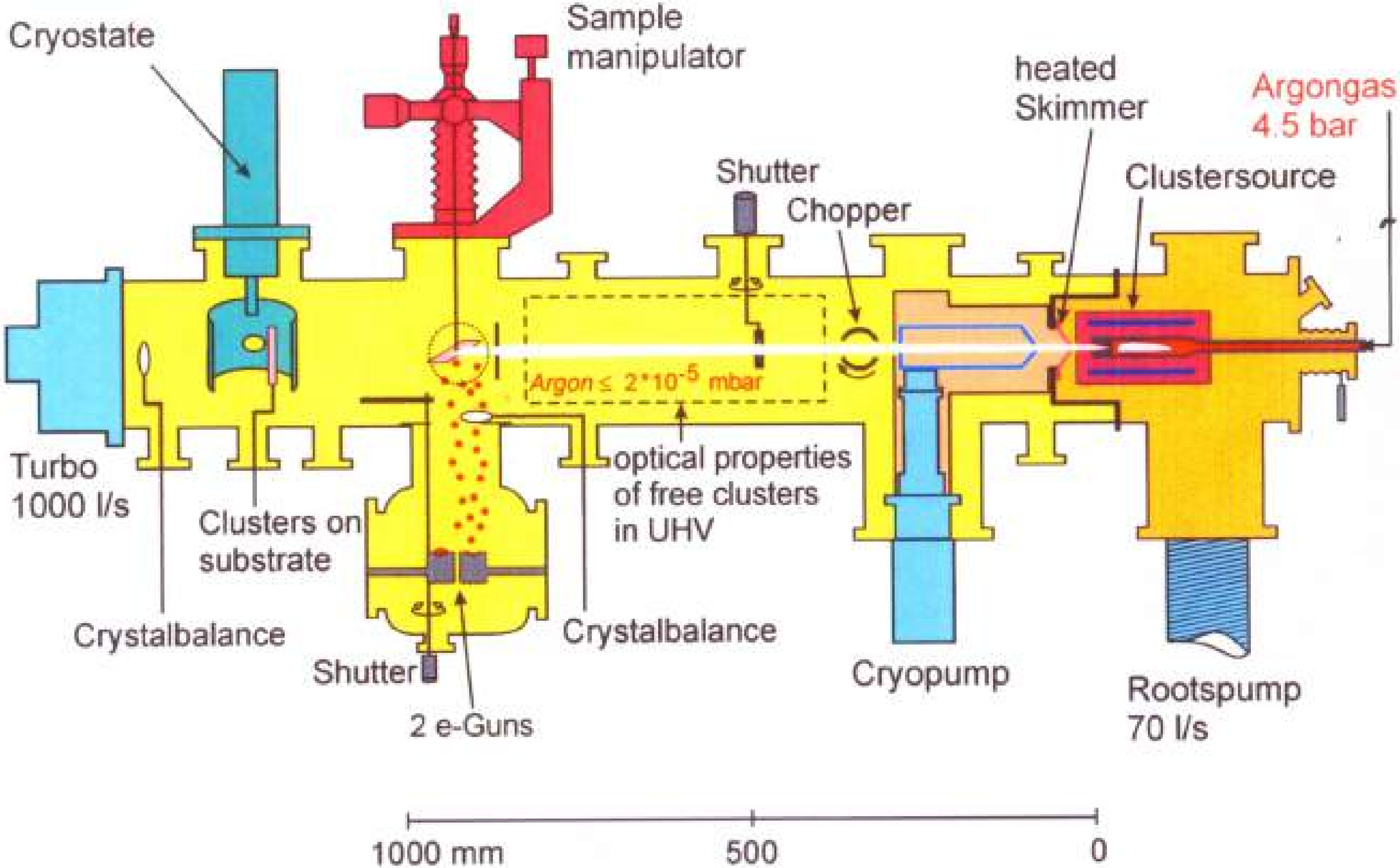

characterisation by AFM and TEM

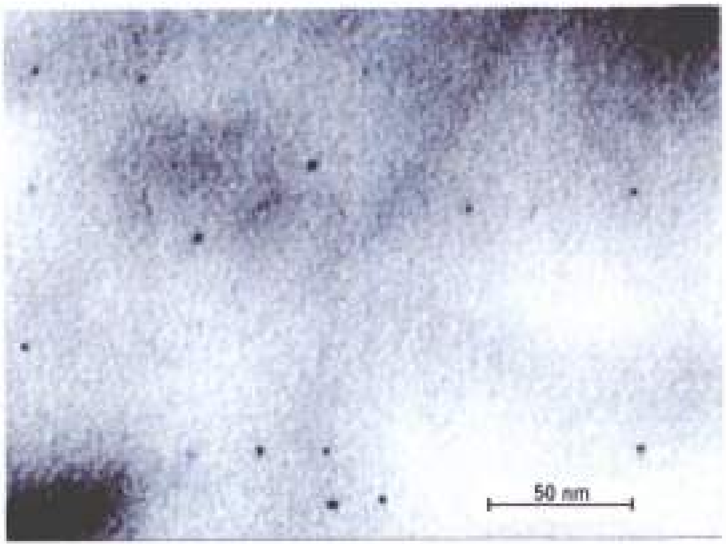

TEM - picture of silver clusters

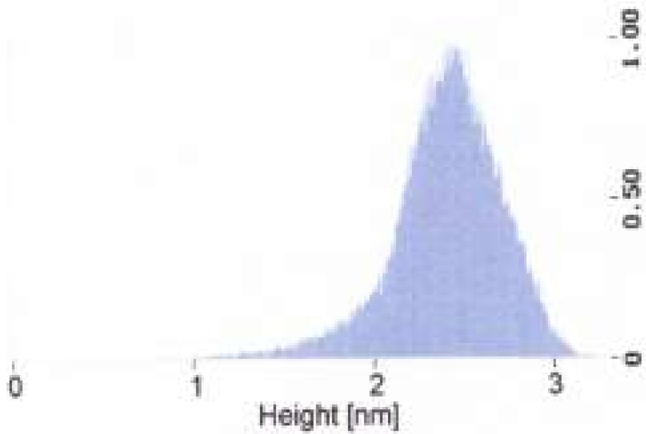

Height distribution by AFM

Size distribution of silver clusters

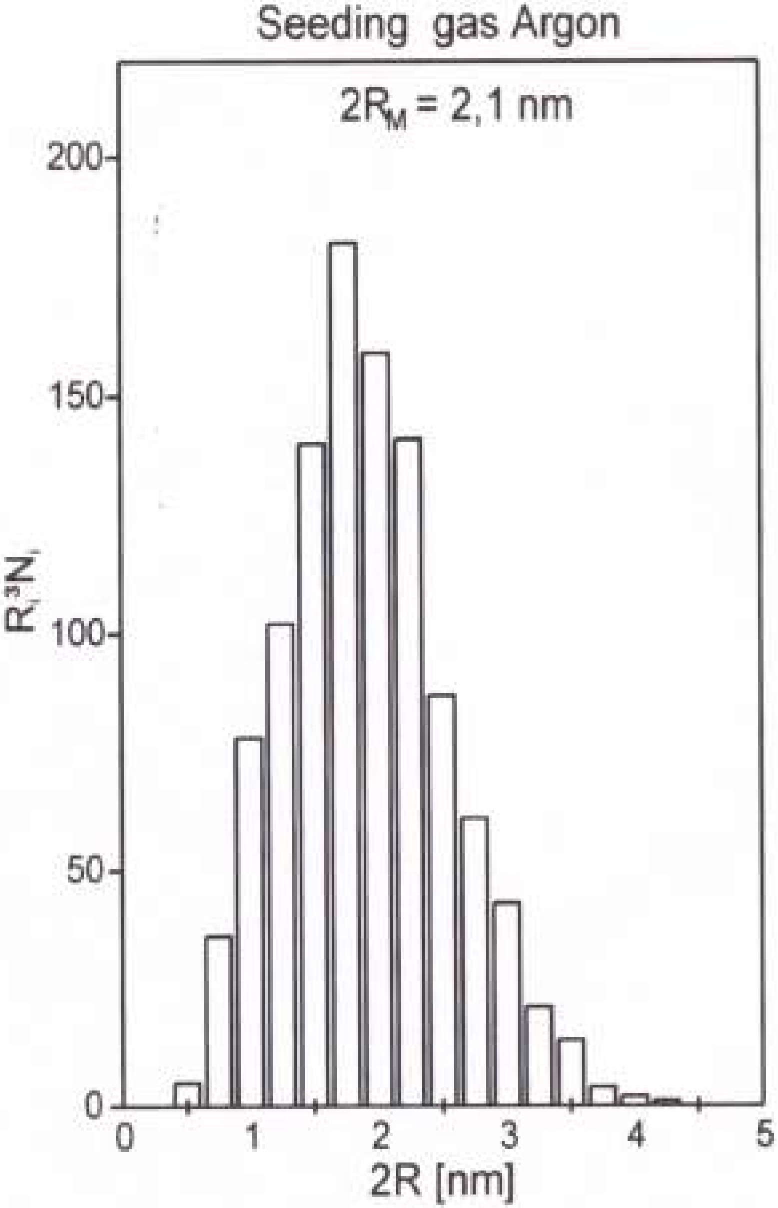

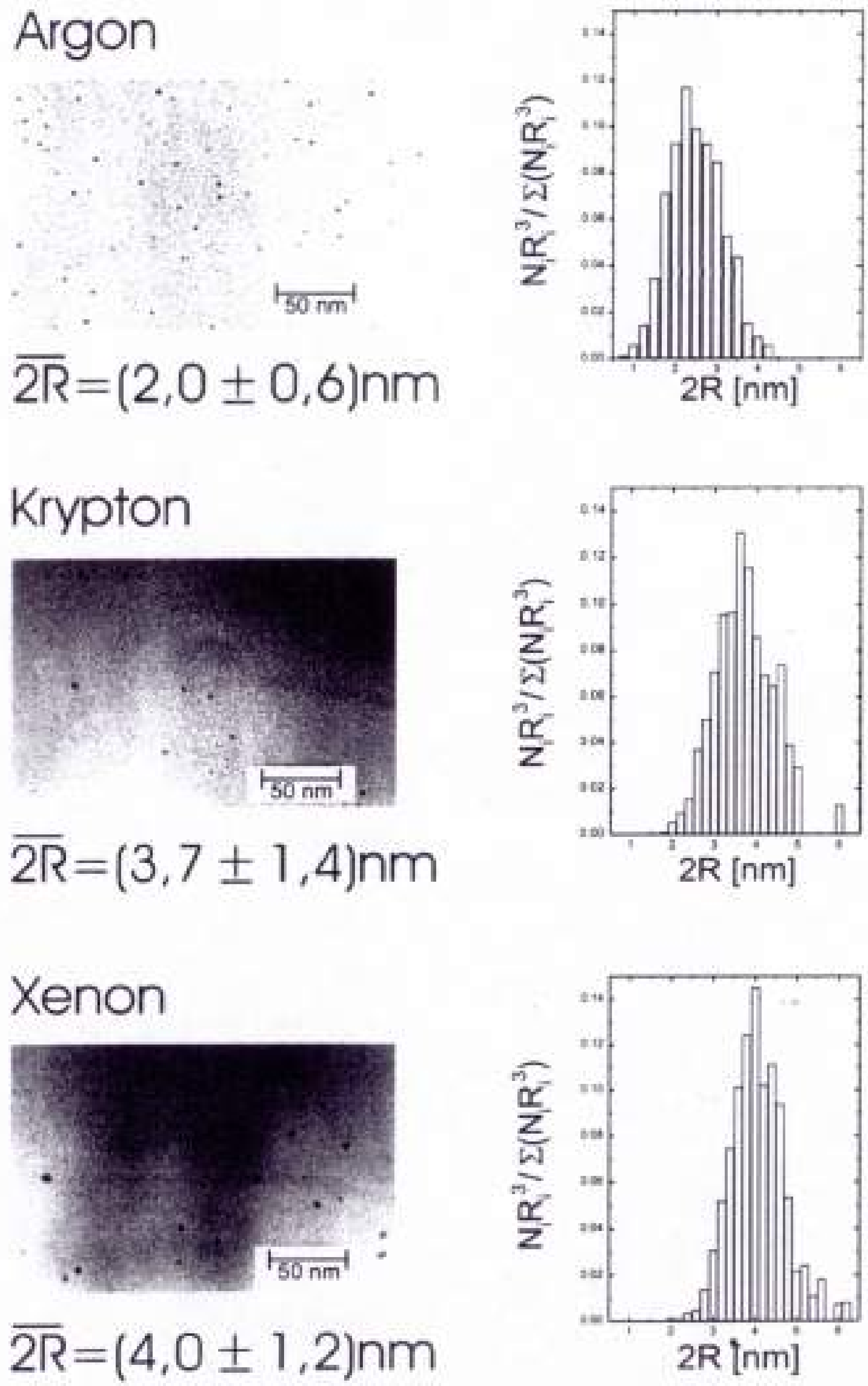

Argon
50 nm
$\overline{2R} = (2{,}0 \pm 0{,}6)$nm
$N_iR_i^3/\Sigma(N_iR_i^3)$
2R [nm]
Krypton
50 nm
$\overline{2R} = (3{,}7 \pm 1{,}4)$nm
$N_iR_i^3/\Sigma(N_iR_i^3)$
2R [nm]
Xenon
50 nm
$\overline{2R} = (4{,}0 \pm 1{,}2)$nm
$N_iR_i^3/\Sigma(N_iR_i^3)$
2R [nm]

MIE - PLASMON - POLARITON LIFETIMES :
(Phase relaxation times)

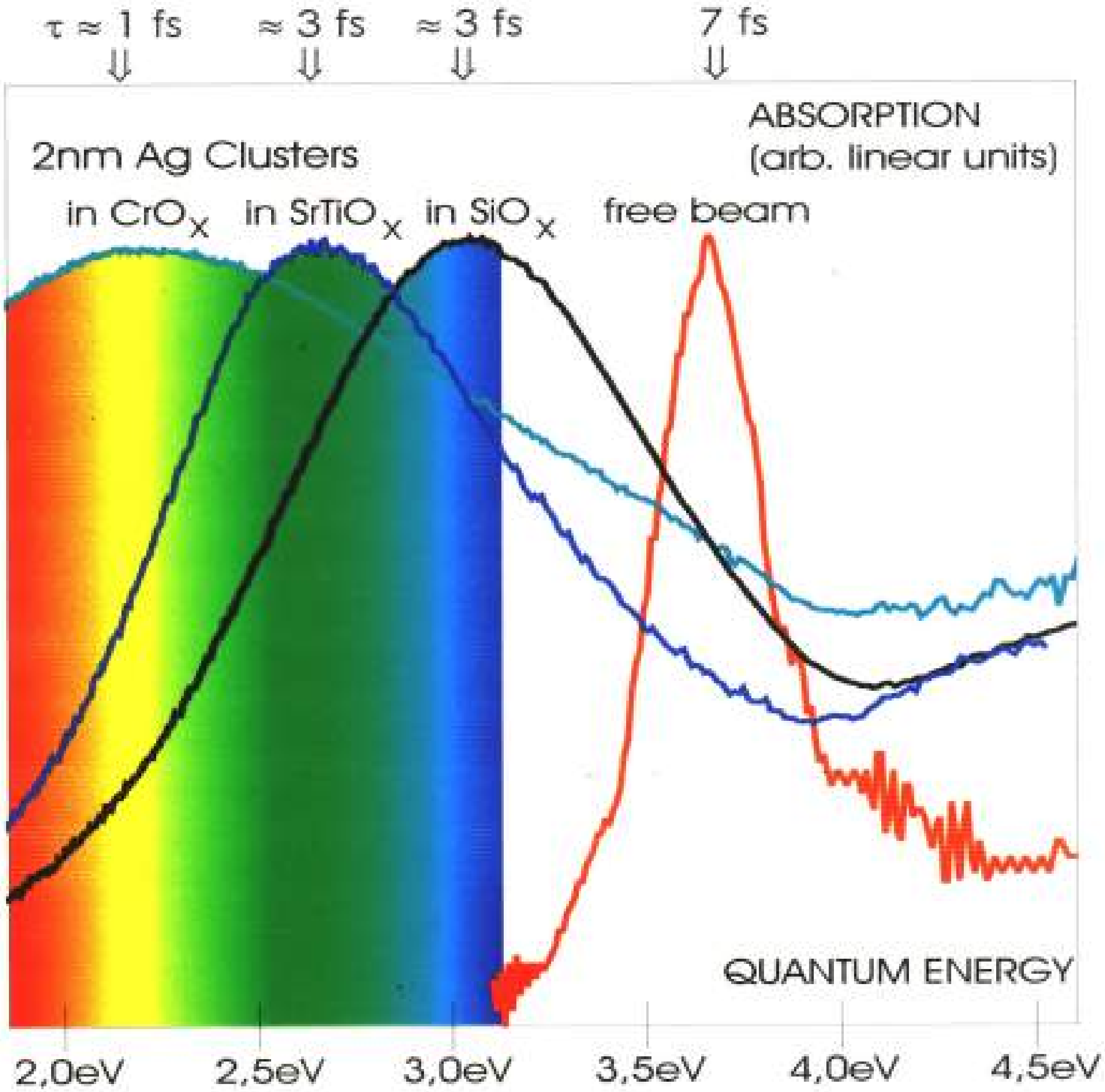

(Hilger et al. *Handbook of Optics*, ed.Hummel,Wissmann, CRC 1997)

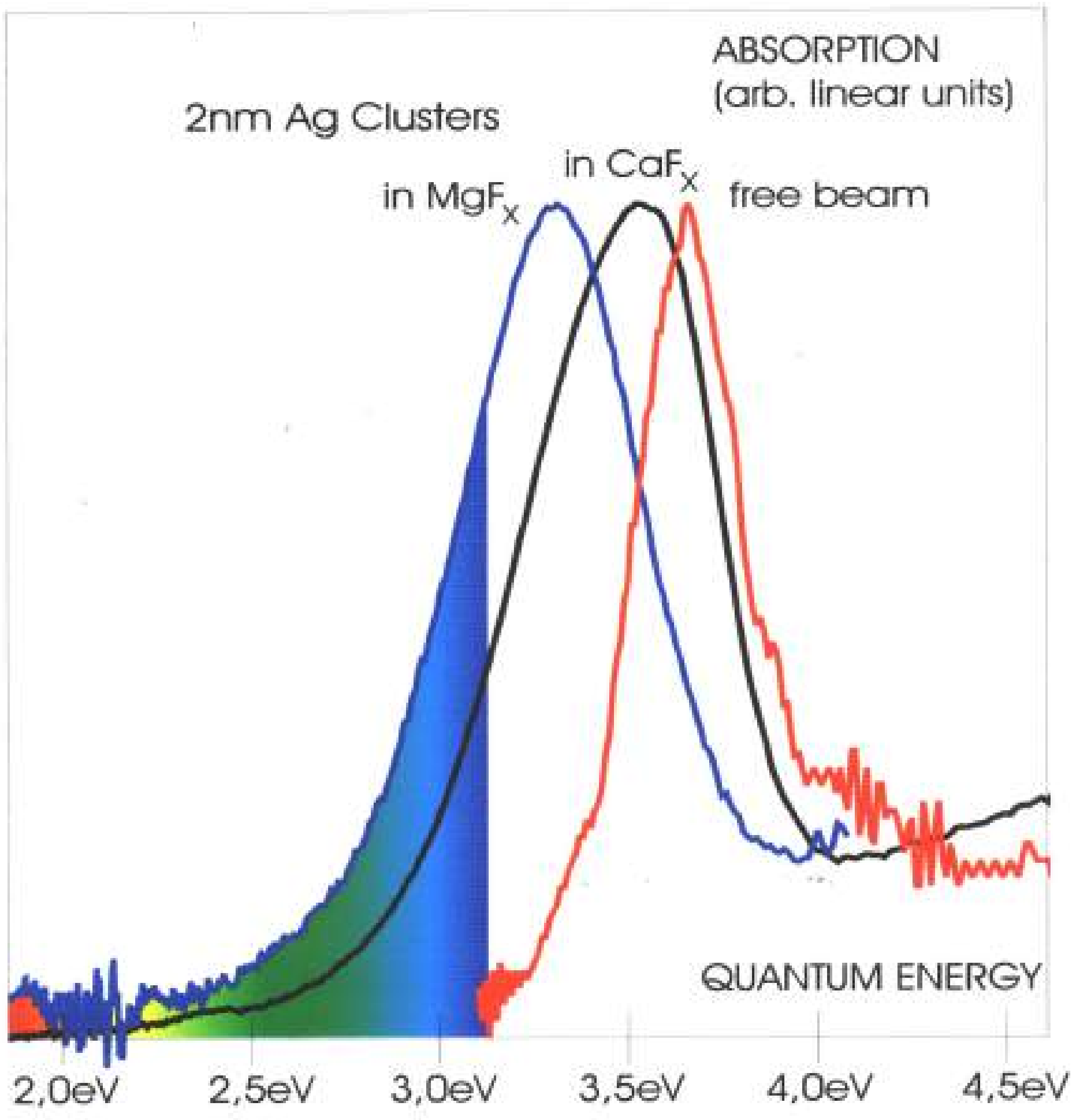

(Hilger et al. Eur.Phys.J. 2000)

A-PARAMETERS OF AG-CLUSTERS IN VARIOUS MEDIA

Data : *Theory* : Persson et al. (1994)
Experiments: *Solid gases*: Schulze et al. (1984)
Other solid media: Kreibig (1970); Cüppers, Fröba, Gartz, Hilger, Hövel, Maaß, Nusch, Pidun, Relitzki, Sonntag, Tenfelde (papers, theses, diploma works 1994 -99)

Matrix material	Theory	Experiment	Mie plasmon lifetimes
Free clusters	0.29	0.25	7 f s (2R=2 nm)
Solid Ne	0.29	0.25	
Ar		0.3	
O_2	0.6	0.5	
CO_2	1.1	0.9	
Na-Si-O-glass	1.0	1.0	
Ice		0.5	
Li $F_{(x)}$		0.72	
$CaF_{2(-x)}$		0.76	
$MgF_{2(-x)}$		0.80	
Fullerite (C_{60})		1.0	
$SiO_{2(-x)}$		1.3	
ITO		1.5	
$SrTiO_x$		1.5	
$Al_2O_{3(-x)}$		1.7	
$TiO_{2(-x)}$		1.8	
$P(C_6H_5)_3$		2.0	
SbO_x		2.0	
Si (+O impurities)		≈ 3.0	0.6 f s (2R=2 nm)
CrO_x		≈ 3.0	
Substrates			
$MgF_{2(-x)}$		0.55	
ITO		0.57	
SiO_2 (110K)		0.55	
SiO_2 (300K)		0.59	
CrO_x		0.59	

(U.Kreibig, M.Gartz, A.Hilger
Ber. Bunsenges.Phys.Chem. 1997)

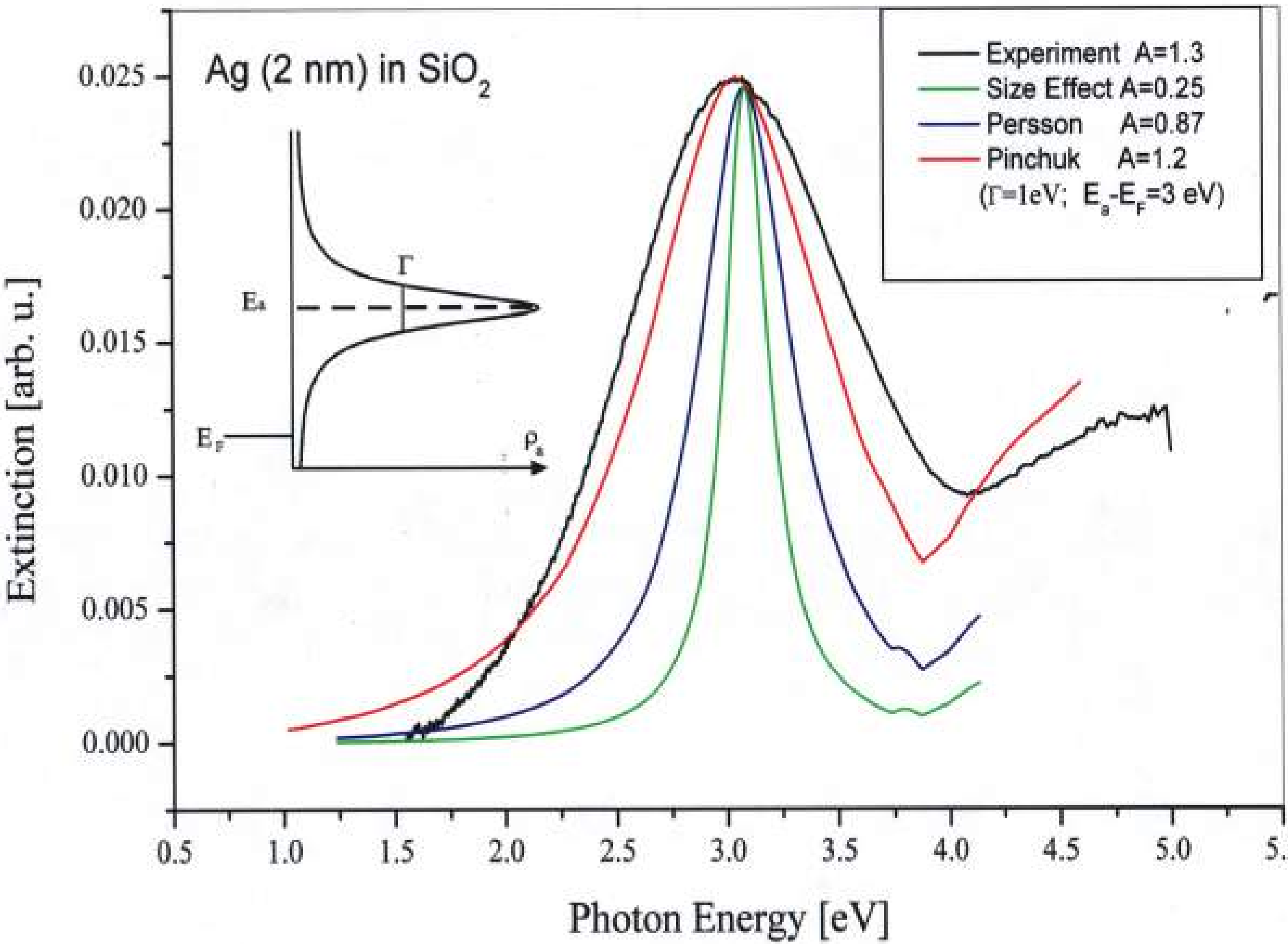

Ag (2 nm) in SiO2
Experiment A=1.3
Size Effect A=0.25
Persson A=0.87
Pinchuk A=1.2
(Γ=1eV; Ea-EF=3 eV)
Γ
Ea
EF
ρa
0.025
0.020
0.015
0.010
0.005
0.000
Extinction [arb. u.]
0.5
1.0
1.5
2.0
2.5
3.0
3.5
4.0
4.5
5.0
5.5
Photon Energy [eV]

MIE - PLASMON - POLARITON: PHASEN - ZERFALL DURCH DYNAMISCHEN LADUNGSTRANSFER

$$dN_{kohärent} / N_{kohärent} \Rightarrow \exp\{-t / \tau_{Phase}\}$$

Dephasierungszeit τ_{Phase} :

$1 / \tau_{Phase} \approx$ (Oberflächen-Stoßhäufigkeit) • (Übergangswahrscheinlichkeit in Adsorbat-levels)

$$1 / \tau_{Phase} \approx (v_{Fermi} / R) \cdot A_{interface}$$

$$A_{interface} = F \cdot \Phi \cdot \rho(E_{Fermi}) \cdot T$$

Φ = **Adsorbat-Oberflächenbedeckung**

$\rho(E_{Fermi})$ = **Dichte der unbesetzten Adsorbat-Zustände nahe E_{Fermi}**

T = **Grenzschicht-Transferwahrscheinlichkeit**
= 1 (ohne Tunnelbarriere)
< 1 (mit Tunnelbarriere)

F = **Normierungsfaktor**

PLASMONEN - ZERFALL :

ENERGIE - DISSIPATION

KASKADEN VON ELEKTRON-LOCH-ANREGUNGEN

ELEKTRON-GITTER-ANREGUNGEN

ELEKTRON-GITTERFEHLER

IMPULS - RELAXATION

„ELASTISCHE“ WECHSEL-WIRKUNGEN

PHASEN - RELAXATION

ZERSTÖRUNG DER KOHÄRENZ DER KOLLEKTIVEN LEITUNGS-ELEKTRONEN-ANREGUNG (MIE-PLASMONEN)

HIERARCHY OF RELAXATION-TIMES :

Phase Relaxation > Momentum Relaxation > Energy Relaxation

EXPERIMENTAL NUMBERS (Ag, Au Nanos):

(1) Electron - Lattice Relaxation
(fs-spectroscopy : Perner et al (1997)) **$1 - 10^2$ ps**

(2) Electron - Electron Relaxation
(fs-spectroscopy : Perner et al (1997)) **10^2 fs - 1 ps**

(3) Phase relaxation, De-phasing, De-coherence **1 - 15 fs**
(Lamprecht et al (1997) SHG autocorrelation)
(Kreibig et al (1997) optical, variation with surrounding media)
(Klar et al (1998) single nano in TiO_2)
(Rubahn et al (1998) optical)
(v. Plessen et al (1998) near field, hom. bandwidth)
(Lamprecht et al (1999) THG autocorrelation) 1999)
(Stietz et al (2000) "hole burning")

MIE-PEAK POSITIONS OF FLUORIDES AND OXIDES :

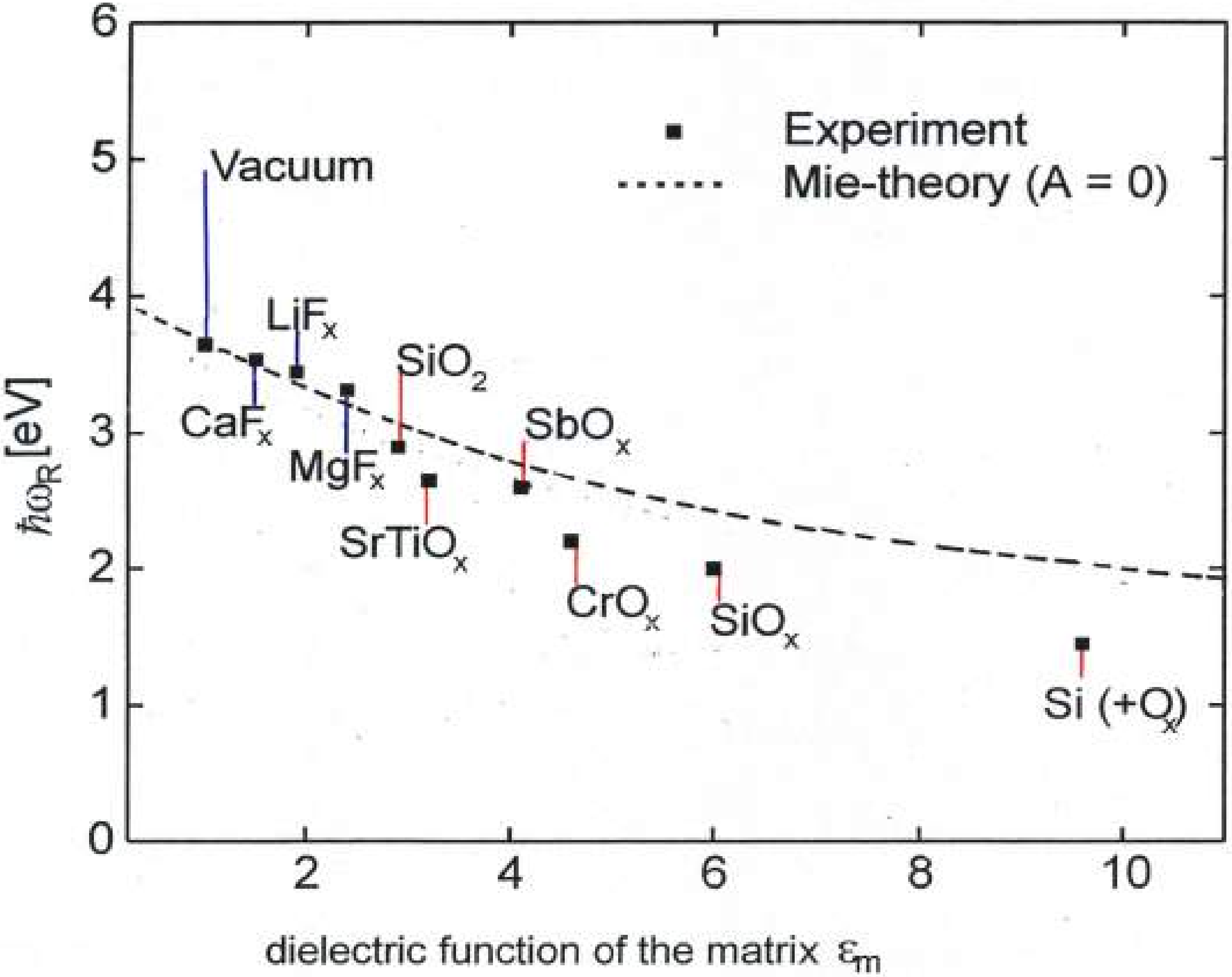

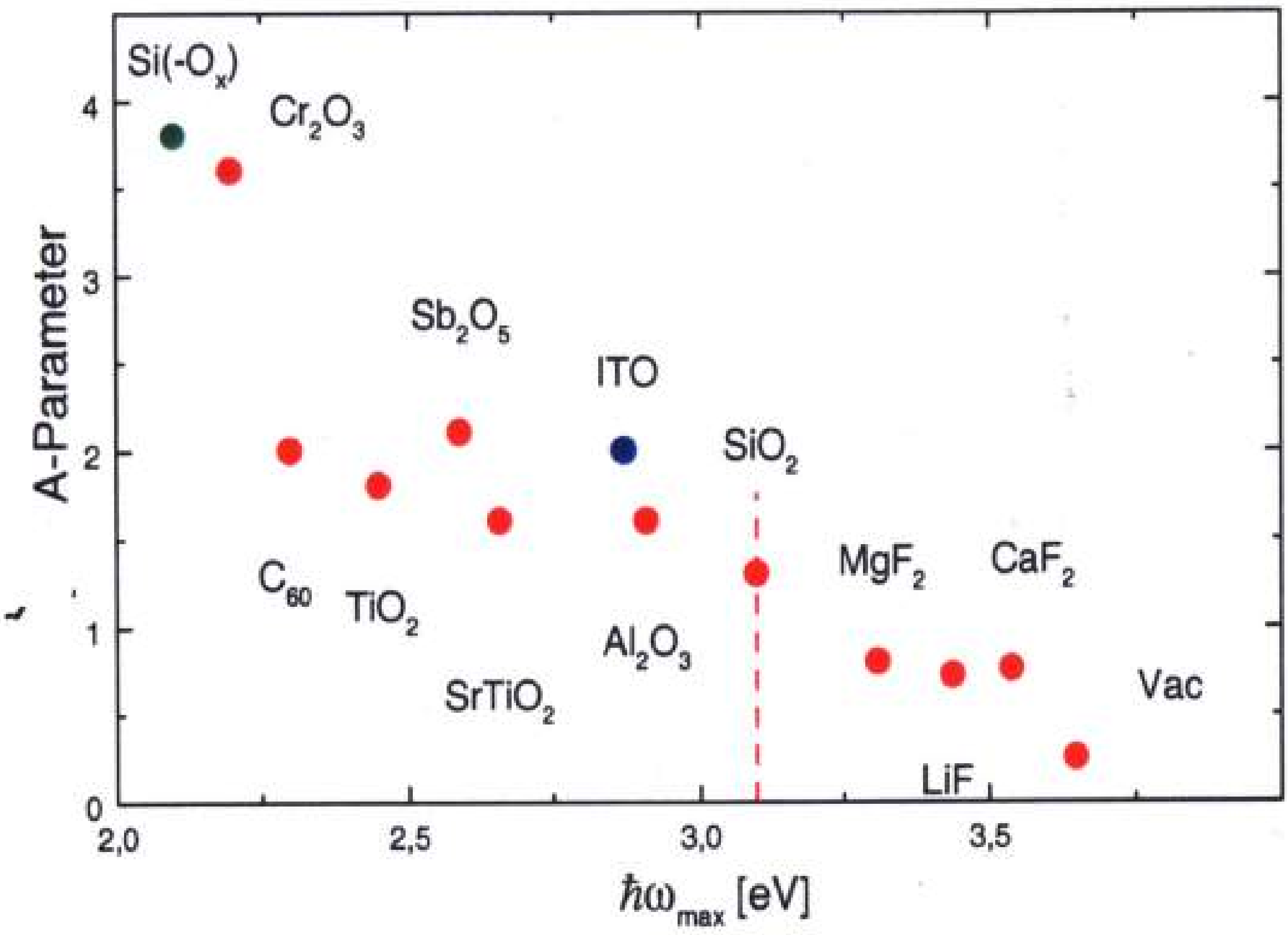

Si(-Ox)
Cr2O3
Sb2O5
ITO
SiO2
MgF2
CaF2
C60
TiO2
Al2O3
SrTiO2
Vac
LiF
A-Parameter
0
1
2
3
4
2,0
2,5
3,0
3,5
ħω max [eV]

STATIC VERSUS DYNAMIC CHARGE TRANSFER

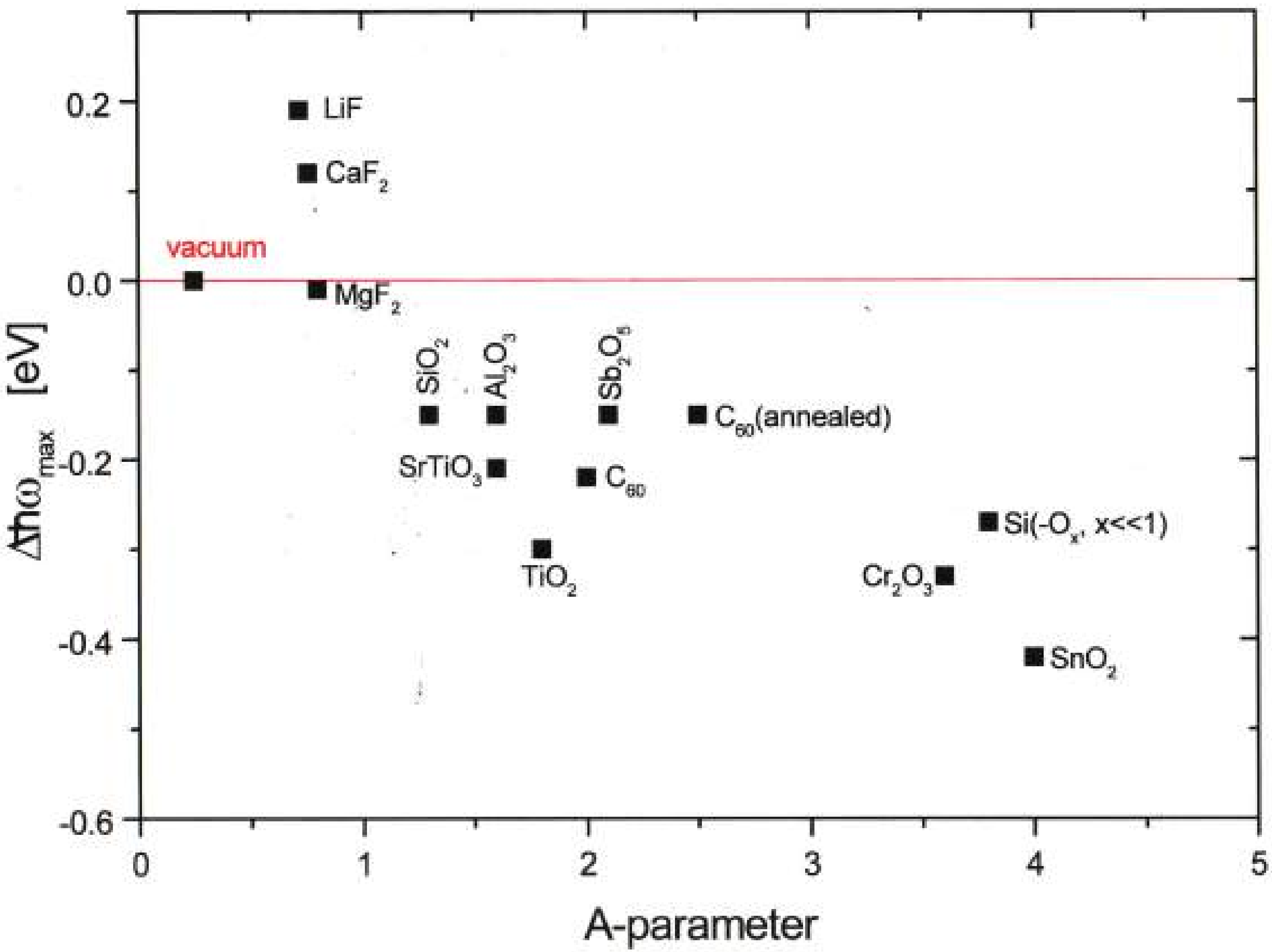

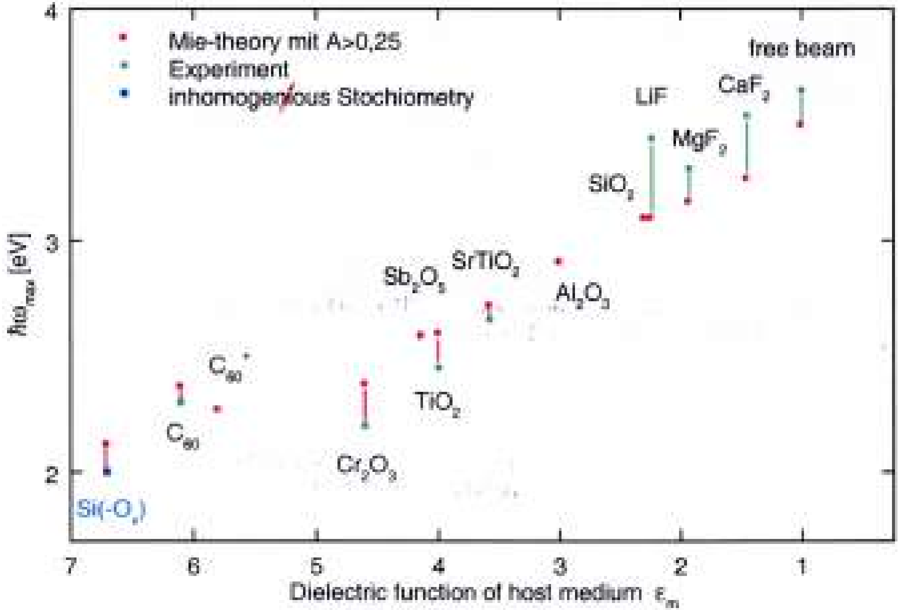

Abbildung 4.26: Silbercluster der Größe $\overline{2R}$=2nm im freien Strahl und eingebettet in Oxide und Fluoride. Aufgetragen ist die Lage der gemessenen Mie-Resonanz $\hbar\omega_{max}$ gegenüber der dielektrischen Funktion der Umgebung ε_m. Der shift von Δ=0,15eV im freien Strahl tritt in der gleichen Richtung beim Einbetten in Fluoride auf. Die Richtung des shifts kehrt sich bei der Einbettung in Oxide um. Die Materialien ITO, In_2O_3 und SnO_2 wurden ausgeschlossen, da eine Ag-Legierungsbildung bei Indium-Zinn-Oxid (ITO) nachgewiesen werden konnte.

NANOPARTICLES

ON

SUBSTRATES

Ag - clusters on SiO_2 - substrate at T = 110 K produced with different seeding gases (experiment)

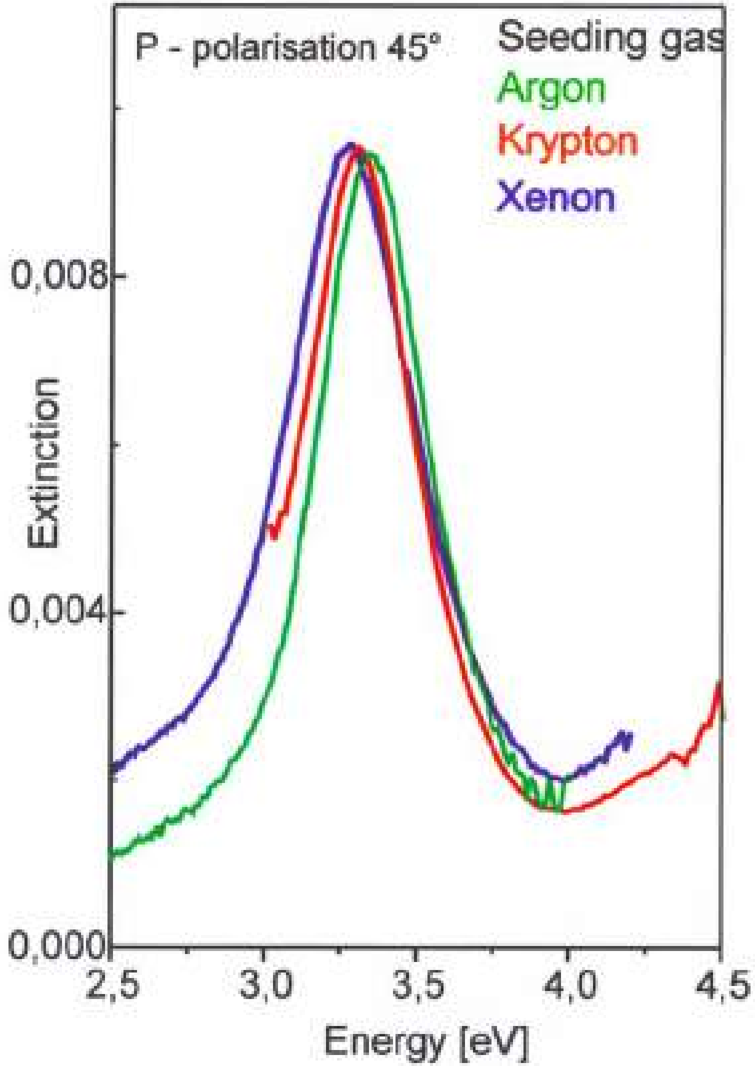

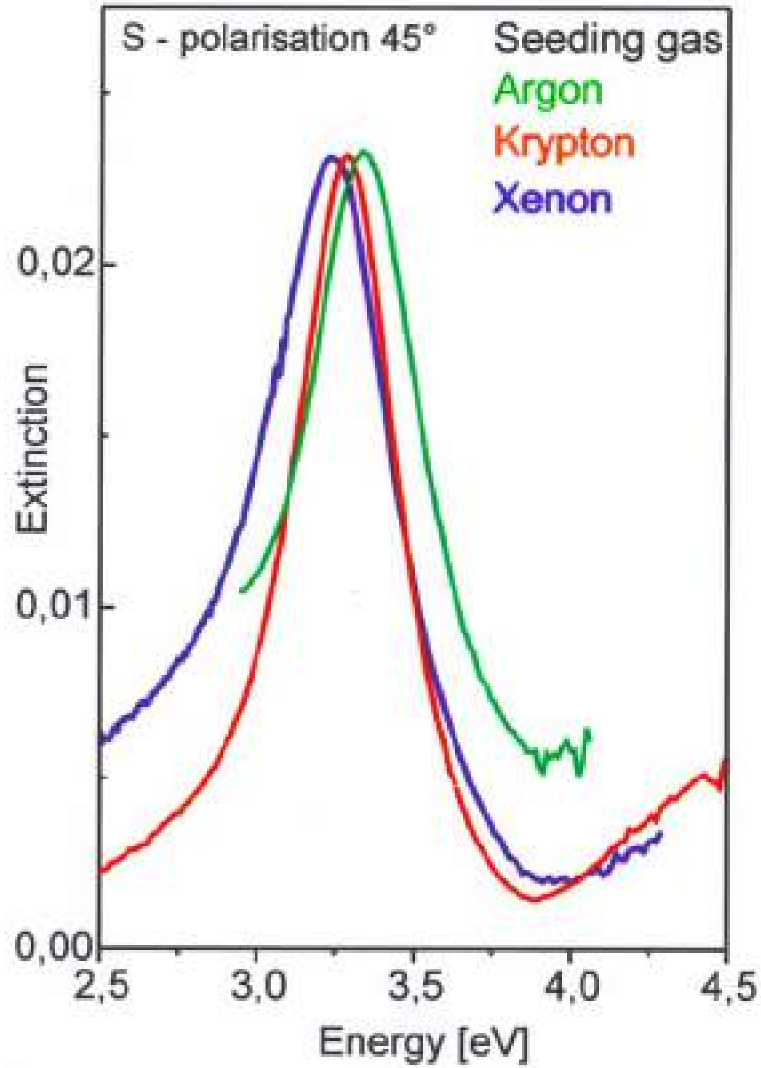

Deposition on different Substrates :

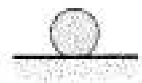

Experiment: P - Polarisation 45°

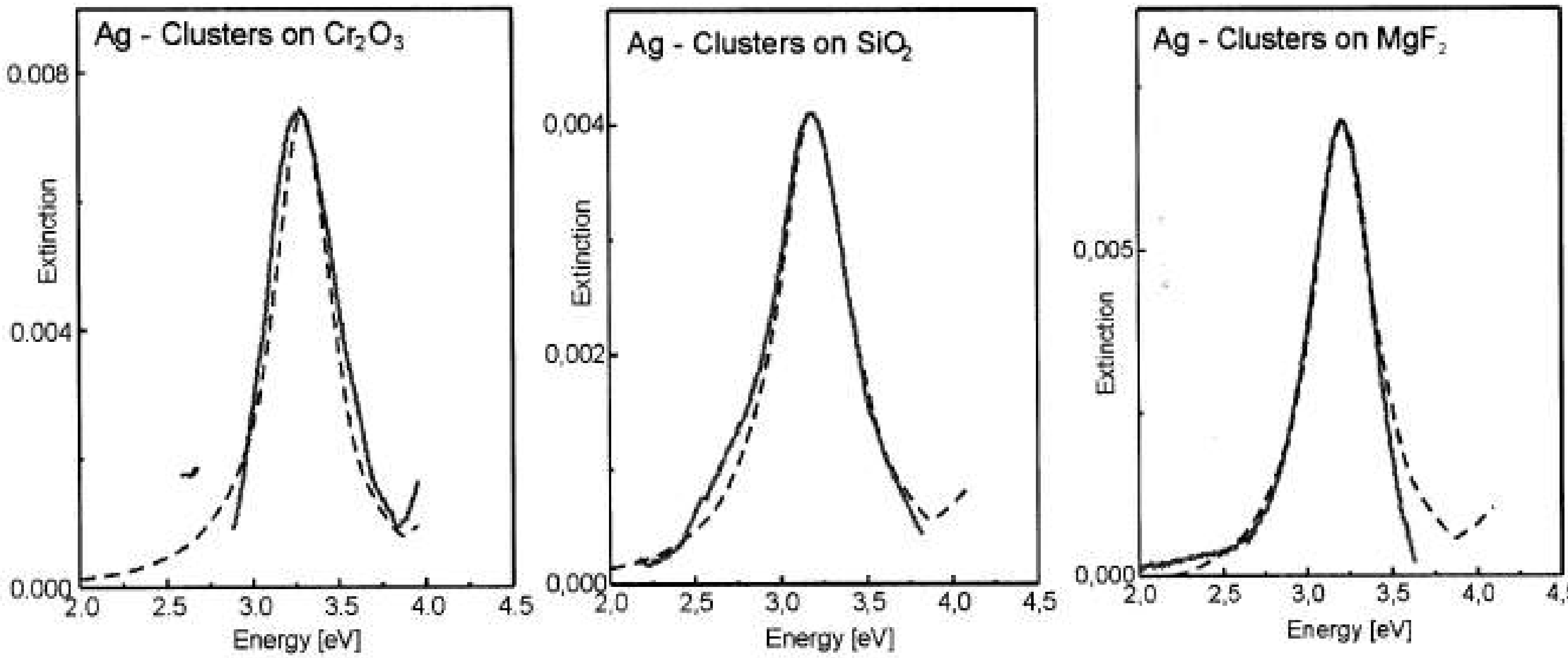

A - Parameter: A = 0,55 - 0,6

verschiedene_Substrate.cdr

CONTACT AREAS OF SILVER-CLUSTERS DEPOSITED ON VARIOUS SUBSTRATES

(M. Tenfelde, Diploma work Aachen 1999)

Substrate	MgF_x ($x \approx 2$)	SiO_x ($x \approx 2$)	Cr_2O_x ($x \approx 3$)
Contact Area (Interface)	15 %	9.5 %	< 3 %
A - Parameter (Deposition)	0.55	0.59	0.59
A - Parameter (Embedding)	0.83	1.3	3.0

Temperature Dependence of the Mie Absorption Peak :

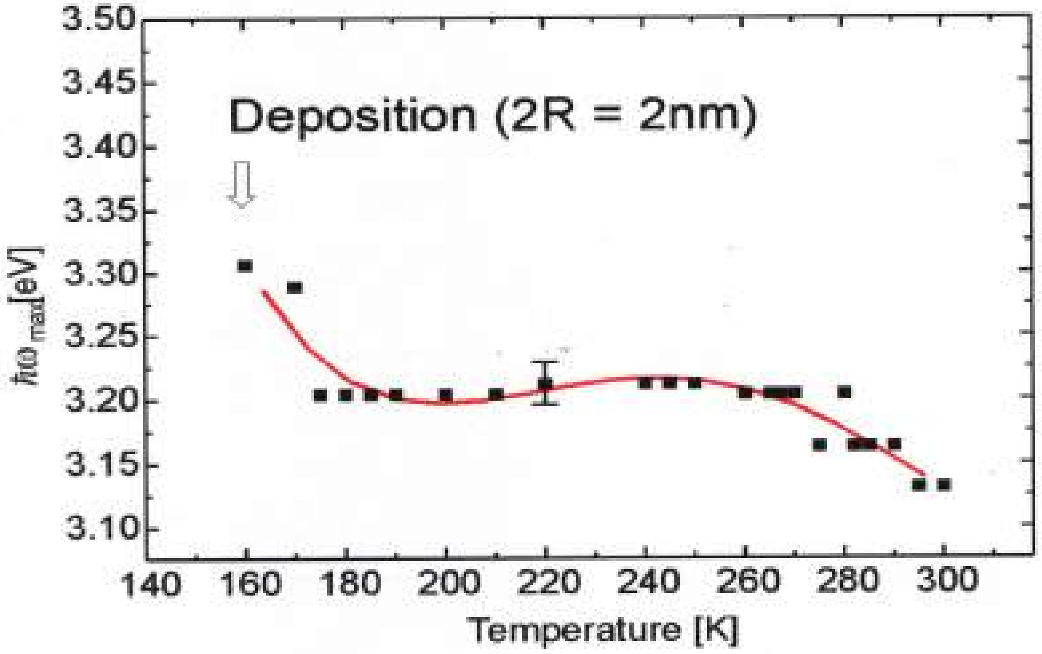

- increasing ellipticity
- increasing contact area

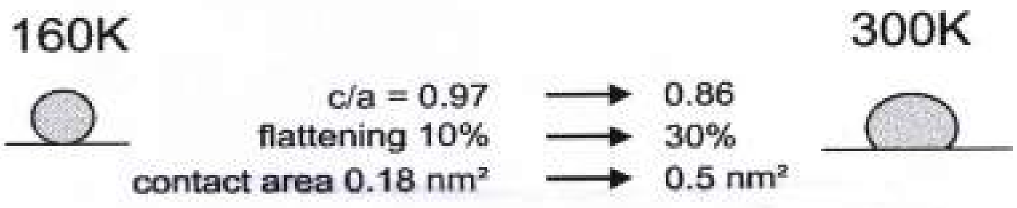

CHEMICAL REACTIONS

ON

NANOPARTICLE

SURFACES / INTERFACES

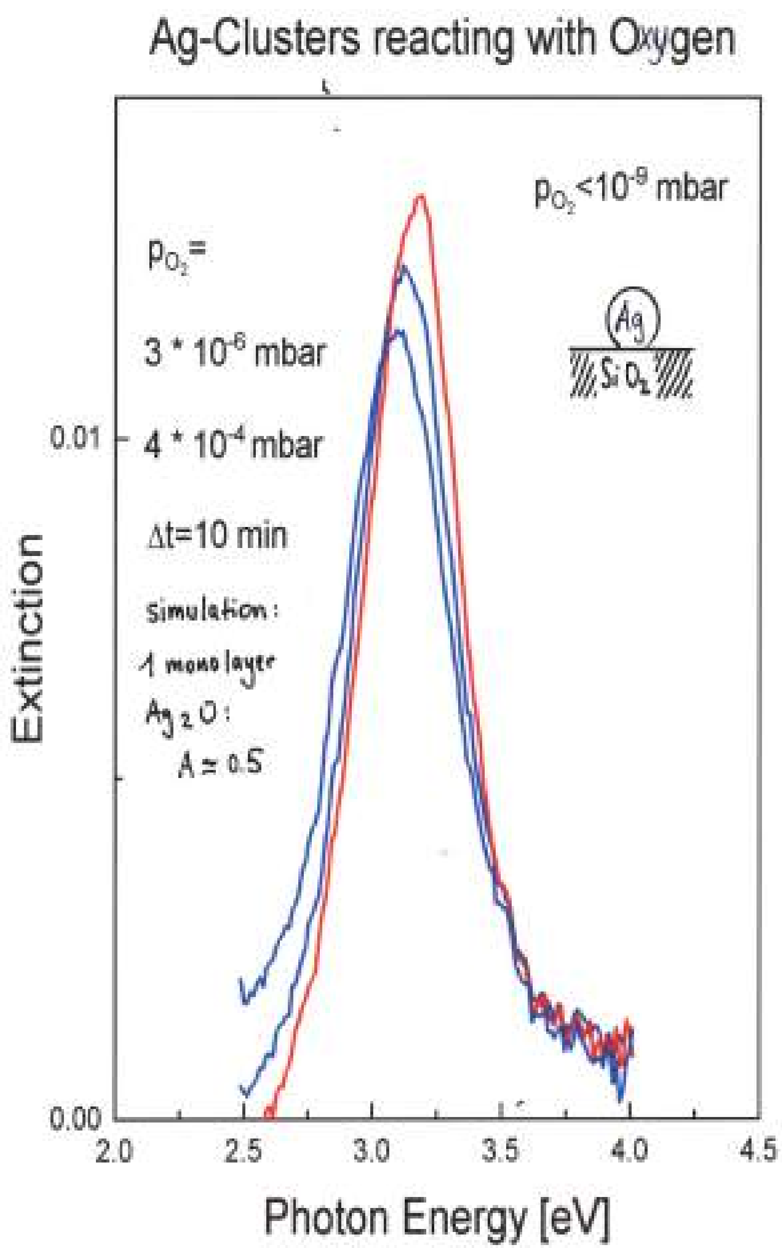

Ag-Clusters reacting with Oxygen
p_{O_2}<10^-9 mbar
p_{O_2}=
3 * 10^-6 mbar
4 * 10^-4 mbar
Δt=10 min
simulation:
1 monolayer
Ag2O:
A ≈ 0.5
Ag
SiO2
Extinction
0.01
0.00
2.0
2.5
3.0
3.5
4.0
4.5
Photon Energy [eV]

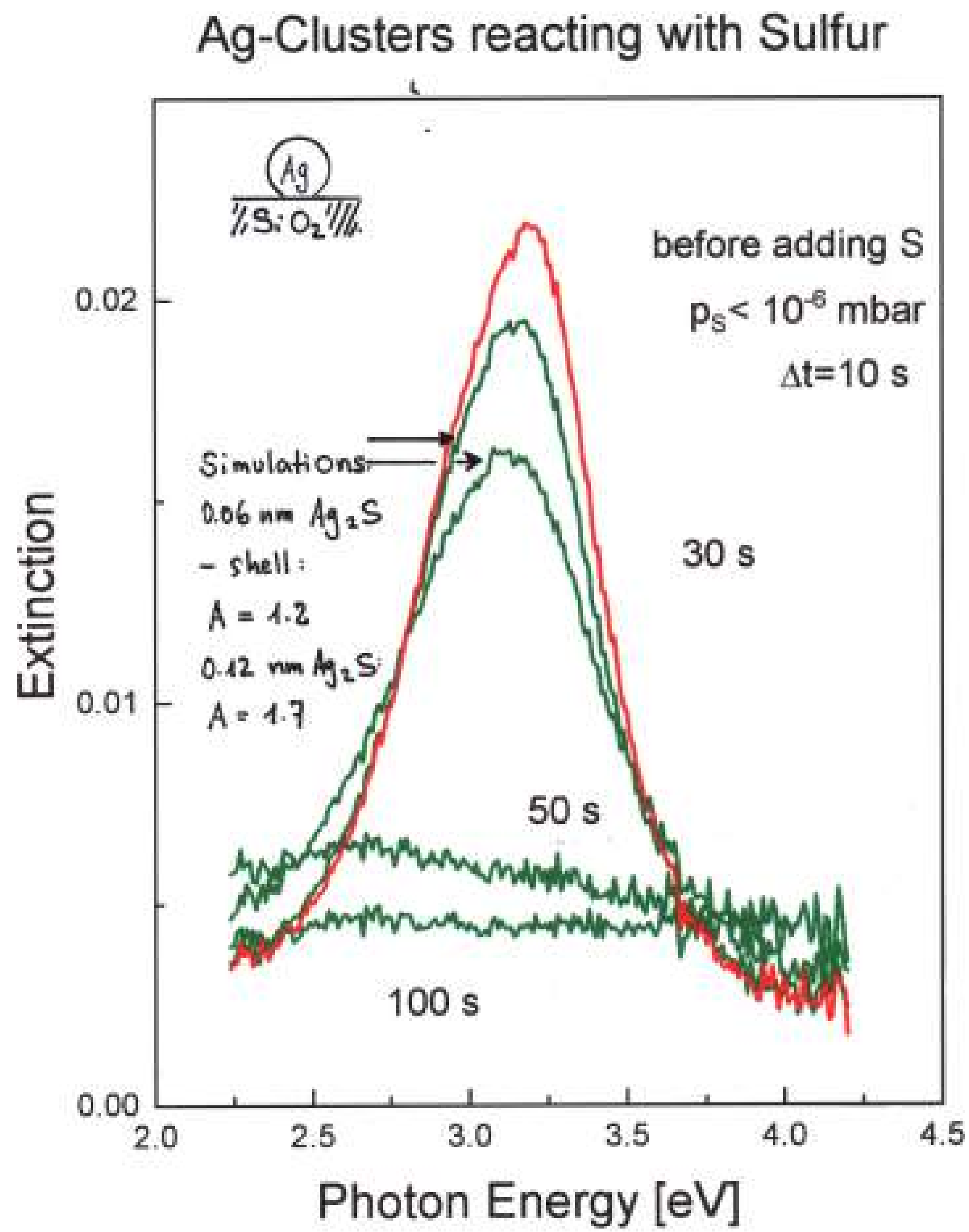

Ag-Clusters reacting with Sulfur
Ag
SiO2
before adding S
p_S< 10^-6 mbar
Δt=10 s
Simulations
0.06 nm Ag2S
- shell:
A = 1.2
0.12 nm Ag2S
A = 1.7
30 s
50 s
100 s
Extinction
0.02
0.01
0.00
2.0
2.5
3.0
3.5
4.0
4.5
Photon Energy [eV]

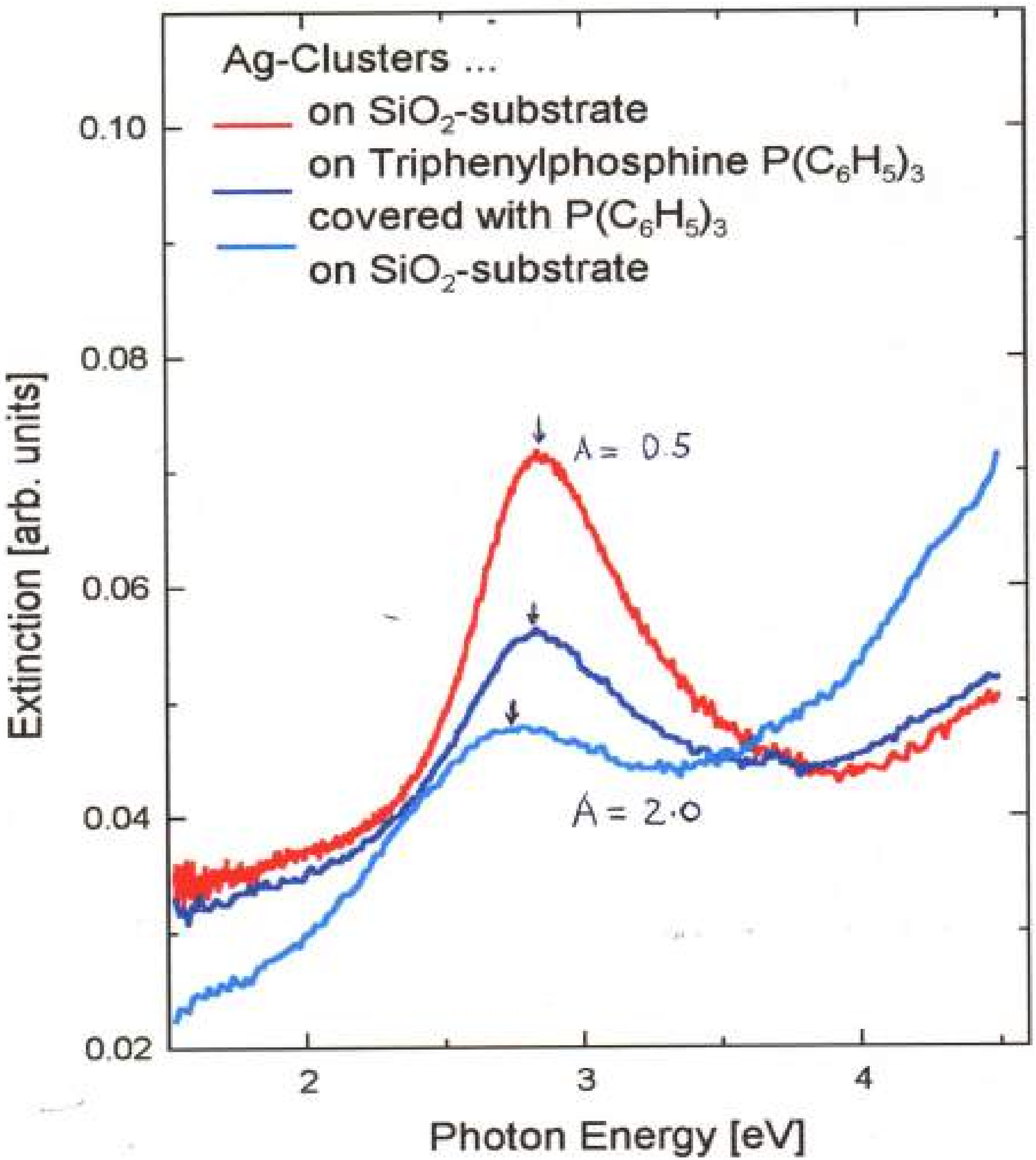

Ag-Clusters ...
on SiO_2-substrate
on Triphenylphosphine $P(C_6H_5)_3$
covered with $P(C_6H_5)_3$
on SiO_2-substrate
A = 0.5
A = 2.0
Extinction [arb. units]
Photon Energy [eV]
0.10
0.08
0.06
0.04
0.02
2
3
4

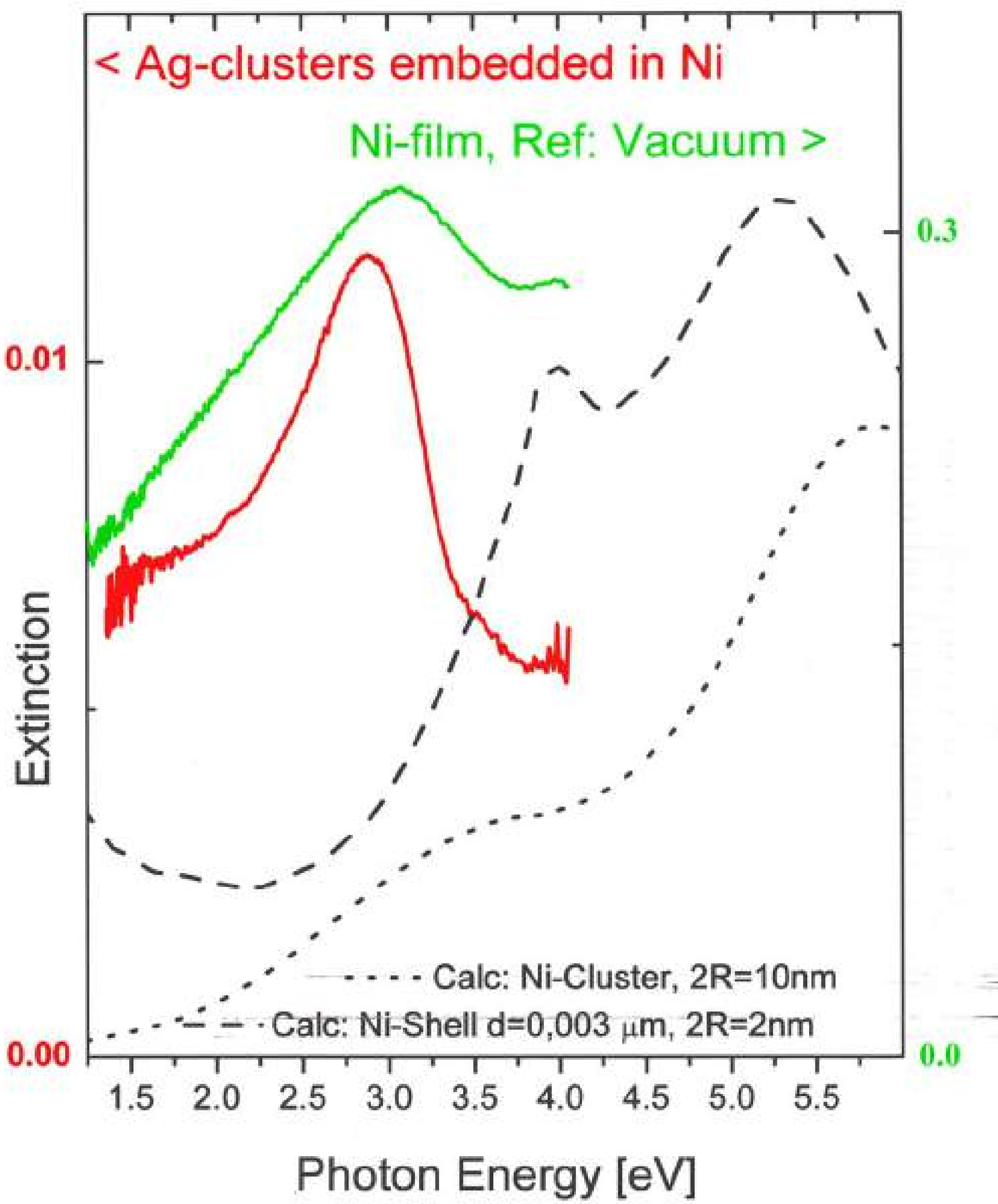

< Ag-clusters embedded in Ni
Ni-film, Ref: Vacuum >
0.01
0.00
0.3
0.0
Extinction
Calc: Ni-Cluster, 2R=10nm
Calc: Ni-Shell d=0,003 μm, 2R=2nm
1.5
2.0
2.5
3.0
3.5
4.0
4.5
5.0
5.5
Photon Energy [eV]

ELECTRODYNAMIC COUPLING

AMONG

DENSELY PACKED PARTICLES

IN

MANY-PARTICLE-SYSTEMS :

THE GENERALIZED MIE -THEORY

(GMT)

WEAK SELF-ASSEMBLY OF LIGAND-STABILIZED AU-CLUSTERS
(Kreibig, Schmid)

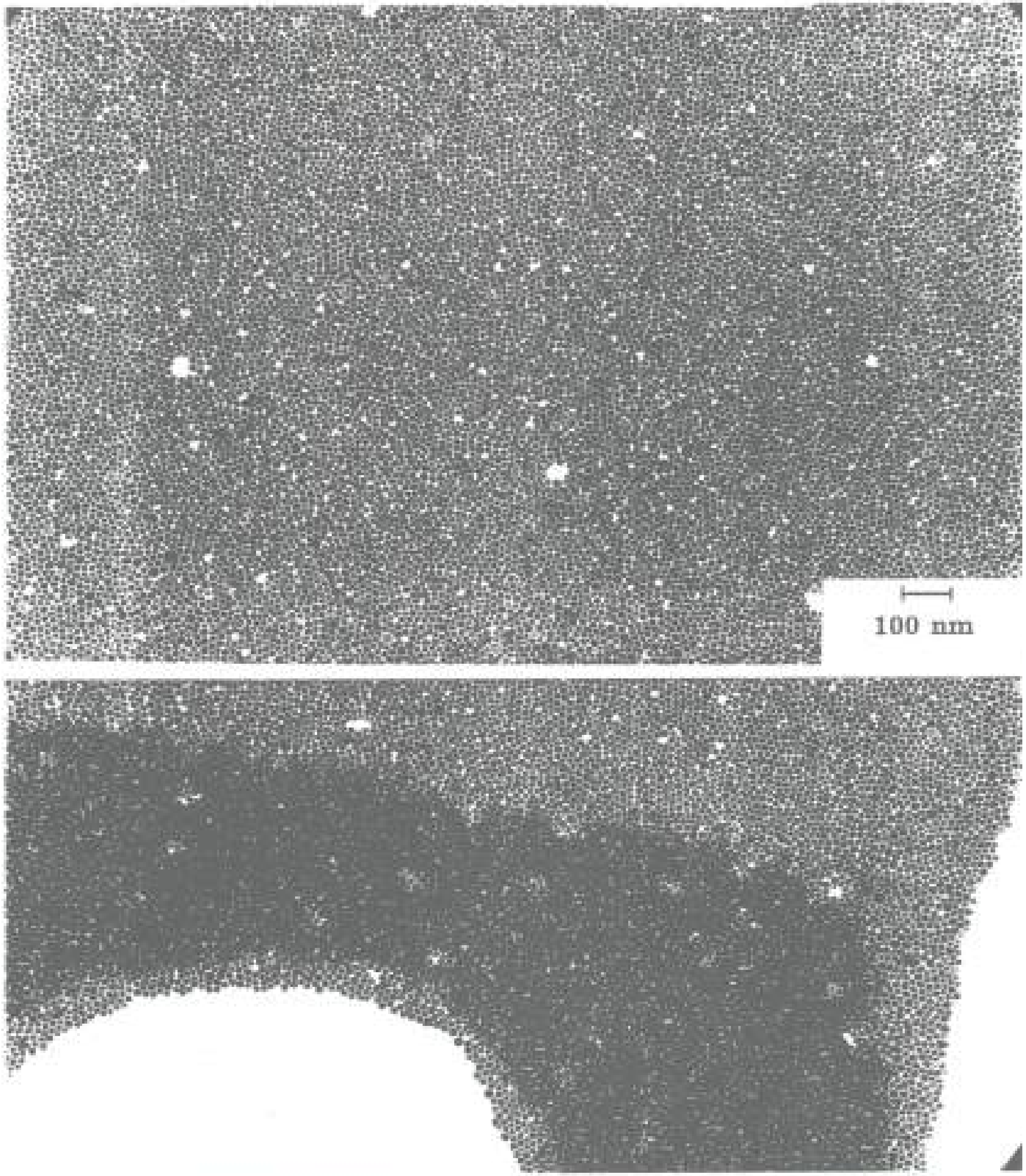

QUASI-FRACTAL AU-PARTICLE ARRAYS
2R~20 nm; TPP-Stabilized; Scales 1:10

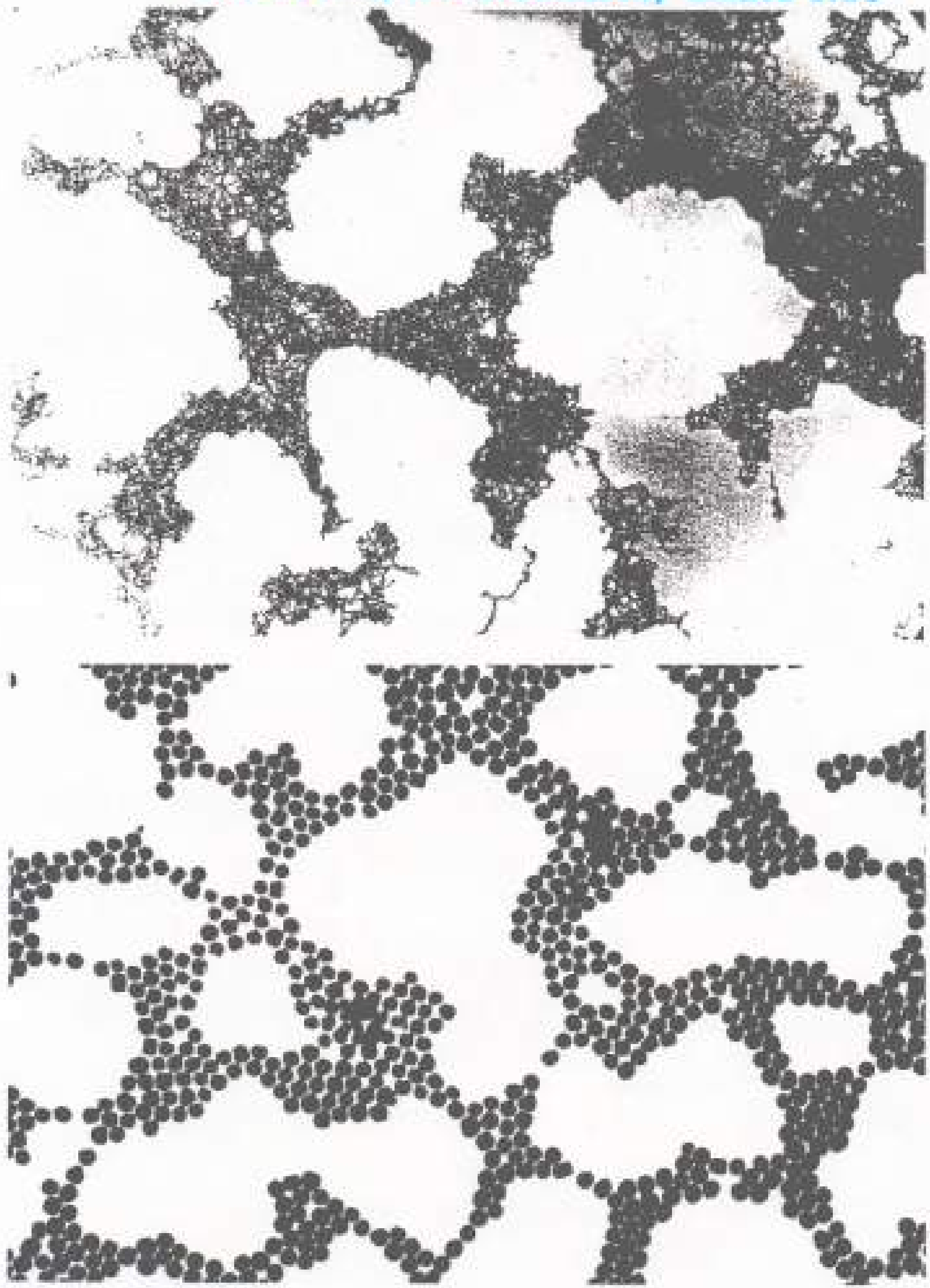

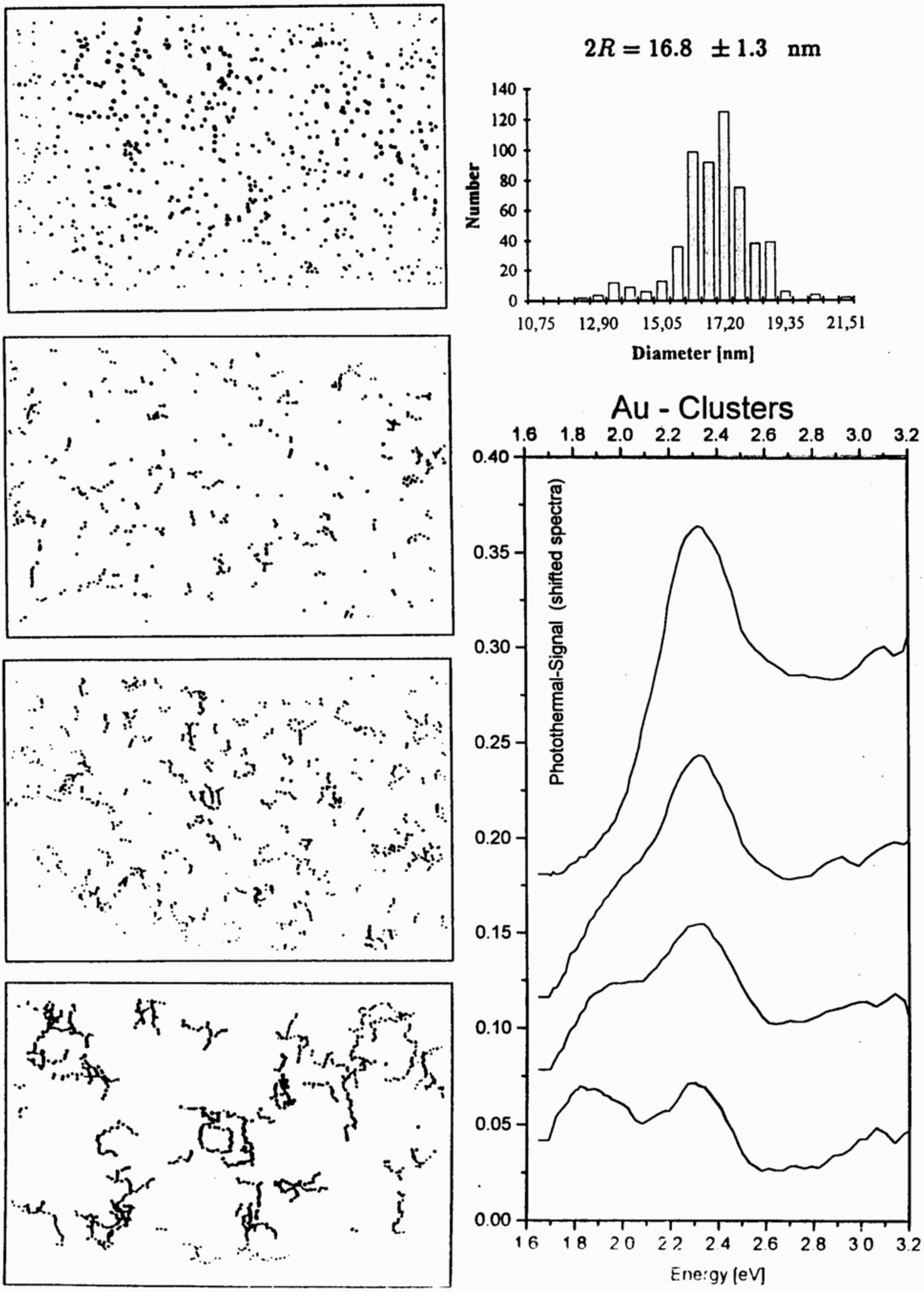

$2R = 16.8 \pm 1.3$ nm
Number
0
20
40
60
80
100
120
140
10,75
12,90
15,05
17,20
19,35
21,51
Diameter [nm]
Au - Clusters
Photothermal-Signal (shifted spectra)
0.00
0.05
0.10
0.15
0.20
0.25
0.30
0.35
0.40
1.6
1.8
2.0
2.2
2.4
2.6
2.8
3.0
3.2
Energy [eV]

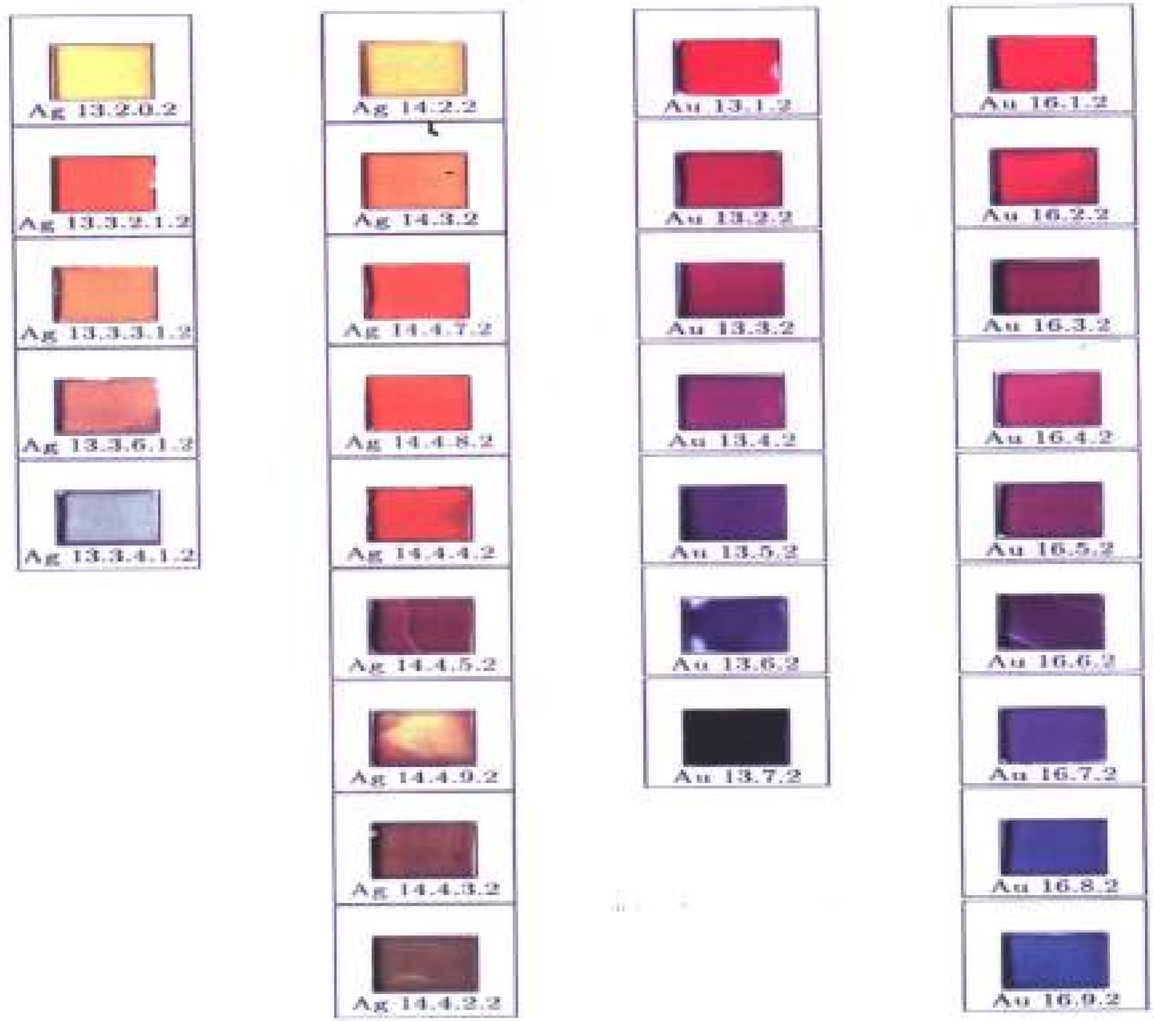

MIE-PLASMON-COUPLING
IN
CLUSTER-MATTER

ROWS: 1: Silver (23±3 nm); 2: Silver (20±3 nm);
3: Gold (17±2 nm); 4: Gold (10±1 nm)
VERTICAL: decreasing mean cluster distance

AGGREGATION UND KOALESZENZ

IN WÄSSRIGEN EDELMETALL - KOLLOIDEN

Diplomarbeit von Guido Reuter
I. Physikalisches Institut
der R W T H (1994)

REZEPTE :

(1) Zitrat - Methode (Gold)
(2) Zitrat Tannin - Methode (Gold)
(3) Zsigmondy'sche Keimmethode (Gold, Silber)

FÜLLFAKTOREN : f 10^{-5} - 10^{-6}

AGGREGATION :

Änderung des pH-Wertes : Verschiebung zum Sauren durch Beigabe von stark verdünnten wässrigen $CuSO_4$ - Lösungen .
Beispiel : Gold (15.5 nm) - Kettenaggregate 2 SPP - Moden
in Abhängigkeit von der mittleren Kettenlänge (1 - 20 Nanopartikel).

SPP - PEAK SHIFTS:

↑ - Mode 2.30 eV > 2.38 e (Δ = + 0.08 eV)
→ - Mode 2.3 eV >1.78 eV (Δ = - 0.52 eV

FARB - ÄNDERUNGEN :

Gold - Sole: Rot > Rosa > Violett > Blau

Silber - Sole : Gelb > Orange > Rotorange > Braun > Grüngrau

STABILISIERUNG :

Zugabe stark verdünnter Gelatine Lösung

Eintrocken auf Substrat oder kohle-befilmten TEM - Netzen

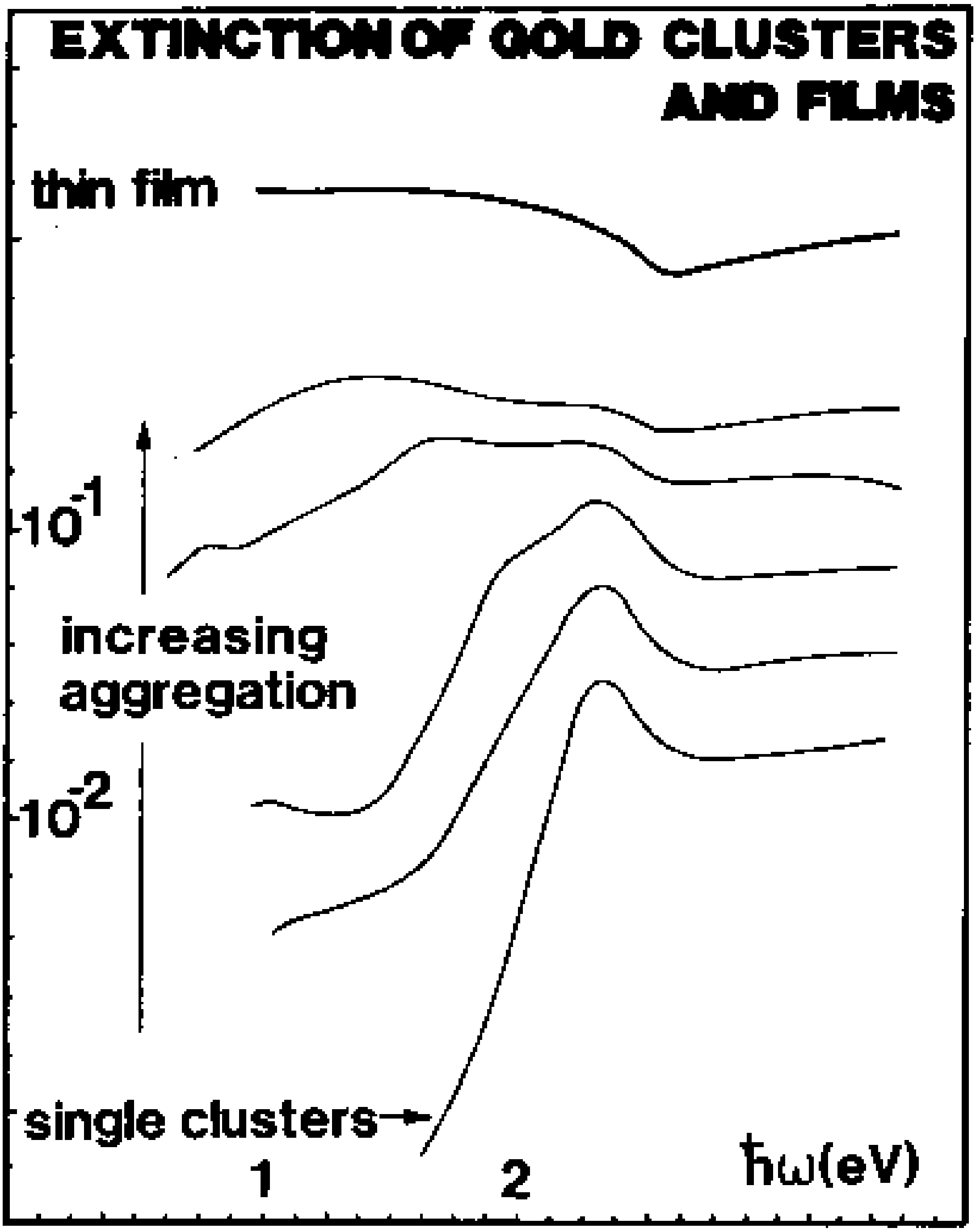
EXTINCTION OF GOLD CLUSTERS AND FILMS
thin film
increasing aggregation
10^-1
10^-2
single clusters
1
2
ħω(eV)

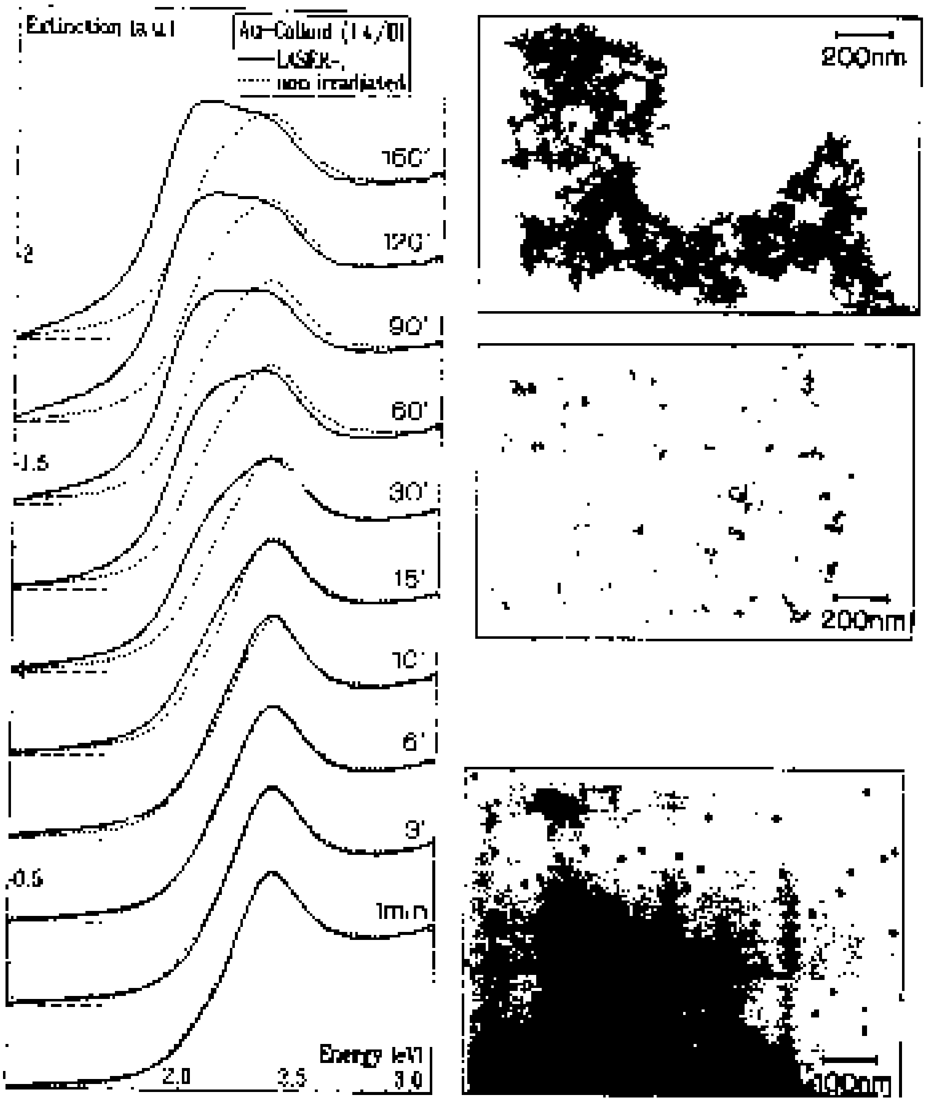

Figure 12 Light-induced aggregation in an aqueous gold colloid ($2R = 10$ nm), shown in the TEM (transmission electron micrograph) lower right. By Ar-514.5 nm laser irradiation, aggregation is induced ("light-induced van der Waals forces" or photochemical effects, see upper right figure), while the nonirradiated sample shows only weak effects (see middle right). The optical extinction spectra of the irradiated and the nonirradiated sample are shown at left. The double peak is due to electromagnetic coupling in the aggregates. (Eckstein, H. and Kreibig, 1993.)

GENERALIZED MIE THEORY (GMT)

The single nanoparticle of Mie's theory is of importance for basic research and understanding. For practical and technical purposes macroscopic many-particles systems are common. If volume concentrations are low, then the application of Lambert-Beer' law, introduced by Mie himself is sufficient.
At concentrations higher than ≈ 10^{-4} cm^{-3} in statistically distributed systems or in systems with aggregation blocks (chains, coagulation clusters) neighboring particles interact with each other during optical excitation via their electromagnetic near fields. As known from coupled oscillators, then resonances split on the frequency scale and strong changes occur in the spectra.

There are different methods with different degrees of accuracy to calculate those spectra. They all assume high particle densities by coagulation, but coalescence is excluded, since this produces novel particles with changed sizes and shapes.

(1) The Effective Medium Theories: They are simple to treat but can be drastically inaccurate. The inhomogeneous sample is approximated by a dielectrically homogeneous system and the resulting "effective dielectric function" (of the whole sample - not of the particle material !) is calculated. We will not treat these roughly approximative methods here, since we have the Generalized Mie Theory (GMT) which is the exact solution of electrodynamics and is exact to the same degree as the Mie theory itself. However, this method requires enormous computer capacities.

(2) The Generalized Mie Theory (GMT) was proposed by Ausloos and Gerardy and fist numerically applied by Quinten and Kreibig. It is based upon

- the exact Mie solution of each single particle,
- the exact position coordinates of each particle in the sample. Experimentally these data may be obtained by electron-microscopic methods (TEM, SXM, SEM etc.),
- the realistic near fields in the spaces between all neighboring particles which induce electromagnetic coupling. All multipolar near fields of all particles n* interact with those of all other particles n and have to be summed up and added to the incident fields. (There are no orthogonality conditions, since all

particles have different positions.). The problem is solved numerically by a self-consistence algorithm which takes much computer time.

To describe the GMT we start with the wave equation in spherical coordinates

$$(\nabla^2 + |\boldsymbol{k}|^2)\Pi_i(r,\theta,\phi) = 0 ,$$

which is solved by multipole expansion (*partial waves* according to Mie) for the following scalar potentials Π_i at position (r,θ,ϕ) of a given particle i in the aggregate:

- Π^{inc} of the incident plane wave
- Π^{in} of the wave inside the particles
- Π^{sca} of the outgoing/scattered wave
- Π^{int} of the scattered waves from all particles $j \neq i$ causing the interaction in the aggregate.

The according fields are the gradients of these potentials. The first three potentials are those of Mie's original theory. The potentials caused by all neighboring scatterers can be transformed into one potential of an additional wave, the interaction potential acting on particle i:

$$\Pi^{\text{int}} = \sum_{j\neq i}^{N_a} \Pi^{\text{sca}}(j) = \frac{1}{|\boldsymbol{k}|^2 r_i} \sum_{l=1}^{\infty} \sum_{m=-1}^{+1} \psi_l(|\boldsymbol{k}|r_i) Y_{l,m}(\theta_i,\phi_i) \times \sum_{j\neq i}^{N_a} \sum_{q=1}^{\infty} \sum_{p=-q}^{+q} A_{lm}^{qp} b_{qp}(j)$$

Here, $\boldsymbol{k}$ denotes the wavevector, Y spherical harmonics, ψ spherical Bessel functions, b_{qp} the complex amplitude coefficients of the scattered wave, and A_{lm}^{qp} the transformation matrix of the spherical coordinates of particle j into those of particle i.

A system of $N_a(2l+1)$ equations (N_a = number of clusters per aggregate; l = maximum number of multipolar modes taken into account) is obtained which allows to calculate self-consistently the complex amplitude coefficients b_{lm} of the wave scattered from particle i. One ends up with the extinction constant of the cluster aggregate

$$\gamma_e = \frac{3c^2}{2\omega^2 \varepsilon_m R^3} \text{Im} \left\{ \sum_{i=1}^{N_a} \sum_{l=1}^{\infty} \sum_{m=-1}^{+1} (-1)^l b_{lm}(i) \right\}$$

by summing up over all particles, all multipoles and the polarization states of the incident light.

- To reduce computer time, smaller but characteristic parts of the sample have to be selected In the dipole-approximation, calculations of some 10^5 particles are realistic, but only of some 10^3 particles if the quadrupoles are also taken into consideration.

Since only samples of limited sizes can be treated, the particles at their limiting boundaries raise problems, since their coordination numbers of nearest neighbors, and, hence the electromagnetic coupling is reduced.

Up to now, none has succeeded in increasing sample sizes so far that the boundary effects could be neglected.

- So, the results are realistic spectra of extinction, absorption and scattering of the whole many-particle sample but not (yet) numerically precise.

Like Mie's theory, GMT can be applied to arbitrary cluster materials, arbitrary distributions of particle sizes and arbitrary particles positions. The only draw-backs are the restriction to the spherical particle shape, the exclusion of coalescence aggregates and the sample size limitations.

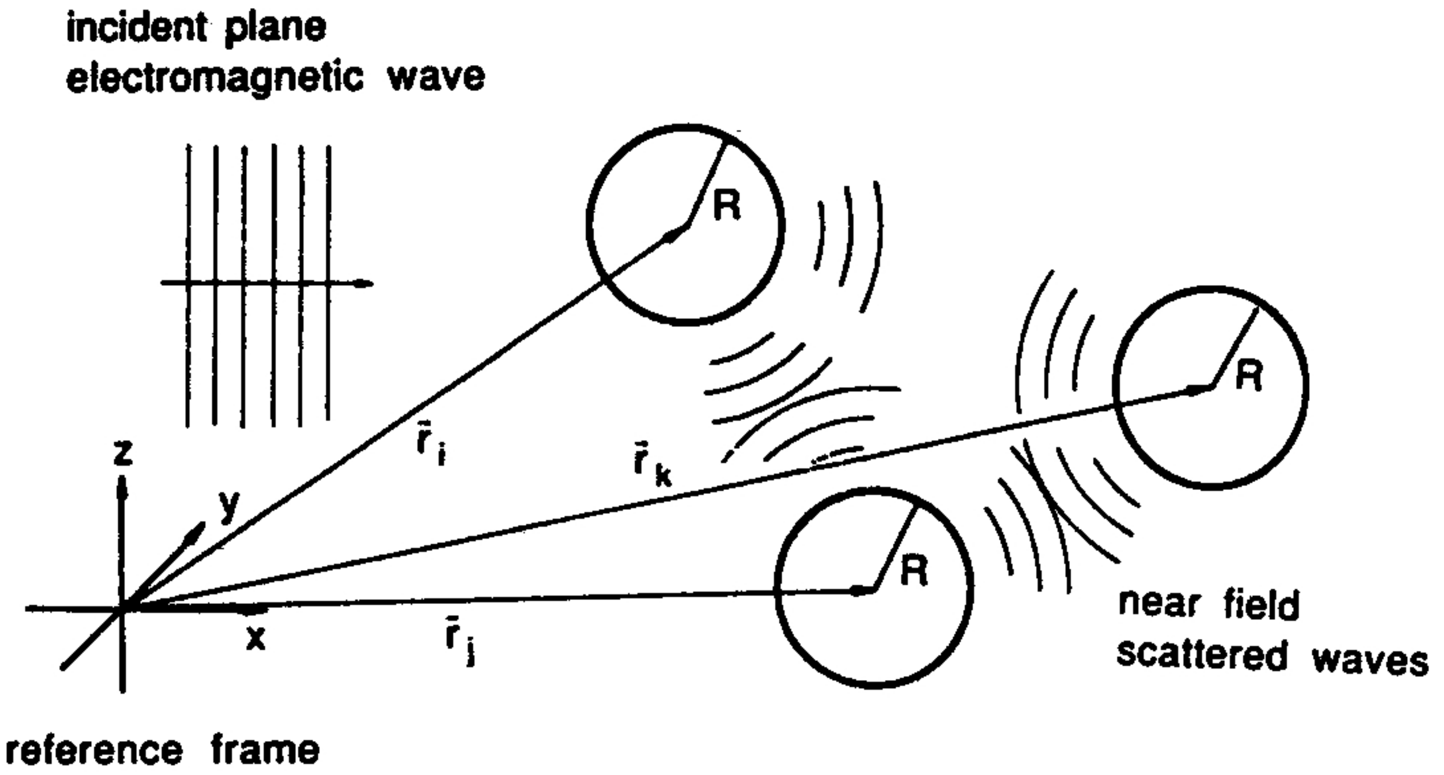

Fig. 2.72. *Generalized Mie theory*: Coordinates for calculation of electromagnetic interactions.

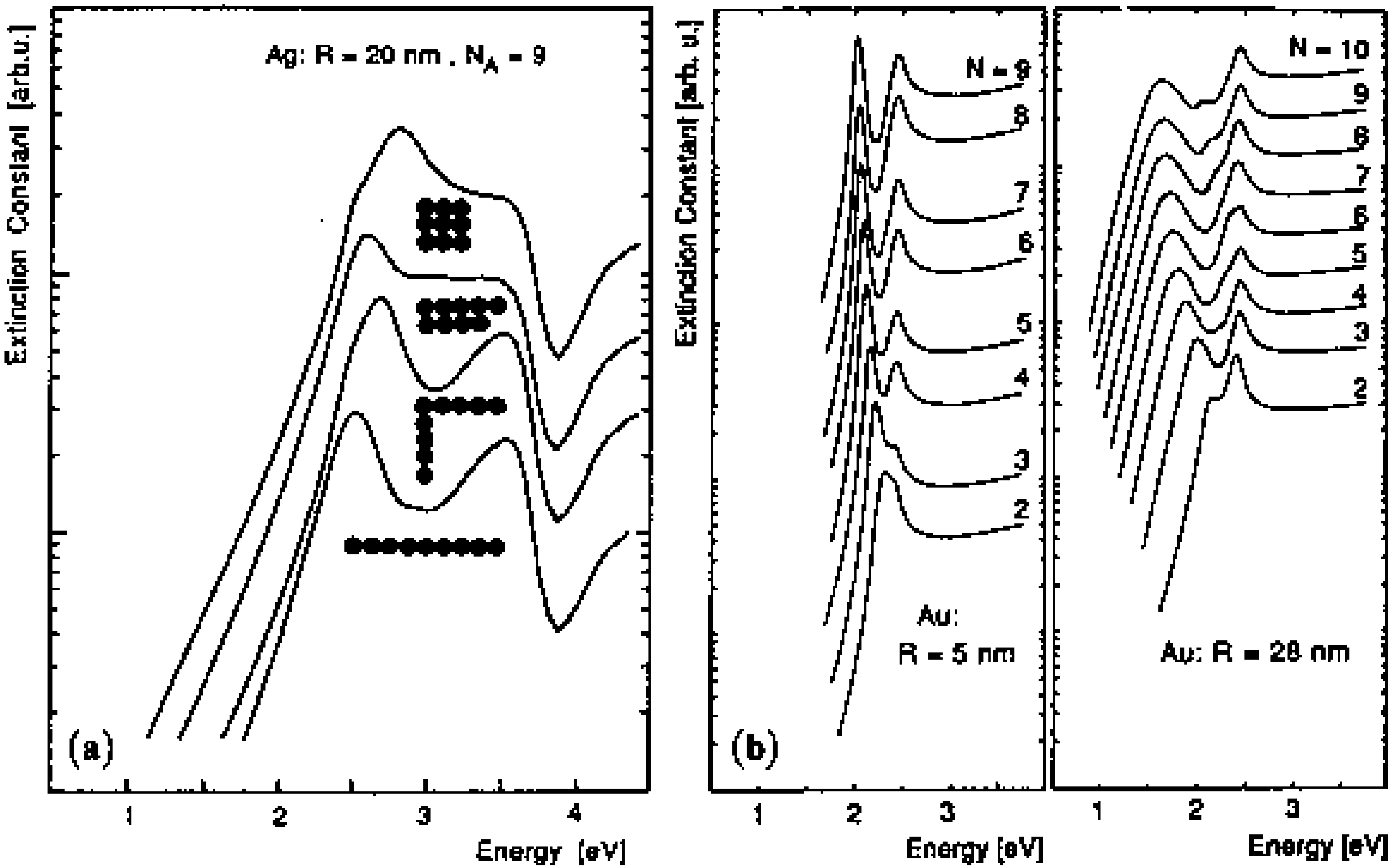

Fig. 2.73. *Generalized Mie theory*: (a) extinction spectra of $N_A = 9$ clusters in aggregates of various topologies. Interactions up to quadrupole order ($L = 1, 2$) are included [after 2.127]). (b) linear chains of Au clusters with various lengths. Cluster sizes are $R = 5\,\text{nm}$ (left) and $R = 28\,\text{nm}$ (right), $\epsilon_m = 1.96$ (after [2.413]). Averaging over the aggregate orientation is included. All curves are vertically shifted by arbitrary amounts for the sake of clarity.

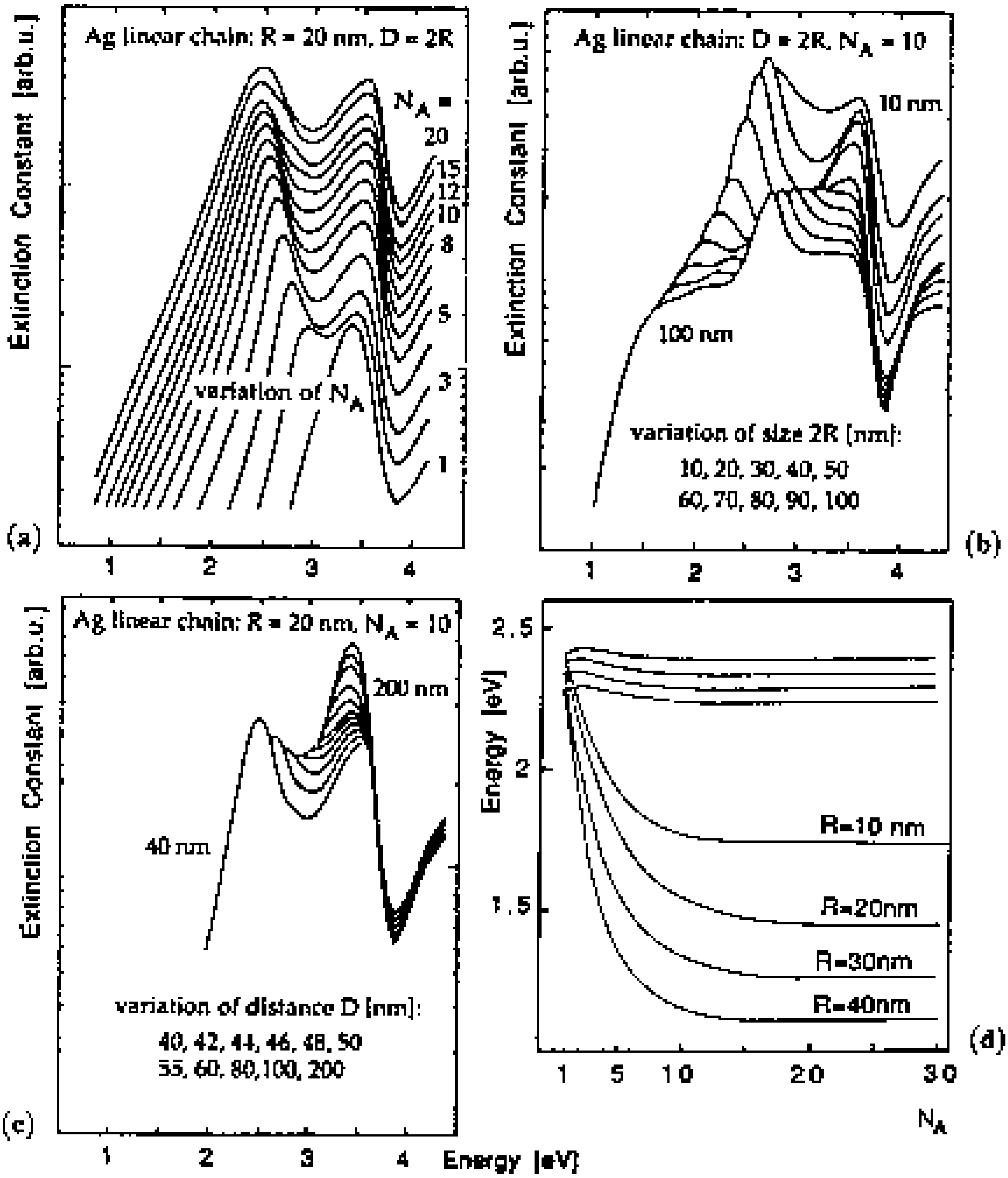

Fig. 2.74. *Generalized Mie theory*: Topological effects on the extinction spectra of linear chains of Ag clusters. Variation of chain length (**a**), cluster sizes (**b**), cluster-cluster distances (center to center) (**c**). Peak positions for varying chain lengths and cluster sizes are shown in (**d**) (courtesy M. Quinten).

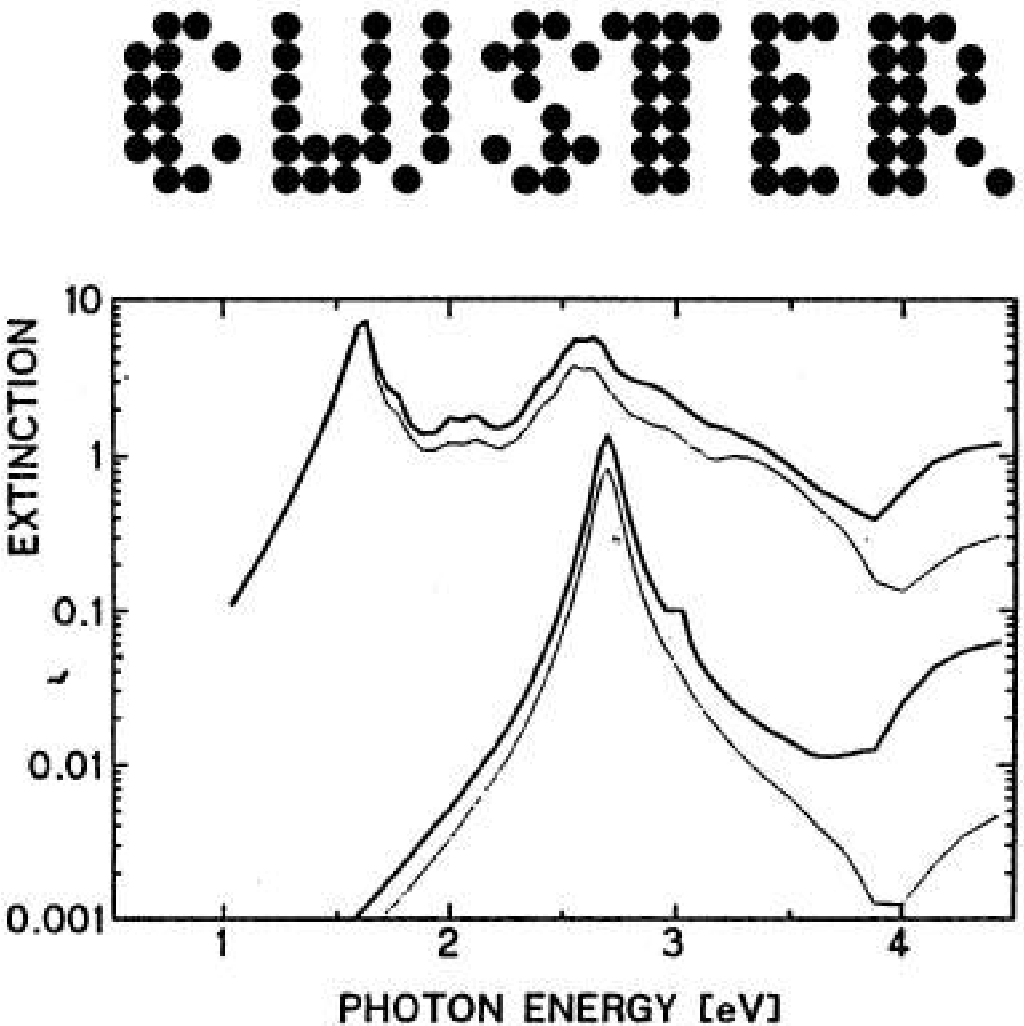

Fig. 2.75. Extinction and scattering spectra (bold and weak lines) of Ag clusters ($2R = 40\,\mathrm{nm}$), computed including retardation effects. The lower two curves correspond to the single clusters, the upper ones to the seven close lying cluster aggregates of, in total, 91 clusters, shown on top (courtesy M. Quinten).